CR-174765

Contract NAS3-23687

Component-Specific Modeling

First Annual Status Report
1983

Prepared By:
R.L. McKnight, Principal Investigator

Approved By:
J.A. McKenzie, Program Manager
M.L. Roberts, Technical Manager

(NASA-CR-174765) COMPONENT-SPECIFIC MODELING Annual Status Report (General Electric Co.) 162 p HC A08/MF A01 CSCL 21L

N85-34140

Unclas
G3/07 26281

NATIONAL AERONAUTICS AND SPACE ADMINSTRATION
LEWIS RESEARCH CENTER
21000 BROOKPARK ROAD
CLEVELAND, OHIO 44135

GENERAL ELECTRIC

AIRCRAFT ENGINE BUSINESS GROUP
ADVANCED TECHNOLOGY PROGRAMS DEPARTMENT
CINCINNATI, OHIO 45212

1. Report No. CR-174765	2. Government Accession No.	3. Recipient's Catalog No.
4. Title and Subtitle Component-Specific Modeling		5. Report Date May 1985
		6. Performing Organization Code
7. Author(s) R.L. McKnight		8. Performing Organization Report No.
		10. Work Unit No.
9. Performing Organization Name and Address General Electric Company Aircraft Engine Business Group Advanced Technology Programs Dept. Cincinnati, Oh 45215		11. Contract or Grant No. NAS3-23687
		13. Type of Report and Period Covered First Annual Status Report
12. Sponsoring Agency Name and Address National Aeronautics & Space Administration Washington, D.C. 20546		14. Sponsoring Agency Code RTOP 533-04-1A

15. Supplementary Notes
Project Manager, M.S. Hirschbein
NASA Lewis Research Center (M.S. 49-6)
21000 Brookpark Road
Cleveland, Ohio 44135

16. Abstract

The overall objective of this program is to develop and verify a series of interdisciplinary modeling and analysis techniques that have been specialized to address three specific hot section components. These techniques will incorporate data as well as theoretical methods from many diverse areas including cycle and performance analysis, heat transfer analysis, linear and nonlinear stress analysis, and mission analysis. Building on the proven techniques already available in these fields, the new methods developed through this contract will be integrated into computer codes to provide an accurate, efficient, and unified approach to analyzing combustor burner liners, hollow air-cooled turbine blades, and air-cooled turbine vanes. For these components, the methods developed will predict temperature, deformation, stress and strain histories throughout a complete flight mission.

17. Key Words (Suggested by Author(s)) Finite element analysis, structural analysis, mission modeling, nonlinear analysis	18. Distribution Statement Unclassified, Unlimited

19. Security Classif. (of this report)	20. Security Classif. (of this page)	21. No. of Pages	22. Price*
Unclassified	Unclassified	162	

* For sale by the National Technical Information Service, Springfield, Virginia 22161

FOREWORD

This report has been prepared to expedite early dissemination of the information generated under the contract. The data and conclusions must be considered preliminary and subject to change as further progress is made on this program. This is a progress report covering the work done during the first 12 months of the contract, and it is not a final report.

TABLE OF CONTENTS

PRECEDING PAGE BLANK NOT FILMED

LIST OF ILLUSTRATIONS

LIST OF ILLUSTRATIONS (Continued)

LIST OF ILLUSTRATIONS (Continued)

LIST OF ILLUSTRATIONS (Concluded)

LIST OF TABLES

1.0 INTRODUCTION

Modern jet engine design imposes extremely high loadings and temperatures on hot section components. Fuel costs dictate that minimum weight components be used wherever possible. In order to satisfy these two criteria, designers are turning toward improved materials and innovative designs. Along with these approaches, they also must have more accurate, more economical, and more comprehensive analytical methods.

Numerous analytical methods are available that can, in principle, handle any problem that might arise. However, the time and expense required to produce acceptable solutions is often excessive. This program addresses this problem by setting out a plan to create specialized software packages which will provide the necessary answers in an efficient, user-oriented, streamlined fashion. Separate component-specific models will be created for burner liners, turbine blades, and turbine vanes using fundamental data from many technical areas. The methods developed will be simple to execute, but they will not be simple in concept. The problem is extremely complex and only by a thorough understanding of the details can the important technical approaches be extracted. The packaging of these interdisciplinary approaches into a total system must conform to the modular requirements for useful computer programs.

The overall objective of this program is to develop and verify a series of interdisciplinary modeling and analysis techniques that have been specialized to address three specific hot section components. These techniques will incorporate data as well as theoretical methods from many diverse areas including cycle and performance analysis, heat transfer analysis, linear and nonlinear stress analysis, and mission analysis. Building on the proven techniques already available in these fields, the new methods developed through this contract will be integrated to provide an accurate, efficient, and unified approach to analyzing combustor burner liners, hollow air-cooled turbine blades, and air-cooled turbine vanes. For these components, the methods developed will predict temperature, deformation, stress, and strain histories throughout a complete flight mission.

This program, to a great extent, draws on prior experience. This base of experience is invaluable for understanding the highly complex interactions among all the different technical disciplines as well as for estimating the importance of different engine parameters. In particular, there are four specific areas in which experience is especially beneficial.

First, with the recent increases in fuel costs, greater emphasis has been placed on more accurate solutions for stresses and strains in order to understand and improve the durability and life of hot section components. Conventional linear elastic analyses are no longer sufficient; instead, they now provide the boundary values for more refined creep and plasticity calculations. These nonlinear analyses are now performed routinely as part of the design process at General Electric. This extensive experience with these plasticity and creep methods contributes directly to developing component specific models.

Second, advances in 3-D modeling capability are being achieved by the concepts developed under the NASA-supported ESMOSS program. ESMOSS concepts provide the basis to develop an efficient modeling system for geometric and discretized models of engine components.

Third, the NASA-funded Burner Liner Thermal/Structural Load Modeling Program contributes strong support to this program. The specific area addressed, transfer of data from a 3-D heat transfer analysis model to a 3-D stress analysis model, will provide the background and framework for the data interpolation required for all thermomechanical models in this contract.

Fourth, over the past 10 years General Electric has developed internally a family of computer programs: LASTS, OPSEV, and HOTSAM. These programs all have the common thread of using selected points from cycle data, heat transfer, and stress analyses and a decomposition/synthesis approach to produce accurate values of temperature, stress, and strain throughout a mission. These programs are totally consistent with the overall objectives of this program, and represent a proven technology base upon which the component specific models are being developed. Significant advances being made are the inclusion of nonlinear effects and the introduction of improved modeling and data transfer techniques.

The program is organized into nine tasks which can logically be separated into two broadly parallel activities (Figure 1). On the right of Figure 1 we have the Component Specific Thermomechanical Load Mission Modeling path. Along this path a Decomposition/Synthesis approach is being taken. In broad terms, methods are being developed to generate approximate numerical models for the engine cycle and the aerodynamic and heat transfer analyses needed to provide the input conditions for hot parts stress and life analysis.

The left path, Component Specific Structural Modeling provides the tools to develop and analyze finite element nonlinear stress analysis models of combustor liners and turbine blades and vanes. These two paths are shown in more detail in Figures 2 and 3.

Software Development, Task IV, consists of planning and writing the computer programs for both paths, with the necessary interconnections, using a structured, top down approach.

In the Thermomechanical Load Mission Modeling portion of the program (Figure 2), we are developing in Task III a Thermodynamic Engine Model which generates the engine internal flow variables for any point on the operating mission. The method for doing this is described below. Task V is developing techniques to decompose flight missions into characteristic mission segments. In Task VII a Thermomechanical Mission Model is being developed. This uses the flow variables from the Thermodynamic Model to determine metal temperature and pressure distributions for a representative combustor liner and turbine blade and vane.

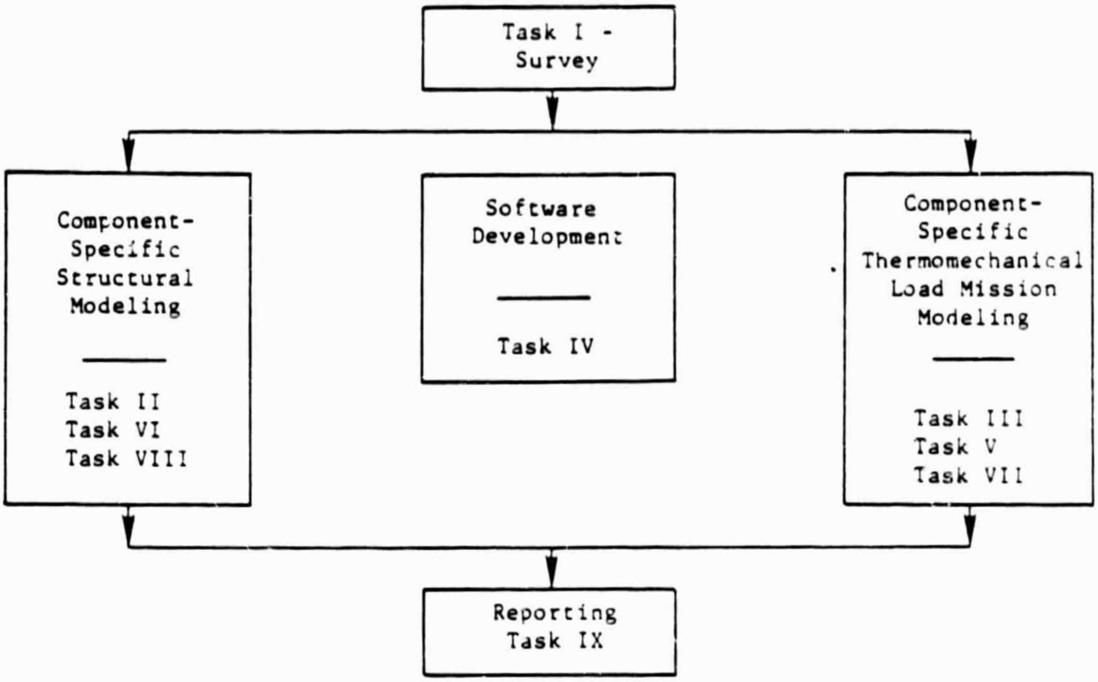

Figure 1. Component Specific Modeling Base Program.

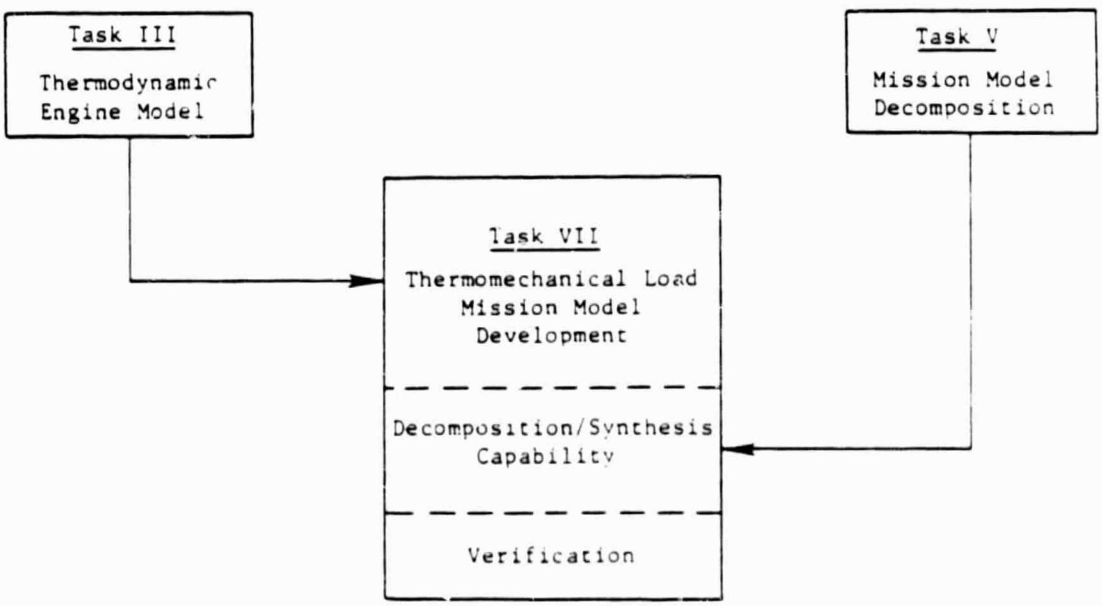

Figure 2. Component Specific Thermomechanical Load Mission Modeling.

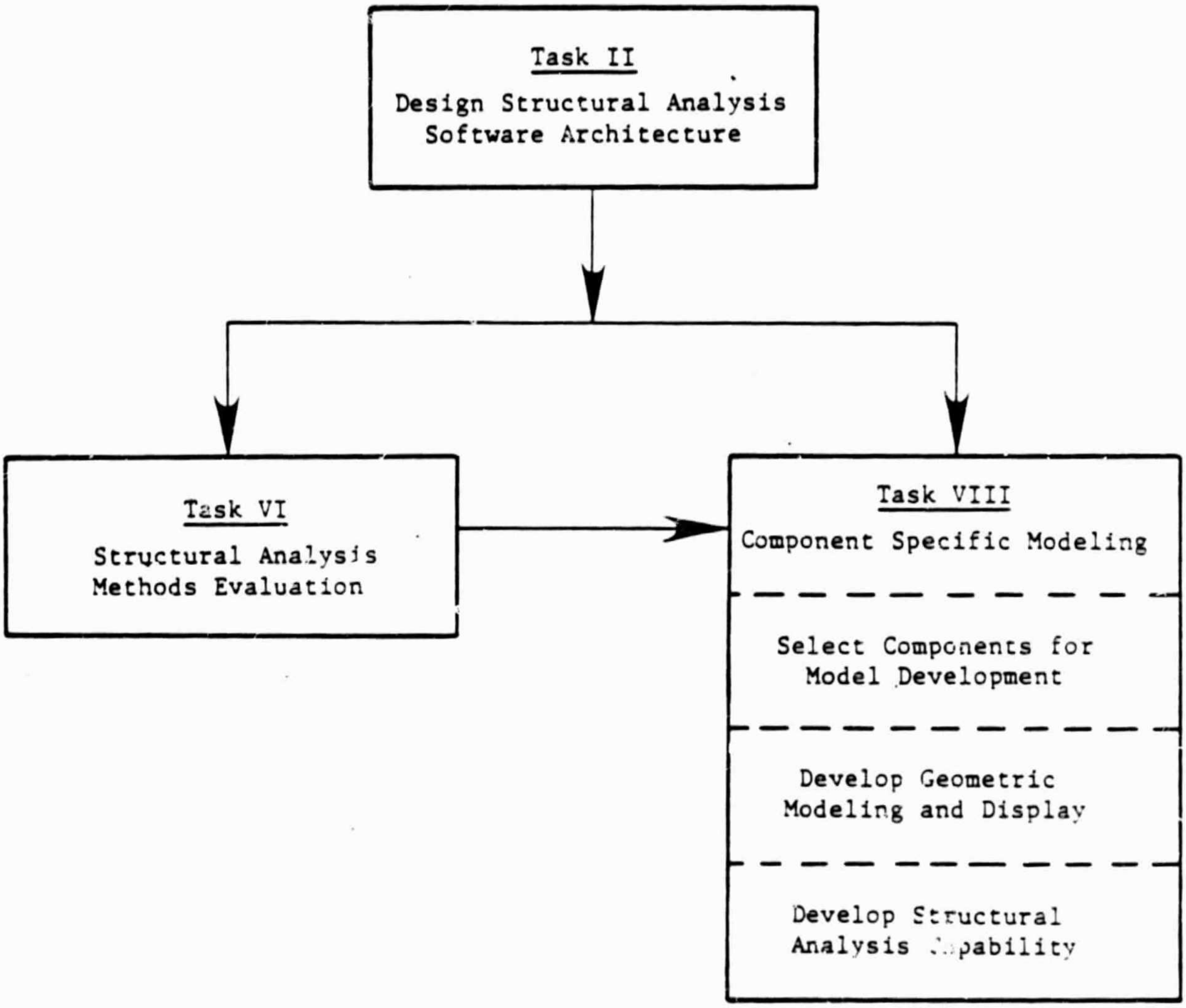

Figure 3. Component Specific Structural Modeling.

Individual tasks for the Structural Modeling activity are shown in Figure 3. The requirements of Software Design, Task II, have been factored into Task VI, the evaluation of the structural analysis methods which were selected for evaluation in Task I. Task VIII provides the capability for structurally modeling current state-of-the-art combustor liners and hollow turbine blades and vanes, given the defining dimensional parameters. These parameters will be chosen to facilitate parametric studies.

The component specific models are being developed in two steps. In the first a geometric model is defined. In the application of the Component Specific Modeling Program these data are then transferred to the Thermomechanical Load Mission Model to provide the geometry for determining component pressures and temperatures. Thus, a data transfer link is being developed to do this in Task IV, Software Development. The capability for generating from the geometric model a discretized, finite element model is also a part of Task VIII. At this point another link between the two paths is needed to transfer the component temperatures and pressures from the Thermomechanical Load Model to the finite element model, interpolating the data as needed to define nodal temperatures and pressures. This also is being completed in Task IV.

2.0 TECHNICAL PROGRESS

2.1 TASK I - LITERATURE SURVEY

The first task of this program was to perform a literature survey of available methods, techniques, and solution strategies that can be used to geometrically model, display, and structurally analyze burner liners, turbine blades, and vanes. NTIS, NASA, DTIC, and internal General Electric Company documents were searched. The fruits of this survey are listed in Appendix A.

2.2 TASK II - DESIGN OF STRUCTURE ANALYSIS SOFTWARE ARCHITECTURE

The software architecture was designed using the methodology developed on the ESMOSS program. The first step in this process was to perform a functional analysis of the problem using Soft Tech's Structured Analysis and Design Technique (SADT). This analysis defined the work of the software system and provided the foundation for the software development of Task IV. This analysis was performed by teams whose members had expertise in all of the pertinent areas. Appendix B contains the diagrams showing the functional decomposition and the current data dictionary.

Figure 4 shows the software architecture defined for the structural analysis portion of COSMOS. This is the architecture developed for internal programs. Subroutine ELKIND determines the element type, the output option, the material number, the orthotropic orientation set, the stiffness computation code, the area load set, and the line load set. This information is then bit packed into one word. Subroutine NODDOF determines the degree of freedom per node consistent with the element type. Subroutine FIXITY determines zero displacement boundary conditions and sets counters to eliminate the proper equations from the solution. Subroutine PREDIS determines all other prescribed boundary conditions. Subroutine CONNEC reads the element nodal connectivity. Subroutine CONSTR establishes any constraint equations. Subroutine XYZCOR reads the global coordinates of each node. Subroutine MIDNOD generates midside nodes for those elements requiring them. Subroutine SKWDOF reads any skew boundary conditions. Subroutine MTABLE reads material property data. Subroutine ELDATA establishes the element specific data. Subroutine COLHT establishes the column heights for the linear solver subroutine. Subroutine SBLOCK determines the number of solution blocks required by the linear equation solver. Subroutine FILCOR allows for more portability of of code by establishing logic to determine whether there is sufficient core or whether files are needed. Subroutine ELSTIF develops the element stiffness. Subroutine ELMASS develops the element mass. Subroutine ELDAMP develops the element damping. Subroutine ADDSTF assembles the global stiffness matrix. Subroutine MODSTF modifies the global stiffness matrix for boundary conditions. Subroutine EIGEN performs an eigenvalue solution and outputs the answers.

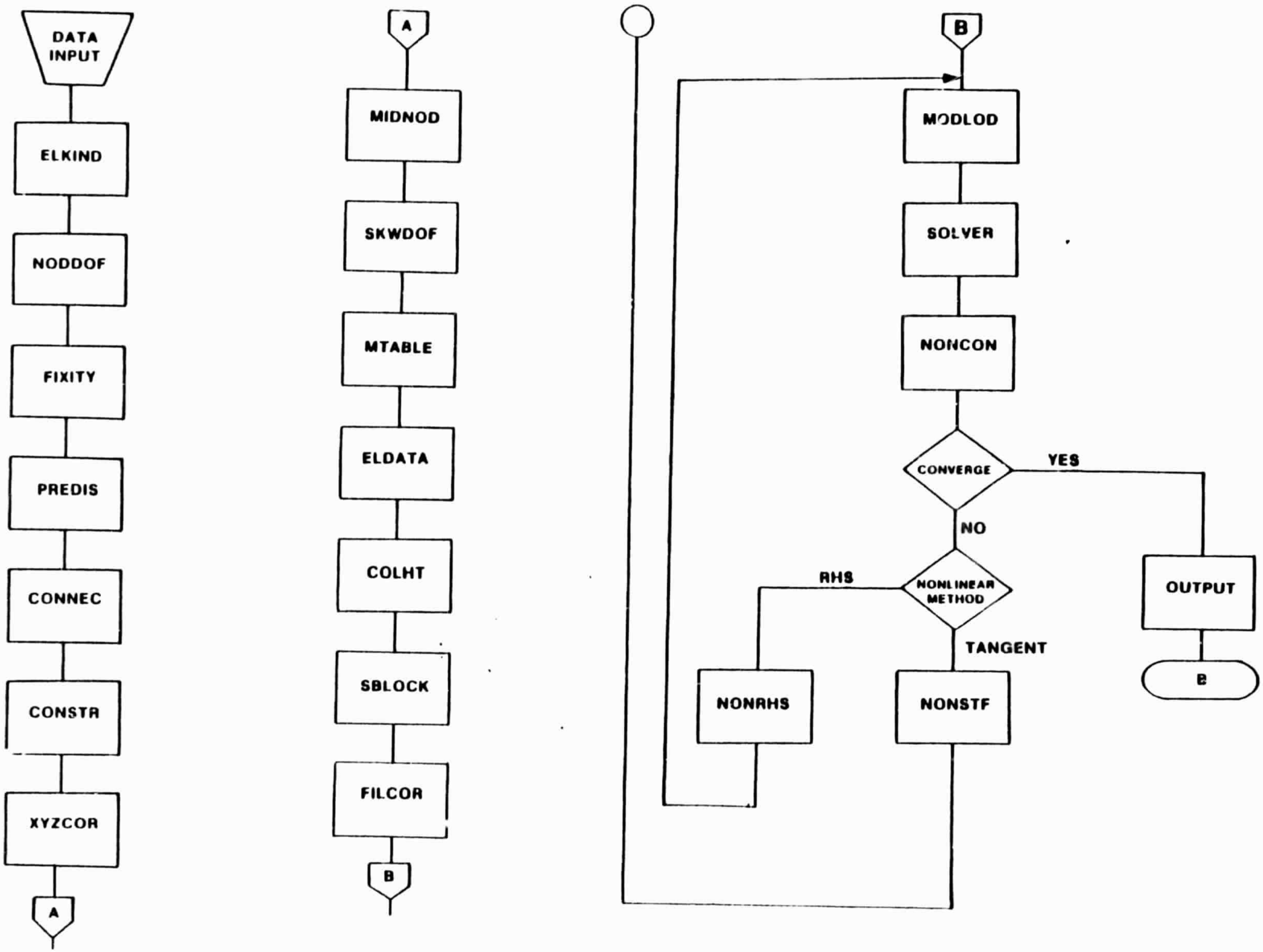

Figure 4. Logic Flow Chart for the Structural Analysis Program.

Subroutine LOADS develops the right-hand side vector. Subroutine MODLOD modifies the right hand side vector for the prescribed boundary conditions. Subroutine SOLVER solves the set of linear equations. Subroutine NONCON develops the nonlinear constitutive equation information. Subroutine NONSTF develops the nonlinar stiffness terms for a tangent modulus solution methods. Subroutine NONRHS develops the nonlinear right hand side terms for a right hand side pseudoforce solution method. Subroutine OUTPUT develops the requested results and sends them to the proper I/O device. This structure is both modular and growable.

2.3 TASK III - THERMODYNAMIC ENGINE MODEL

The Thermodynamic Engine Model has been completed. The model has been developed as a simple calculations tool which will take as inputs the three variables altitude (h), Mach number (M), and power level (PL) or the allowed flight map of an engine, as shown in Figure 5. In addition, ambient temperature deviations from the standard atmosphere, airframe bleed air requirements, and engine deterioration can also be included as part of the input to the thermodynamic model. For each input condition specified by h, M, and PL, the thermodynamic model will calculate gas weight flow ($\dot{w}$), temperature (t), and pressure (p) at selected aerodynamic engine stations as needed to determine component thermal loadings. These stations are shown in Figure 6.

The technique for developing a thermodynamic engine model is shown in Figures 7 and 8. The engine to be analyzed must be defined thermodynamically by an engine cycle deck (computer program) that can be run to generate the internal flow variables at the chosen aerodynamic stations (Figure 7). To encompass the complete engine operating map (Figure 5), 148 operating points are chosen and $\dot{w}$, t, and p are calculated using the cycle deck for the selected stations as well as N_1 and N_2, the fan and core speeds. From this station data, an engine performance cycle map is constructed. This is essentially a set of three-dimensional data arrays that map the station data ($\dot{w}$, t, p, N_1, and N_2) onto the engine operating map (Figure 5). Given an arbitary operating point defined by h, M, and PL, it is then possible in principle to interpolate on the engine performance cycle map to determine station data. In practice the station parameters are nonlinear functions of the input parameters, and considerable effort is needed to develop these multidimensional interpolations. The computer programs used to generate the engine performance cycle map from the engine cycle deck output has been developed as part of Task III. The functioning of the thermodynamic engine model is shown in Figure 8. Given an engine mission, as shown schematically in Figure 9, it can be defined by values of the input variables h, M, and PL at selected times through the mission. Using these input variables and the engine performance cycle map, an interpolation program developed in this effort will calculate engine station parameters throughout the mission (Figure 8). These are then used to define station mission profiles of $\dot{w}$, t, p, N_1, and N_2 as functions of time at each aerodynamic station. These station mission profiles then become the input to the thermomechanical engine model.

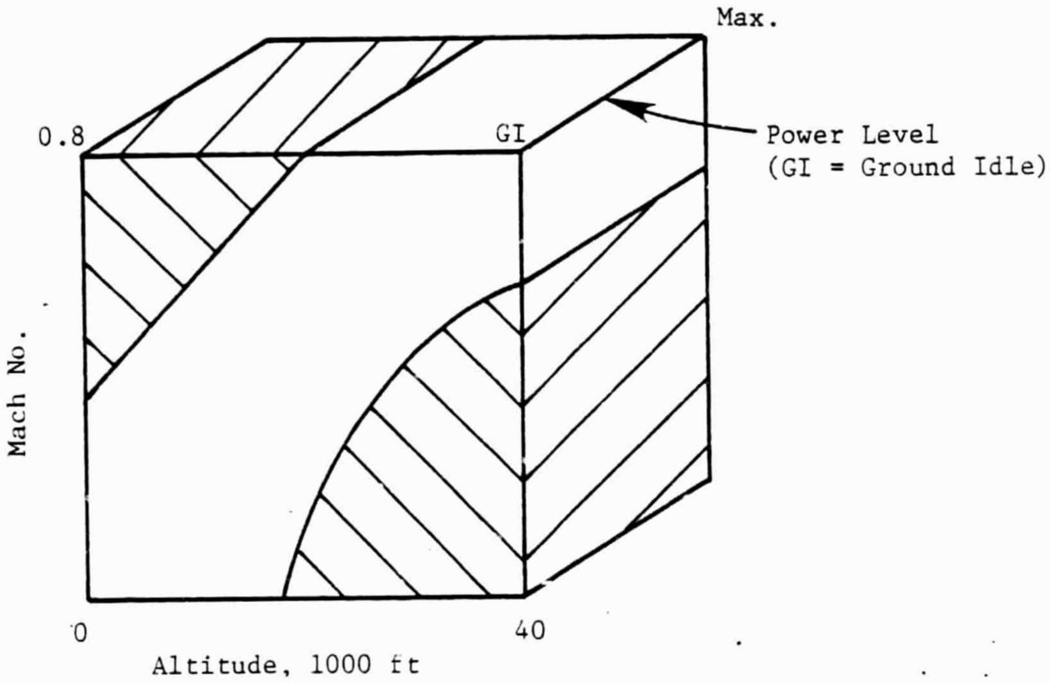

Figure 5. Engine Operating Map.

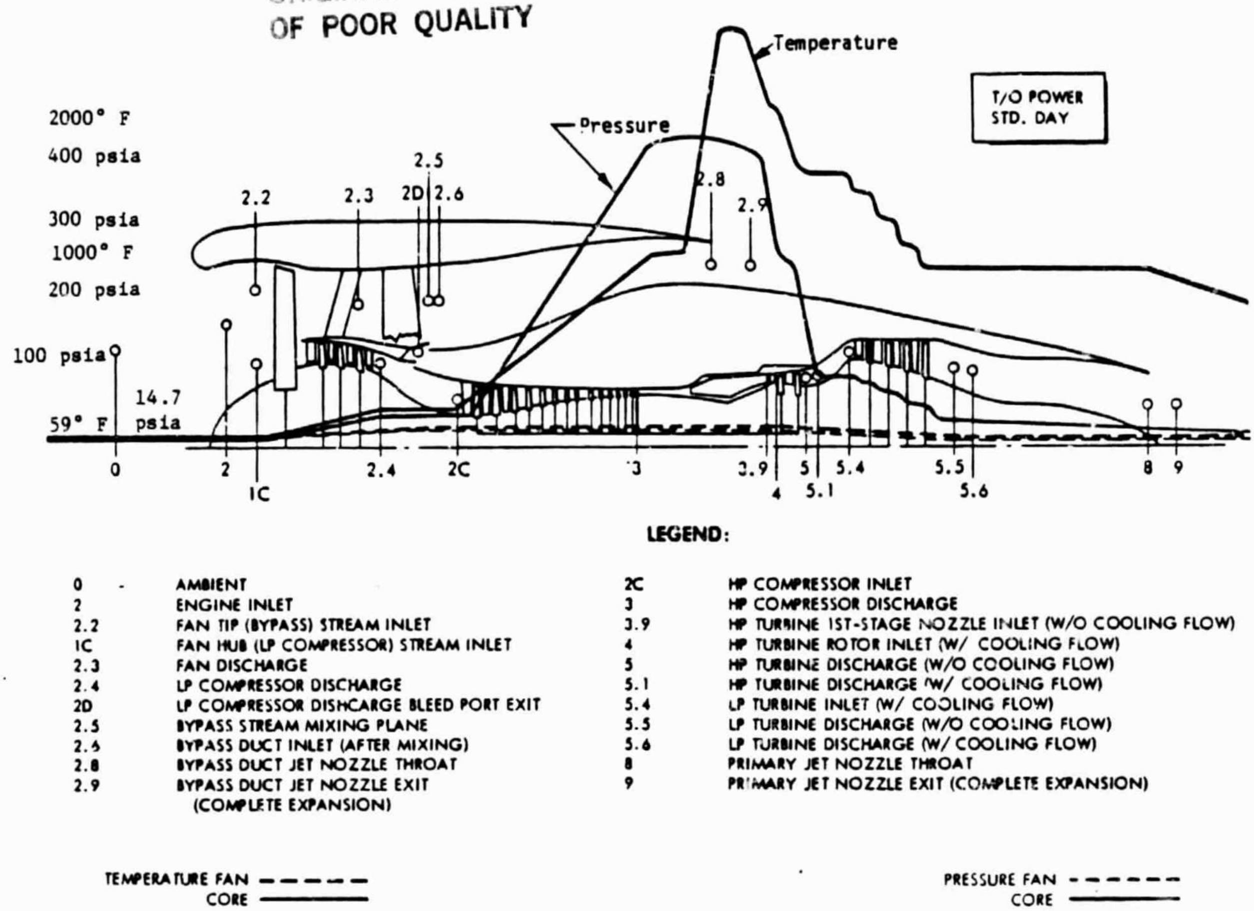

Figure 6. CF6 Aerodynamic Stations.

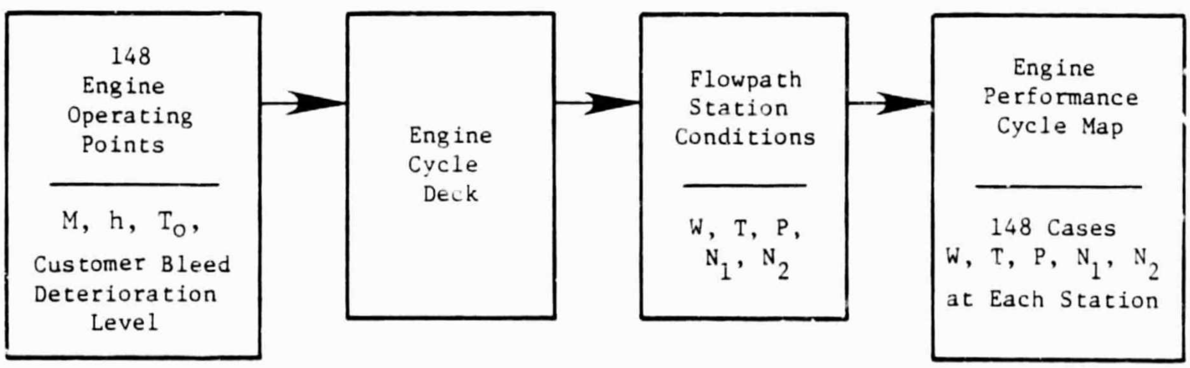

Figure 7. Themodynamic Engine Model Cycle Map Generation.

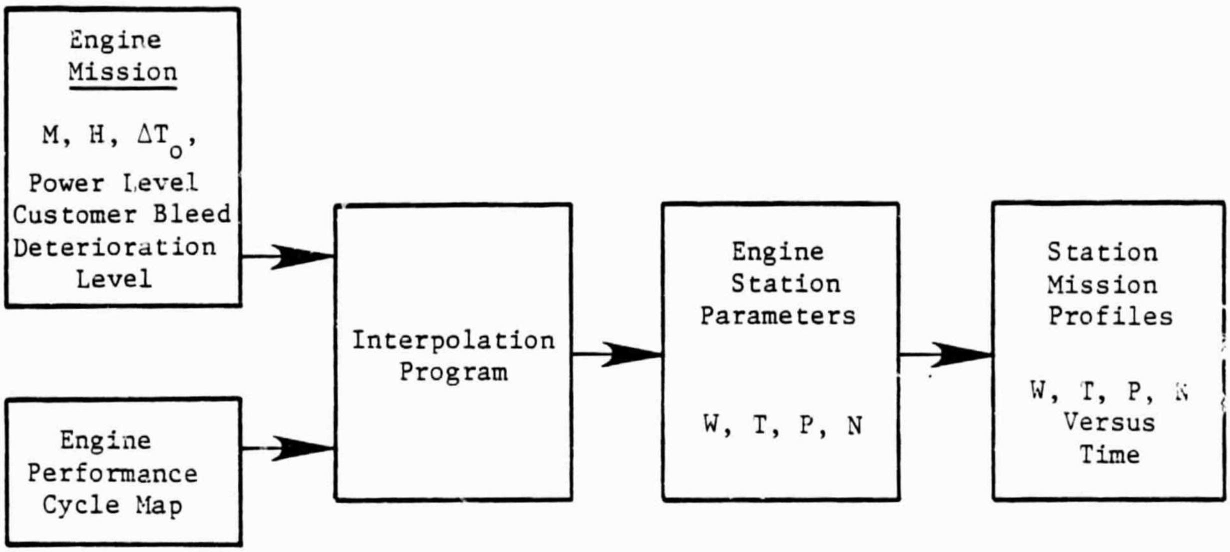

Figure 8. Thermodynamic Engine Model.

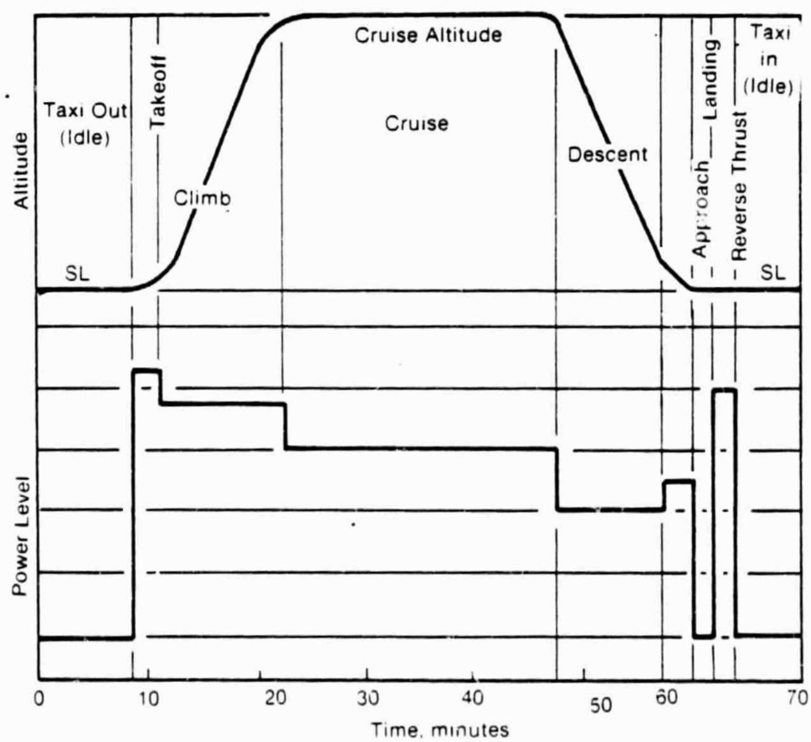

Figure 9. Typical Flight Cycle.

2.3.1 Detailed Specification and Requirements

The first step in this task was to develop detailed specifications and requirements for the thermodynamic engine model software. This specification, which was approved by the NASA Program Manager, is presented in Appendix C.

2.3.2 Model Design and Development

Based on the detailed specifications, the thermodynamic engine model software was generated and a set of 148 performance cases was obtained to load this model. The next task was to establish interparameter interpolation functions. To assist in this effort, 103 special cases that would maximize interpolation errors were chosen from the cycle deck.

A master interparameter linearity study was executed to evaluate interpolation functions. A computer program (STATPAC) was available that could take 30 input performance parameters, perform transformations on the data, and generate crossplots of the transformed function. The linearity of these crossplots was the criterion of excellence in the selection of interpolation functions. One hundred validation cases were run with 30 parameters each, giving 3000 individual comparisons. Sixty-three additional performance cases were used to perform the interparameter linearity study for the Mach number and altitude control variables.

Based on the above program, a set of interparameter interpolation functions and transformation functions was defined and encoded in the TDE model software. The accuracy that can be achieved with these is excellent. As a final "trial run," this model was tested against the CFM56 engine flight conditions.

The TDE user's manual is in preparation.

2.4 SUPPORTING TASKS

2.4.1 Task IV - Software Development

This task consists of planning and writing the computer codes for both paths of this program with the necessary interconnectors. As such, it is a continuous and ongoing effort; the substance is covered under the other task headings.

2.4.2 Task VI - Structural Analysis Methods Evaluation

The objective of Task VI was to evaluate the basic methods to be used in developing the structural-analysis capabilities of the component-specific models. The task has been completed, and selected items are being implemented in Task VIII.

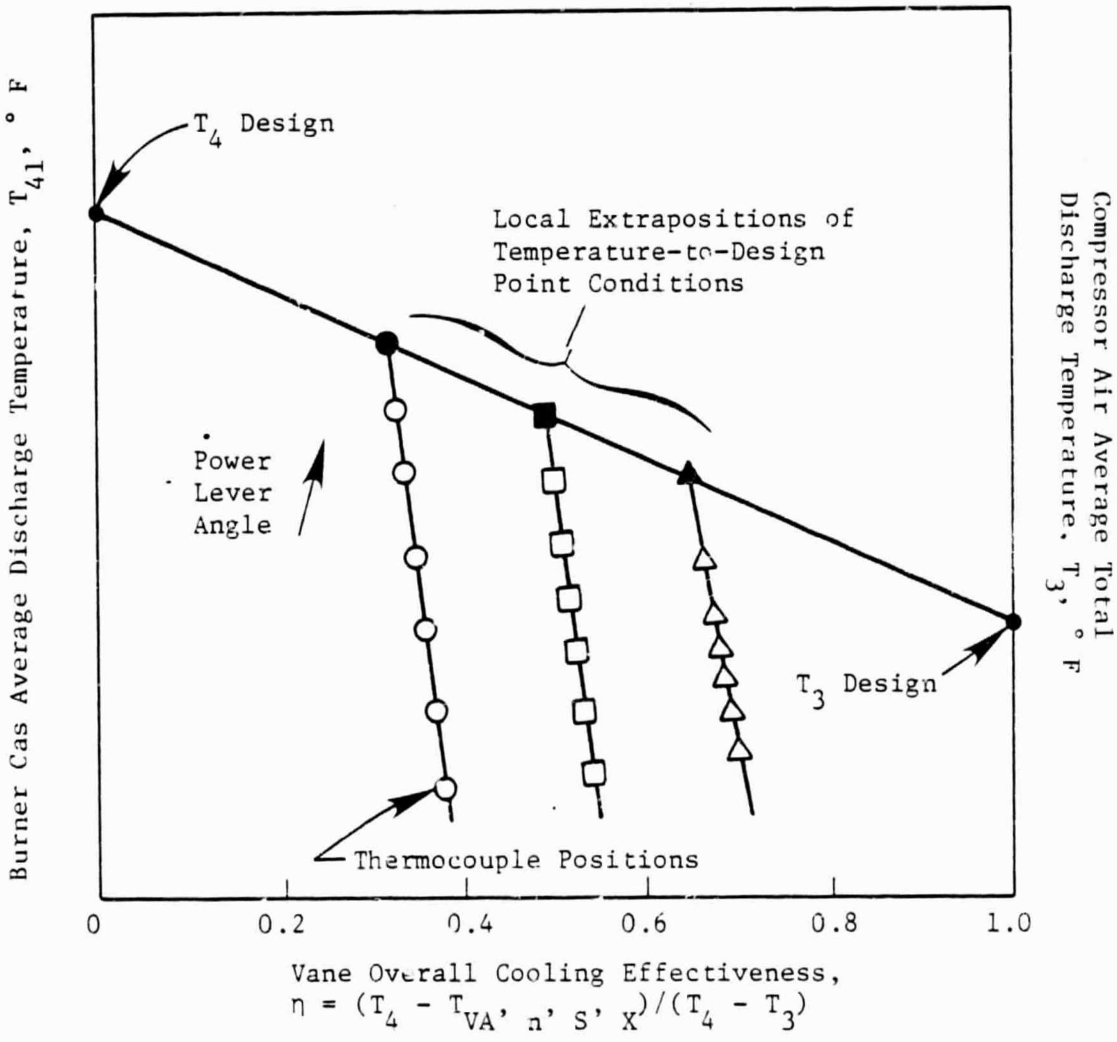

Figure 10. Turbine Vane Cooling Effectiveness.

2.5 TASK V - MISSION MODEL DEVELOPMENT

The thermomechanical model is still under development. The form is based on types of correlations previously developed within GE. Figure 10 shows a representative correlation for a turbine vane. Metal temperatures at various points on the vane T_{VA} are correlated in terms of a vane overall cooling effectiveness η, station gas temperature T_3 at compressor discharge, and T_4 at combustor discharge. Using the station mission profiles, it is possible to calculate the temperatures at selected locations on each component as functions at time, given the input parameters h, M, and PL that define the engine mission. These provide the boundary conditions for the component stress and analyses.

2.5.1 Combustor Liner Temperature and Pressure Decomposition and Synthesis

Introduction

Work has been completed on a generalized procedure established to predict liner temperatures and pressure drop for a rolled ring combustor. This procedure was developed using available data, both measured and and calculated, from several sources. The correlating procedure was demonstrated using engine test data at sea level conditions. Since no engine data at altitude conditions were available, high pressure sector data for a CF6-80A rolled ring liner were used to demonstrate that the method could be used at altitude conditions. A THTD (transient heat transfer - Version D) two-dimensional calculation for the rolled ring combustor at takeoff condition was used to generate the cooling effectiveness data for the entire panel (Panel 7 outer) that was selected for analysis. The development of the procedure and the steps leading to the final cooling effectiveness curve and pressure drop data are described below.

Liner Temperature Distribution

A large amount of engine test data is available for the CF6-50 rolled ring combustor. For the test of the engine, all panels were instrumented with the largest amount of thermocouples on Panels 3 and 7 of the outer liner. Using the metal temperature data, the combustor exit temperature T_4, and the compressor discharge temperature T_3, a cooling effectiveness η_c was evaluated from:

$$\eta_c = \frac{T_4 - T_{liner}}{T_4 - T_3} \quad (1)$$

The results for Panel 7 outer are shown in Figure 11 for several conditions from idle to takeoff power. As shown in the figure, the method correlates the data for several instrumented locations over a wide range of sea level conditions and also shows a slight increase in cooling effectiveness for several of the liner postions as the power level (pressure) decreases.

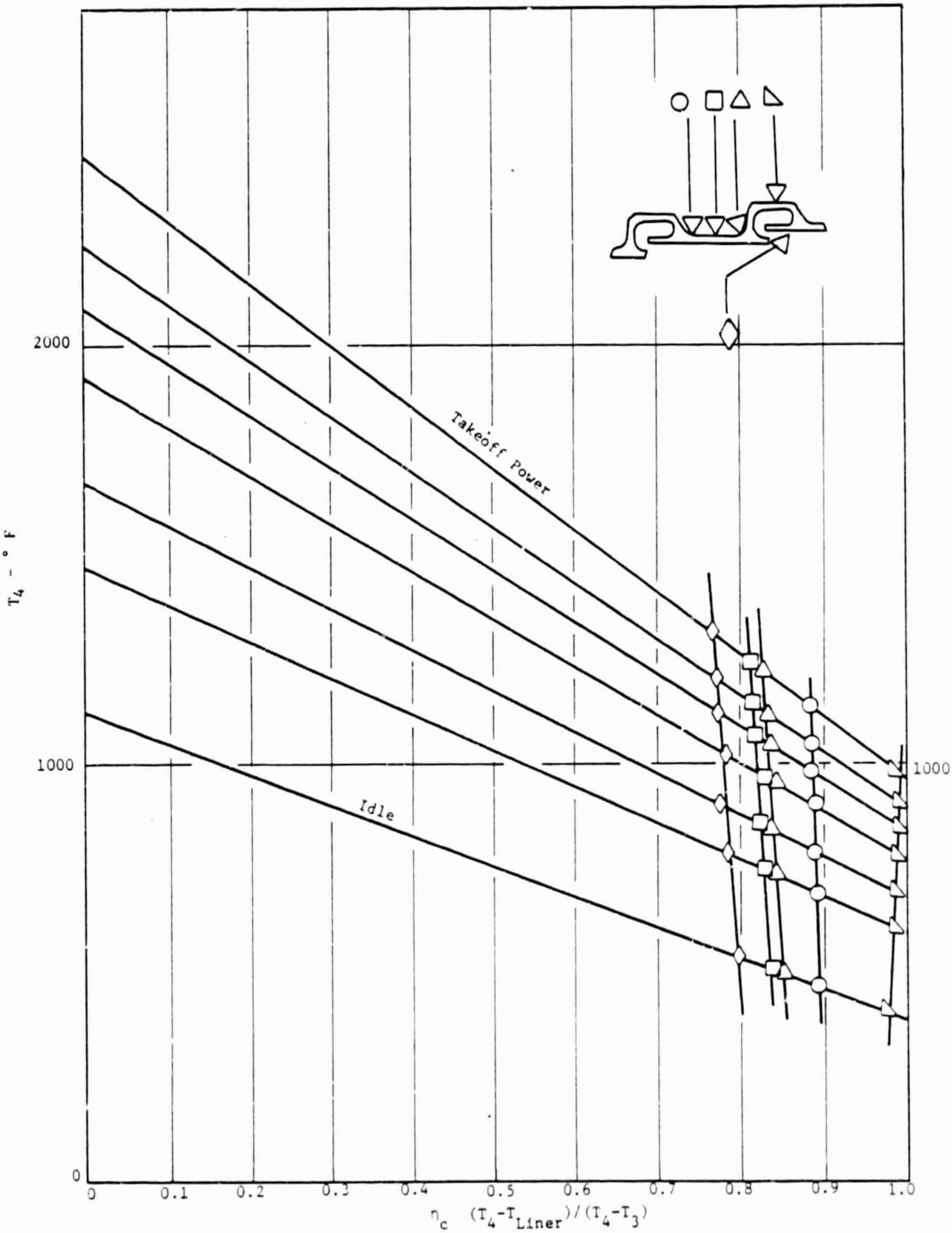

Figure 11. Cooling Effectiveness, Panel 7.

This pressure effect is illustrated in Figure 12 where the ratio of the effectiveness at a given power to the effectiveness at takeoff power is plotted versus pressure. As shown, the ratio for Panel 7 outer increases to about 1.03 at the idle condition. This ratio was plotted for all panels. It was found that the ratio increased to about 1.08 on the forward panels and was about 1.03 for all panels downstream of the aftmost dilution panel. This difference is probably due to the difference in the contributions of flame radiation and convection to the total heat load to the liner. The heat load on the forward panels is controlled by radiation, which is a power function of the local gas temperature. The gas temperatures are lower and the gas velocities are higher on the aft panels. Thus, the heat load is controlled by convection and is a direct function of the local gas temperature. If the pressure effect is not used, then the predicted temperatures at the idle condition would be only about 15° F higher on the aft panels than if the correction is used. The difference on the forward panels would be about 55° F at the idle conditions. Therefore, the pressure correction can be neglected and not cause serious errors in the stress/life calculations.

Data at altitude conditions were not available from the engine test; however, both altitude and sea level data were available from a high pressure sector test of a rolled ring combustor, which has the same type of liner construction as the engine test combustor. These data, converted to cooling effectiveness, are shown in Figure 13 and illustrate that the generalized procedure can be used at both altitude and sea level conditions.

As mentioned earlier, a THTD analysis of Panel 7 was used to generate a cooling effectiveness curve for the entire panel length. This curve was generated for maximum (hot streak) and average panel temperatures. Generally, hot streaks exist around the circumference of the liners and streak for each fuel injector. These streaks result from locally high gas temperatures and velocities near the liner surface. Data matching calculations have led to analytical procedures to simulate hot streaks in the THTD predictions. These procedures used factors applied to local gas temperature and velocity to generate the hot-streak heat transfer input. These curves are shown in Figure 14 and the coordinates of the curves for input to the computer model are given in Table I. The coordinate system used in THTD analysis and the model node layout are shown in Figure 15.

Temperature Gradient Through Material Thickness

An expression for the temperature gradient through the material thickness can be derived from cooling effectiveness, compressor discharge temperature and pressure, and combustor exit temperature. The temperature gradient through the material can be calculated from

$$T_H - T_c = \frac{Q/A}{k} \qquad (2)$$

where

T_H = hot side metal temperature, ° F
T_C = cold side metal temperature, ° F

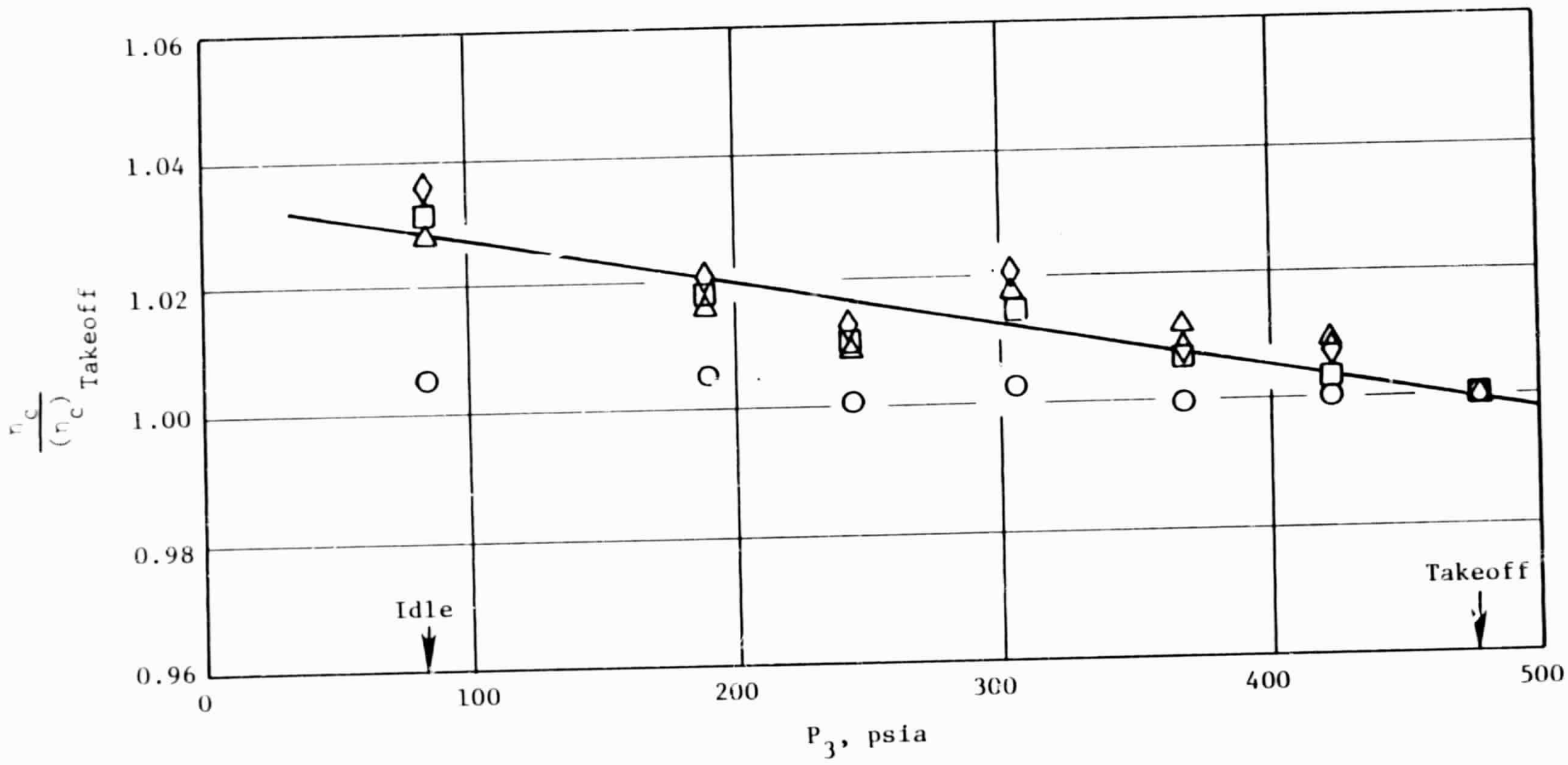

Figure 12. Pressure Effect on Cooling Effectiveness.

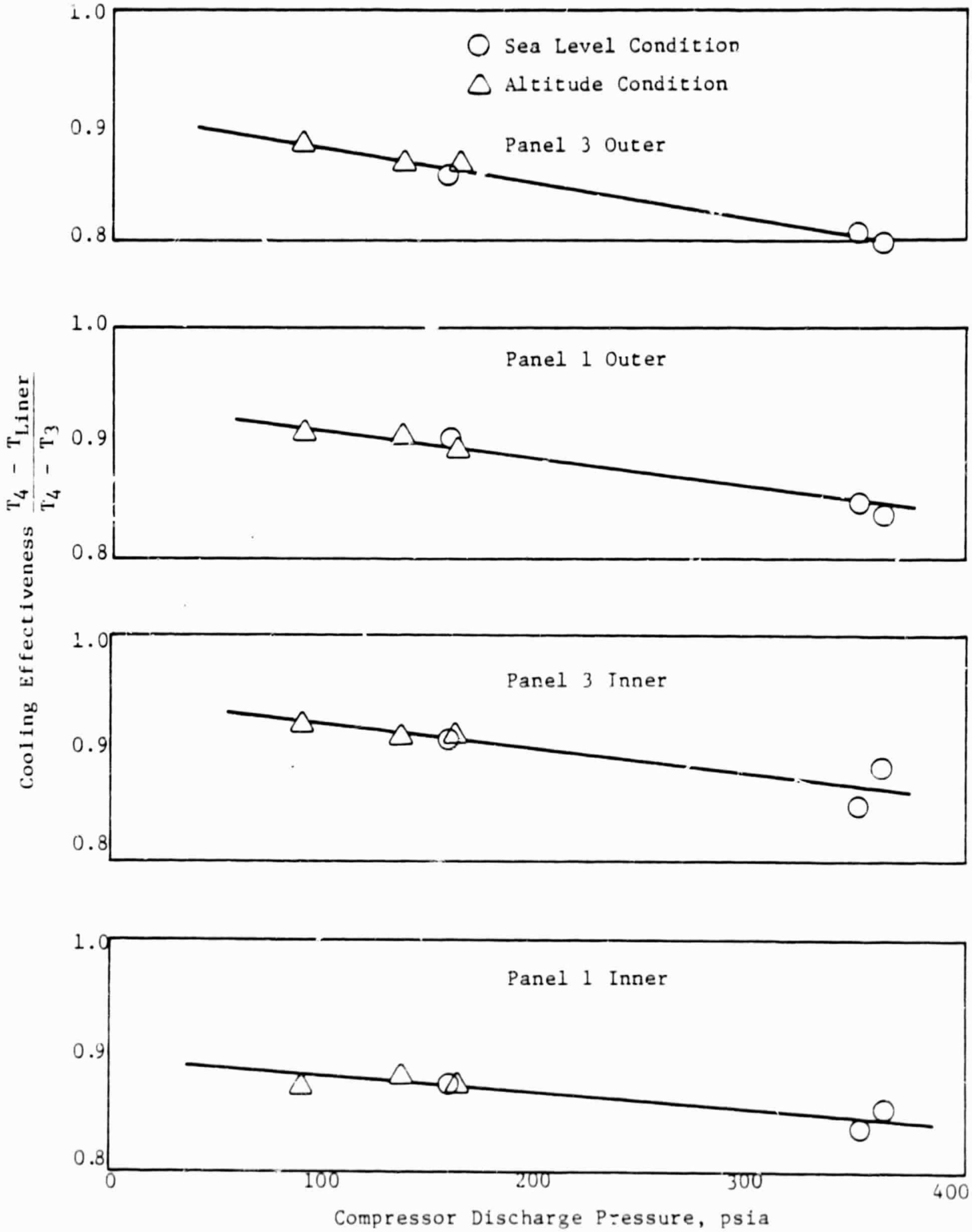

Figure 13. Cooling Effectiveness at Sea Level and Altitude Conditions.

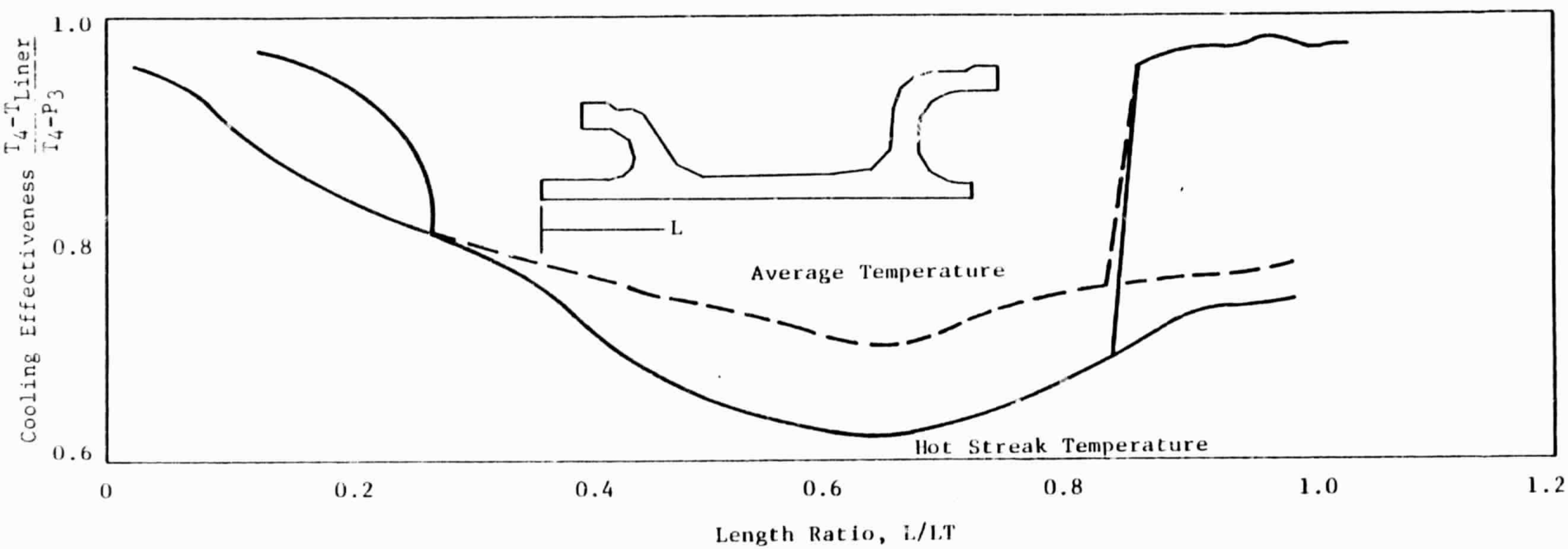

Figure 14. Cooling Effectiveness Distribution, Panel 7 Outer.

Table I. Cooling Effectiveness Coordinates for Panel 7 Outer.

Location	Coordinates, Inch		Cooling Effectiveness	
	X	Y	Hot Streak	Average
Liner	0.034	0.03	0.957	0.957
	0.094	0.03	0.925	0.925
	0.158	0.03	0.880	0.880
	0.208	0.03	0.849	0.849
	0.254	0.03	0.832	0.832
	0.288	0.03	0.819	0.819
	0.340	0.03	0.798	0.802
	0.404	0.03	0.773	0.788
	0.438	0.03	0.706	0.760
	0.584	0.04	0.659	0.739
	0.654	0.04	0.632	0.722
	0.764	0.04	0.623	0.708
	0.854	0.04	0.645	0.739
	0.934	0.044	0.677	0.750
	1.04	0.044	0.713	0.760
	1.074	0.04	0.735	0.767
	1.114	0.03	0.740	0.774
	1.150	0.03	0.744	0.777
Forward Cooling Ring	0.144	0.250	0.968	0.968
	0.194	0.240	0.952	0.952
	0.234	0.230	0.945	0.945
	0.248	0.210	0.933	0.933
	0.284	0.170	0.900	0.900
	0.300	0.124	0.865	0.865
	0.308	0.084	0.838	0.838
Aft Cooling Ring	0.980	0.116	0.791	0.820
	0.984	0.176	0.881	0.890
	0.984	0.234	0.940	0.940
	0.794	0.290	0.956	0.956
	1.024	0.329	0.967	0.967
	1.054	0.34	0.970	0.970
	1.090	0.354	0.973	0.973
	1.124	0.360	0.982	0.982
	1.158	0.366	0.976	0.976
	1.204	0.370	0.944	0.944

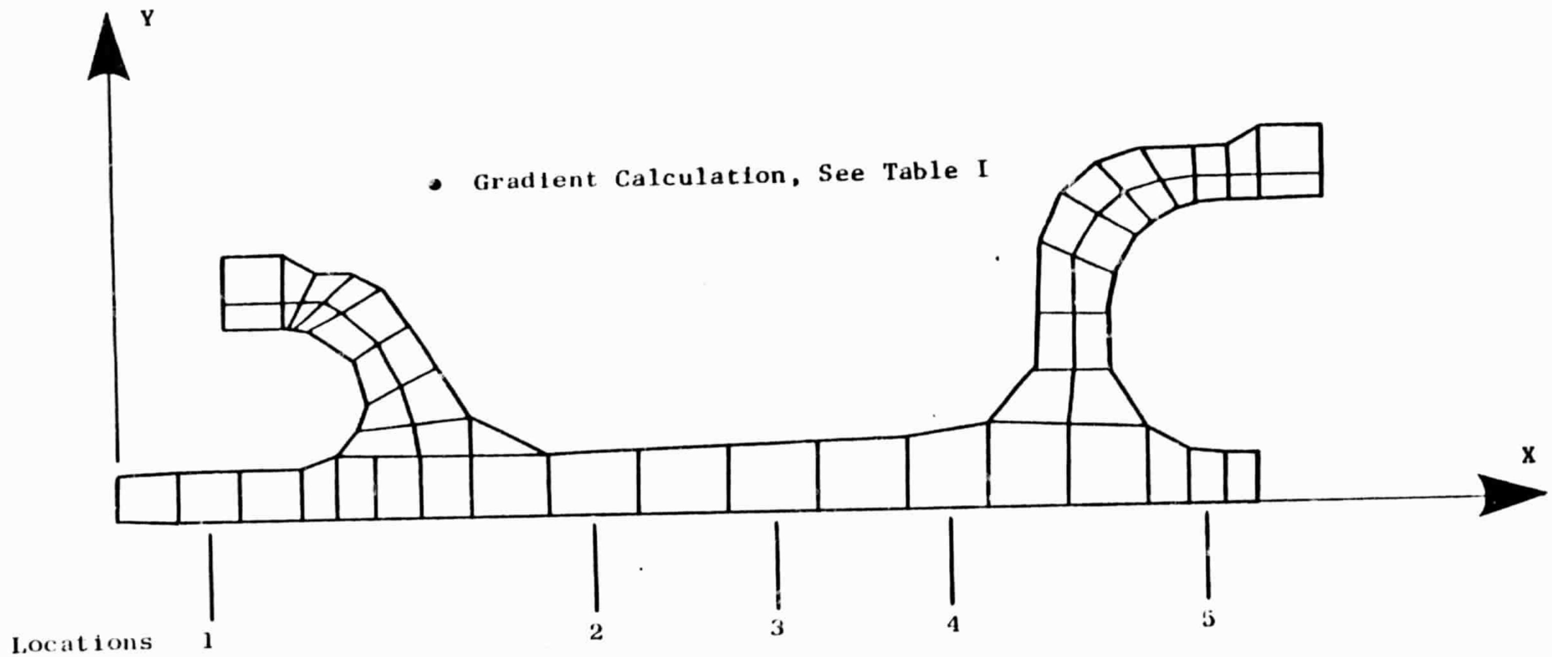

Figure 15. Coordinate System for Cooling Effectiveness.

Q/A = heat flux through material, Btu/hr-ft^2
t = material thickness, ft
k = metal conductivity, Btu-ft/ft^2-hr-° F

The heat flux can be estimated from:

$$Q/A = (h_c + h_r)(T_c - T_3) \quad (3)$$

and is proportional to $(T_{Liner} - T_3)$

$$Q/A \propto (h_c + h_r) T_{Liner} - T_3) \quad (4)$$

where

hc = convection heat transfer coefficient Btu/hr-ft^2-° F
hr = equivalent heat transfer coefficient for radiation to the casing Btu/hr-ft^2-° F

Substituting the heat flux expression into the gradient Equation (2) gives:

$$\frac{T_H - T_c}{T_{Liner} - T_3} \propto \frac{(h_c + h_r)}{k} \quad (5)$$

Using the equation for cooling effectiveness,

$$\eta_c = \frac{T_4 - T_{Liner}}{T_4 - T_3}$$

an equation for $(T_{Liner} - T_3)$ can be written as follows:

$$(T_{Liner} - T_3) = (1 - h_c) T_4 + (h_c - 1) T_3 \quad (7)$$

Substituting Equation (7) into the expression gives (6)

$$\frac{T_H - T_C}{(1 - \eta_c) T_4 + (\eta_c - 1) T_3} \alpha \frac{(\eta_c + \eta_r) T}{k} \quad (8)$$

The convection term η_c varies with pressure; thus, the gradient through the material thickness should be correlated with pressure.

A THTD analysis was done at several pressure conditions and the calculated temperature gradients were plotted versus P_3 for several axial locations. The results are shown in Figure 16. The locations are indicated in Figure 15. As shown in the figure, the gradient data are correlated with pressure. The constants m and b in the equation:

$$\frac{T_H - T_c}{T_{Liner} - T_3} = \frac{T_H - T_c}{(1 - \eta_c) T_4 + (\eta_c - 1) T_3} = mP_3 + b \quad (9)$$

are tabulated in Table II.

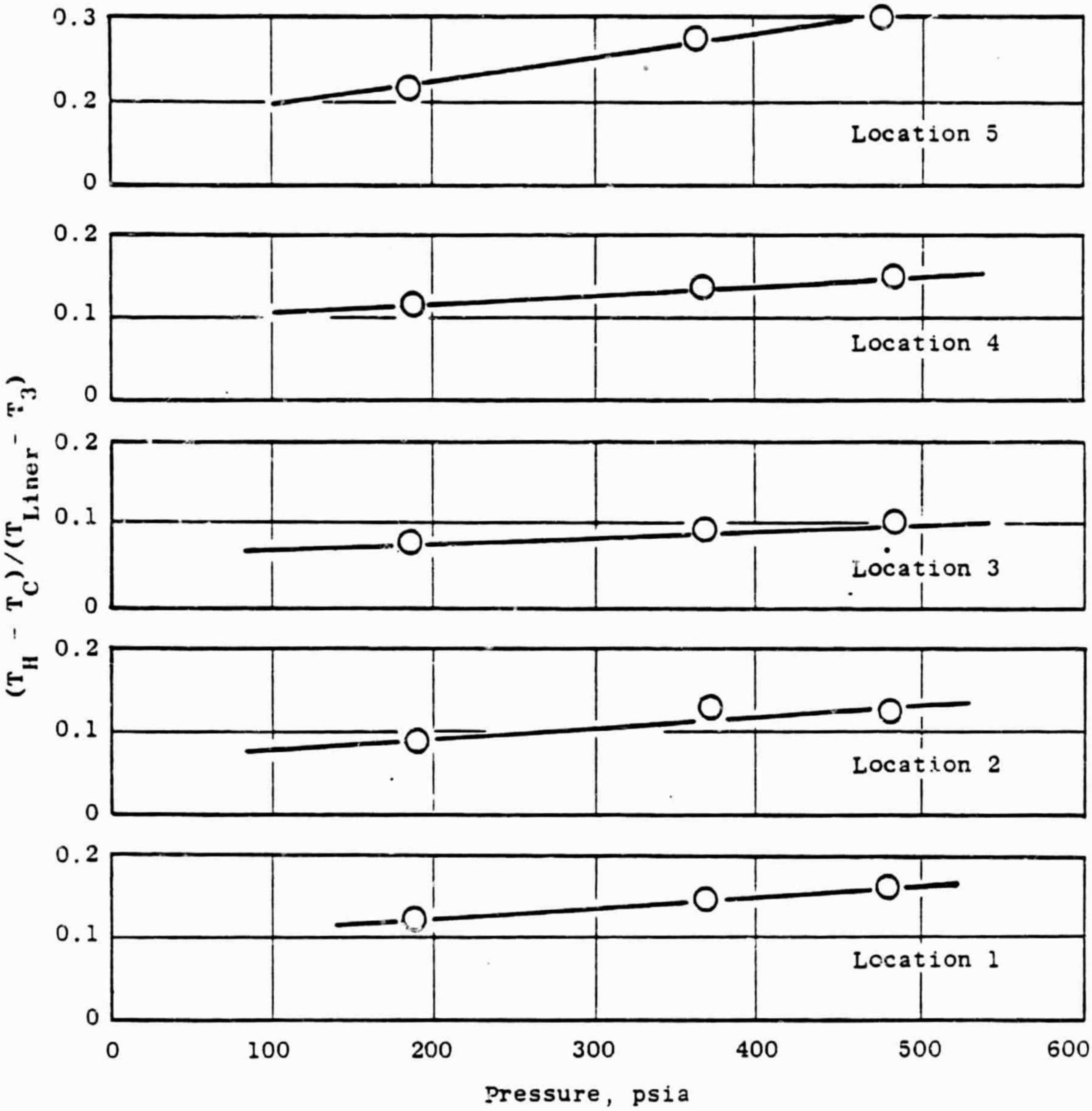

Figure 16. Material Thickness Temperature Gradient.

Table II. Linear Fit Constants for Equation (8).

Location	X, inches	m	b
1	0.094	12.3×10^{-5}	0.100
2	0.438	14.1×10^{-5}	0.061
3	0.654	9.0×10^{-5}	0.061
4	0.854	10.7×10^{-5}	0.092
5	1.114	28.1×10^{-5}	0.168

Given the combustor exit temperature T_4, the compressor discharge pressure P_3, and the compressor discharge temperature T_3, the temperature gradient through material thickness can be calculated from Equation (9) using the cooling effectiveness from Table I and the constants from Table II.

A generalized procedure has been established to predict liner temperature distribution and the temperature drop through the material thickness. The predictions can be made using the above constants and equations and the engine cycle data; that is, the compressor discharge temperature and pressure and the combustor exit temperature.

<u>General Pressure Drop</u>

The pressure drop data from the engine test were reviewed and compared to values predicted by the COBRA (Combustor Analysis) program. The static pressure tap locations are shown in Figure 17 and the comparisons of predicted and measured pressure drop data are shown in Figures 18, 19, and 20 as a function of the combustor flow function squared, $(W_{Comb}/P_{T3})^2\ T_3$. The subscripts shown on the pressure drop curves refer to the static pressure tap locations identified on Figure 17.

In general, the agreement between the measured and predicted values is good except for the values for inner liner. The engine pressure drop to the inner passage is larger than the predicted values for both the forward and aft locations. Data from a full scale, full annular diffuser test were examined and were found to agree with the predicted values. Other data from a combustor test have shown that the forward passage pressures are sensitive to the axial location and that more realistic passage pressures are obtained if the pressure taps are mounted to the casing wall rather than to the combustor cowl or to a film slot as was done in the engine test. If the inner passage measured data are corrected based on the diffuser test data, then the agreement with the COBRA prediction is much better.

The above comparisons indicate that a COBRA analysis can be used to predict the pressure drop across the dome and each of the liners and is related to the square of the combustor flow function by:

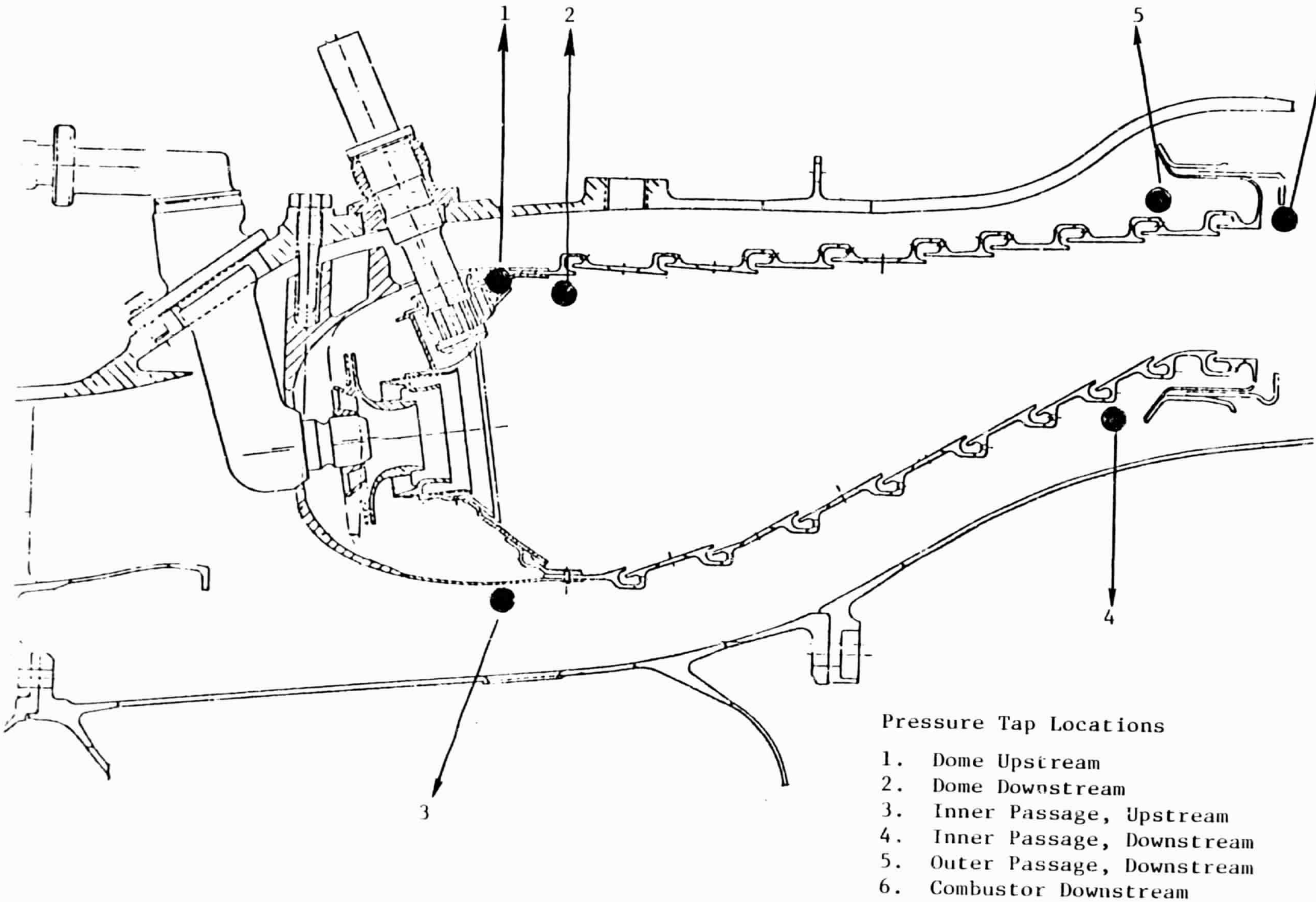

Figure 17. CF6-50 Rolled Ring Combustor.

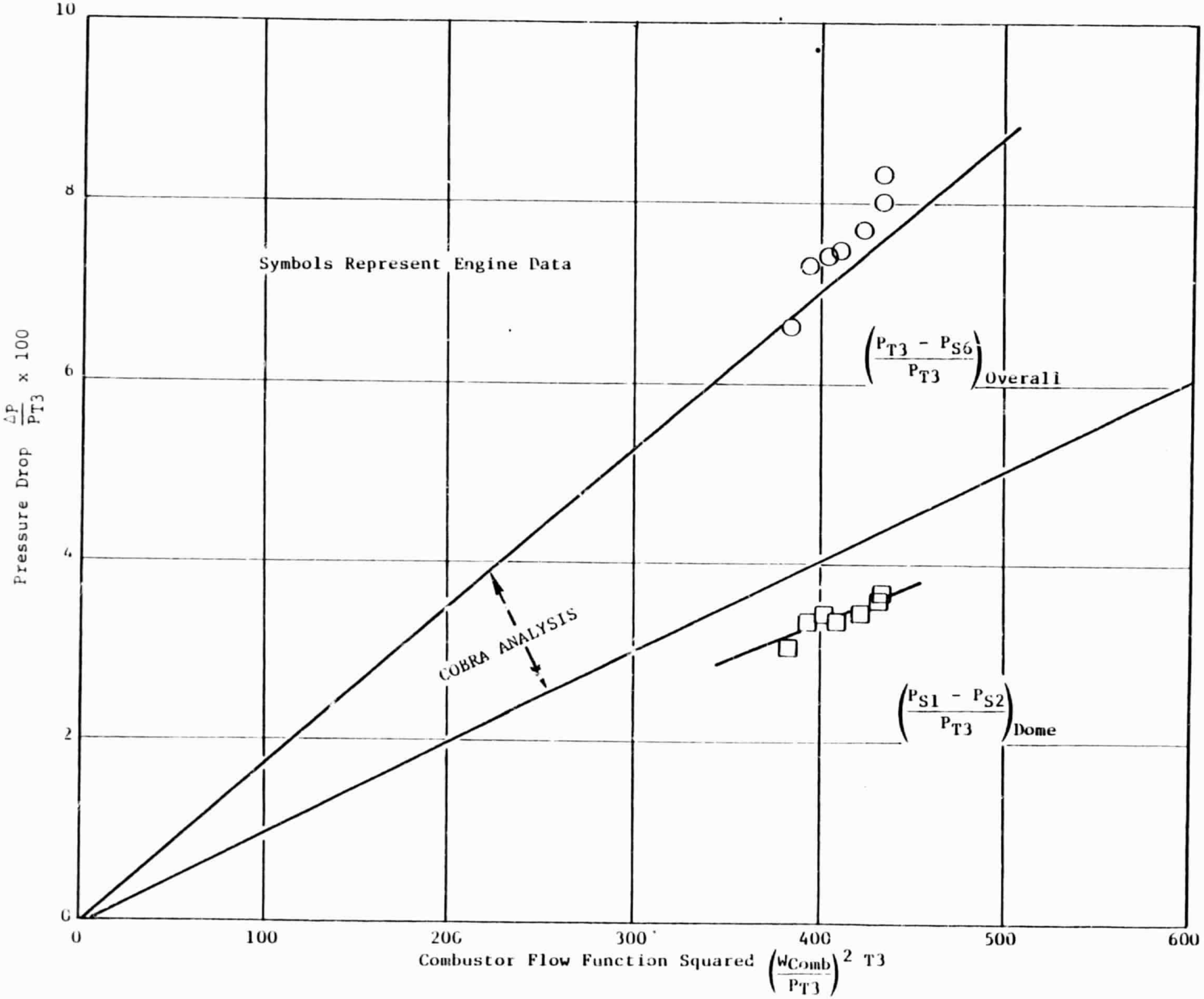

Figure 18. Rolled Ring Combustor Overall and Dome Pressure Drop.

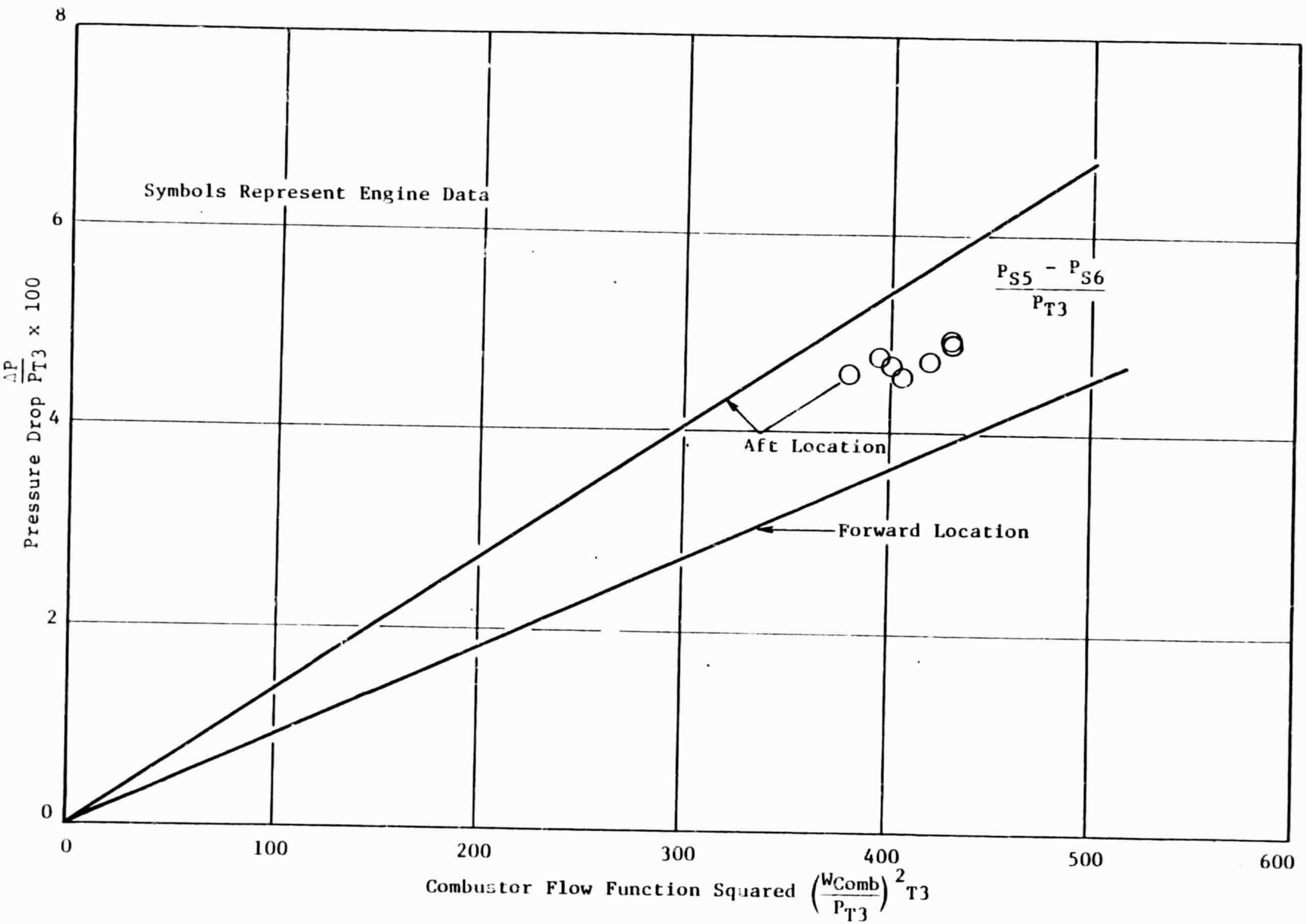

Figure 19. Rolled Ring Combustor Outer Liner Pressure Drop.

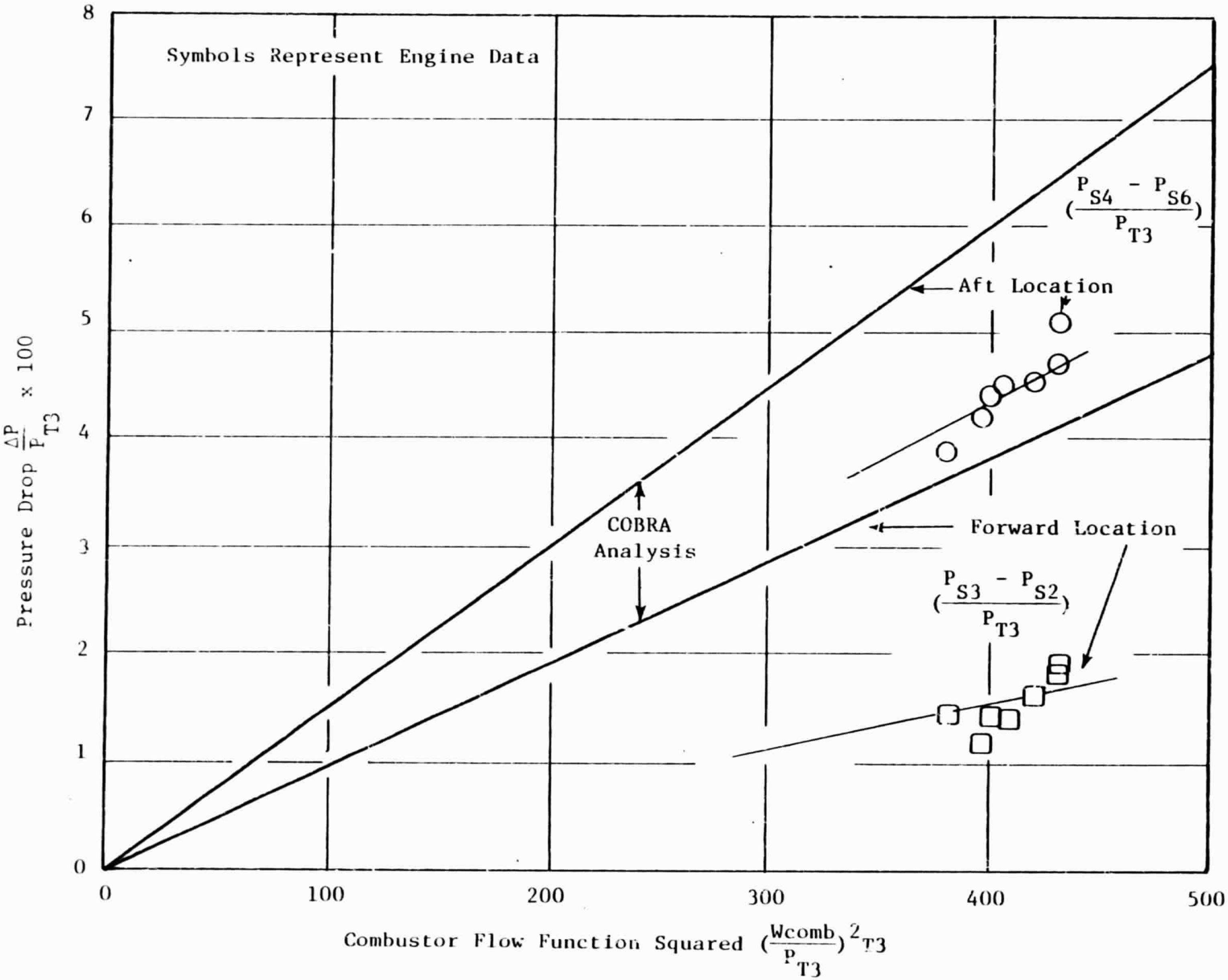

Figure 20. Rolled Ring Combustor Inner Liner Pressure Drop.

$$\frac{\Delta P}{P_3} = K \left(\frac{W_{Comb}}{P_{T3}}\right)^2 T_3 \qquad (10)$$

where K is a constant for each of the various combustor components. The values of K for the locations shown in Figures 18, 19, and 20 are given in Table III.

Table III. Pressure Drop Constants for Equation (10).

Location	K
Dome	10.0×10^{-3}
Outer Liner	
Forward	9.1×10^{-3}
Aft	13.5×10^{-3}
Inner Liner	9.6×10^{-3}
Forward	15.0×10^{-3}
Aft	

Given the combustor flow and the compressor discharge temperature and pressure, the various combustor pressure drops can be calculated.

The above comparisons were based on data obtained at sea level conditions. Additional data were needed at altitude conditions to determine if the sea level prediction curves could be used over the entire flight map. Both sea level and altitude test data are available from a high pressure test of a 60° sector of a rolled ring combustor. The overall pressure drop data are shown in Figure 21. The data from both test conditions correlate together as shown in the figure. Also shown in Figure 21 is the design pressure drop as a function of the sector flow function squared. The COBRA analysis can thus be used to predict the combustor pressure drop and can be applied over the entire flight map.

Summary

Correlations to predict liner temperature, temperature drop through the material thickness, and liner pressure drop have been defined. These correlations use the compressor discharge temperature and pressure as well as the combustor exit temperature to calculate the above values over the entire flight map. The information needed to develop the computer program is summarized below.

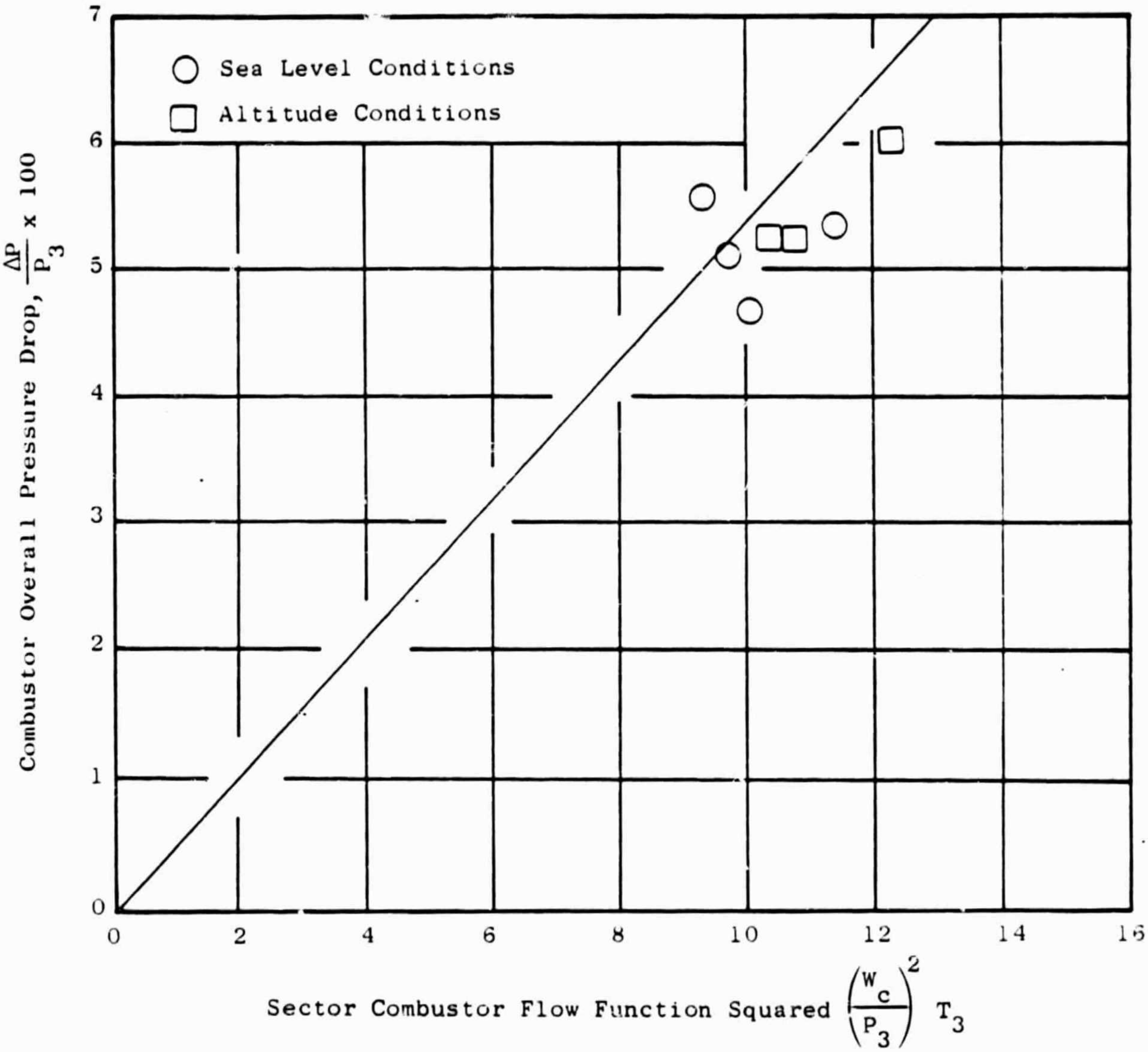

Figure 21. Combustor Pressure Drop.

1. Complete axial temperature distributions are calculated from Equation (1) using the cooling effectiveness values given in Table I.

2. Temperature gradients through the material thickness are calculated from Equation (9) using the values given in Tables I and II.

3. Liner and dome pressure drops are calculated from Equation (10) using the constants in Table III.

2.5.2 Turbine Blade and Vane Temperature and Pressure Decomposition and Synthesis

Our objective was to establish a generalized procedure for predicting the airfoil metal temperature distribution throughout the engine operating power range. Three approaches were initially assessed. They were the following:

1. One-Dimensional Heat Transfer Balance - A generalized one-dimensional heat transfer equation was considered for calculating the metal temperature distribution across the turbine vane or blade. The equation takes the general form

$$\frac{T_g - T_m}{T_g - T_3} = f\,(\text{location, pressure ratio, temperature ratio, gas coolant weight-flow ratio, etc}) \tag{11}$$

2. Predicted Cooling Effectiveness - Use of THTD-predicted design point temperature distributions for vanes or blades to establish the generalized cooling effectiveness equation. These design temperature predictions were collected from CF6-6 and CF6-50 design groups. A total of 20 local temperatures were selected for each vane or blade to establish the local generalized cooling effectivenesses. The airfoil metal temperature could then be calculated by the equation

$$T_m = T_g - \eta_c(T_g - T_3) \tag{12}$$

   where η_c denotes the generalized cooling effectiveness derived from the predicted design temperature distributions, and would be a function of T_g, T_3, and airfoil axial location.

3. Tested Cooling Effectiveness - Similar approach as described in Item 2, but with the cooling effectiveness determined from temperature measured in engine tests rather than predicted values. Measured airfoil temperature data were collected from the CF6 single-shank Stage 1 blade and the Stage 1 vane.

These three approaches in predicting the airfoil metal temperatures distribution were assessed by further detailed studies described below.

Engine test data were collected from two current development engines for the Stage 1 vane and from previous engine tests for the Stage 1 blade. Using the measured temperature along the airfoil surface, T_m, the turbine inlet gas temperature, T_{41}, and the compressor discharge temperature, T_3, the cooling effectiveness η_c can be calculated from

$$\eta_c = \frac{T_{41} - T_m}{T_{41} - T_3} \tag{13}$$

for each thermocouple location.

Figure 22 shows the thermocouple location along the airfoil surface for the vane and blade. Figure 23 is a plot of the cooling effectiveness η_c defined in Equation (1) and derived from the engine test data for the Stage 1 blade. Beginning at a lower power level and progressing to design power level, the test results furnish a series of data points that defines the trends of η_c throughout the engine operating range. Similar plots for the turbine vanes, as derived from engine test results, are given in Figures 24, 25 and 26 for the vane 15%, 50%, and 85% span. These nearly linear η_c lines derived from test data throughout the power level range were used as one of the three approaches to synthesize turbine vane and blade temperatures at selected locations.

The method using THTD-predicted airfoil metal temperatures from design analysis to establish the generalized cooling effectiveness equation for the vanes and blade is described and summarized in the following. Predicted THTD metal temperature distributions for the Stage 1 vane and blade were obtained from two current development engines. Figures 27 and 28 show the surface metal temperature distribution for the airfoil pitchline at design conditions for the Stage 1 vane and blade respectively. Using the predicted temperature along the airfoil surface T_m, and the turbine inlet gas temperature T_{41}, and the compressor discharge temperature T_3, the generalized cooling effectiveness η_c can be evaluated from Equation (13). These generalized η_c's based on predicted metal temperatures are plotted on Figures 29 and 30 for the Stage 1 vane and blade, respectively, compared with the corresponding η_c deduced from engine test data. As can be seen from these figures, the predicted η (denoted by solid symbols) and the η_c extended from test data (open symbols) have the same relative relationship to each other, but absolute quantities do not match. Similar plots are shown in Figures 31 and 32 for the Stage 1 vane 15% and 85% span respectively. The disagreement between these two η_c's is not surprising, and the reasons are thought to be as follows:

- Predicted metal temperatures are based on nominal values of design variables such as T_{gas}, $T_{coolant}$, manufacturing tolerances, and thermal properties

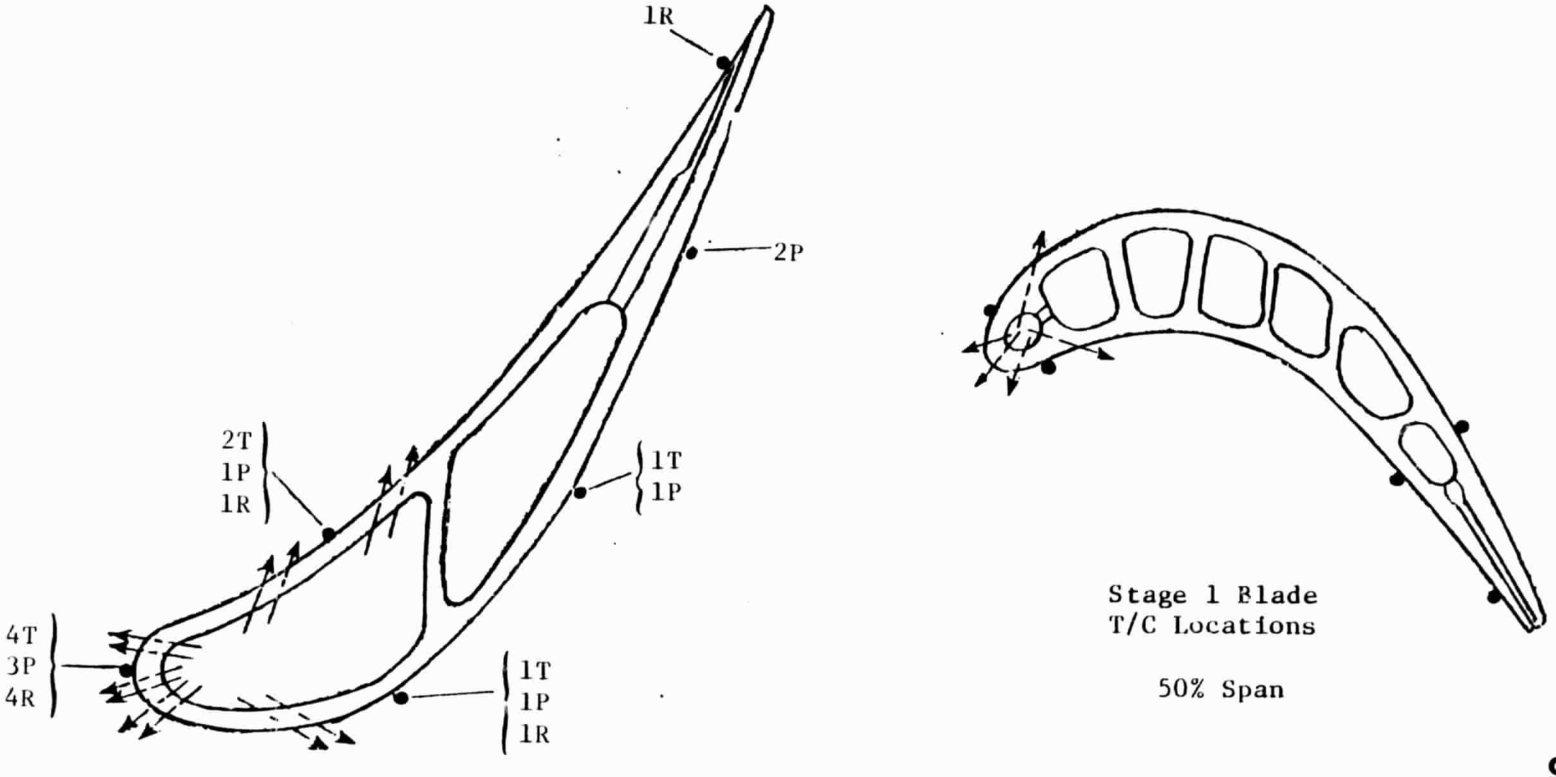

Stage 1 Vane
T/C Locations

T - 85% Span
P - 50% Span
R - 15% Span

Stage 1 Blade
T/C Locations

50% Span

Figure 22. Thermocouple Location for Vane and Blade.

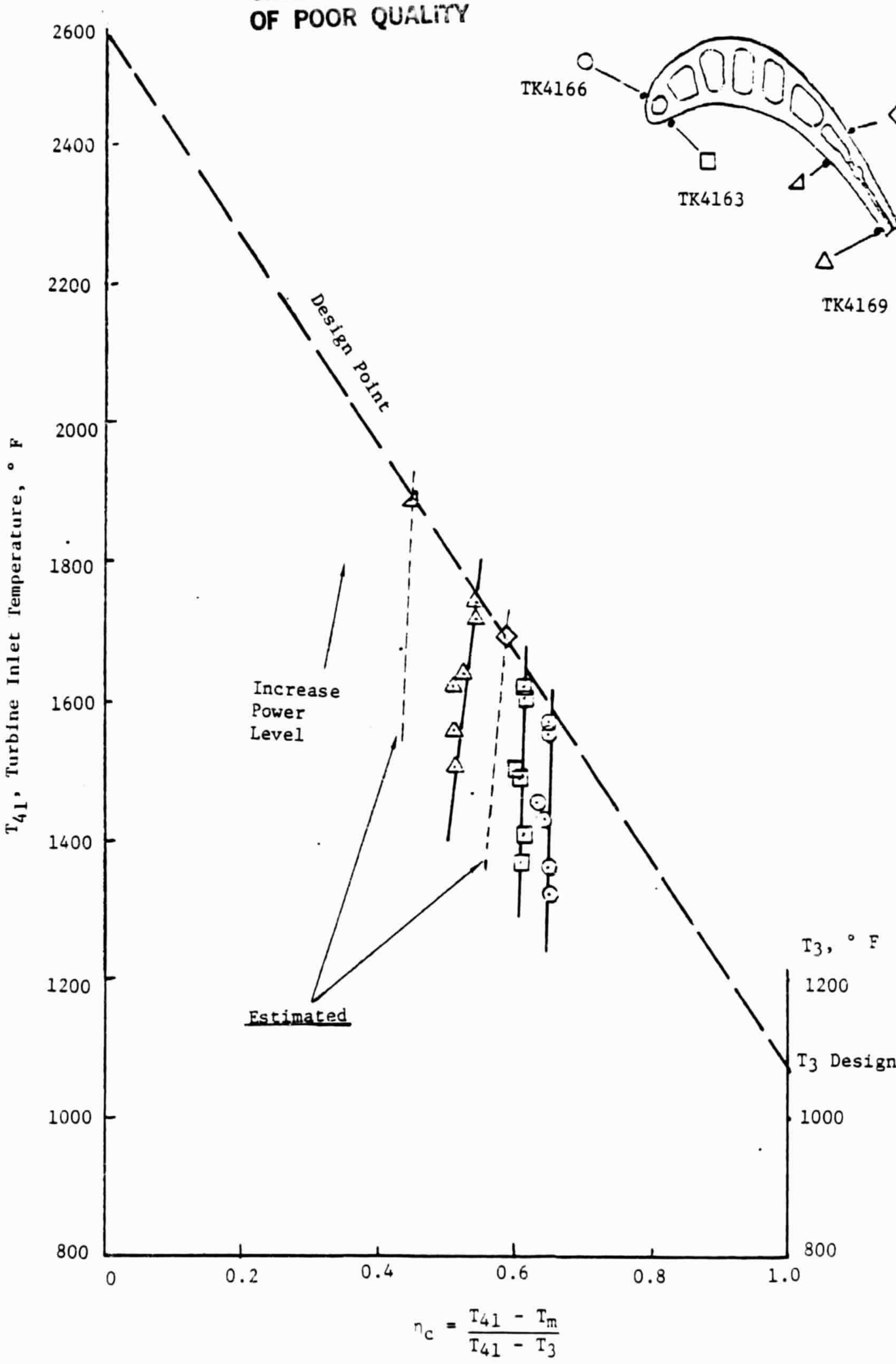

Figure 23. Field Plot of Generalized Turbine Blade Cooling Effectiveness.

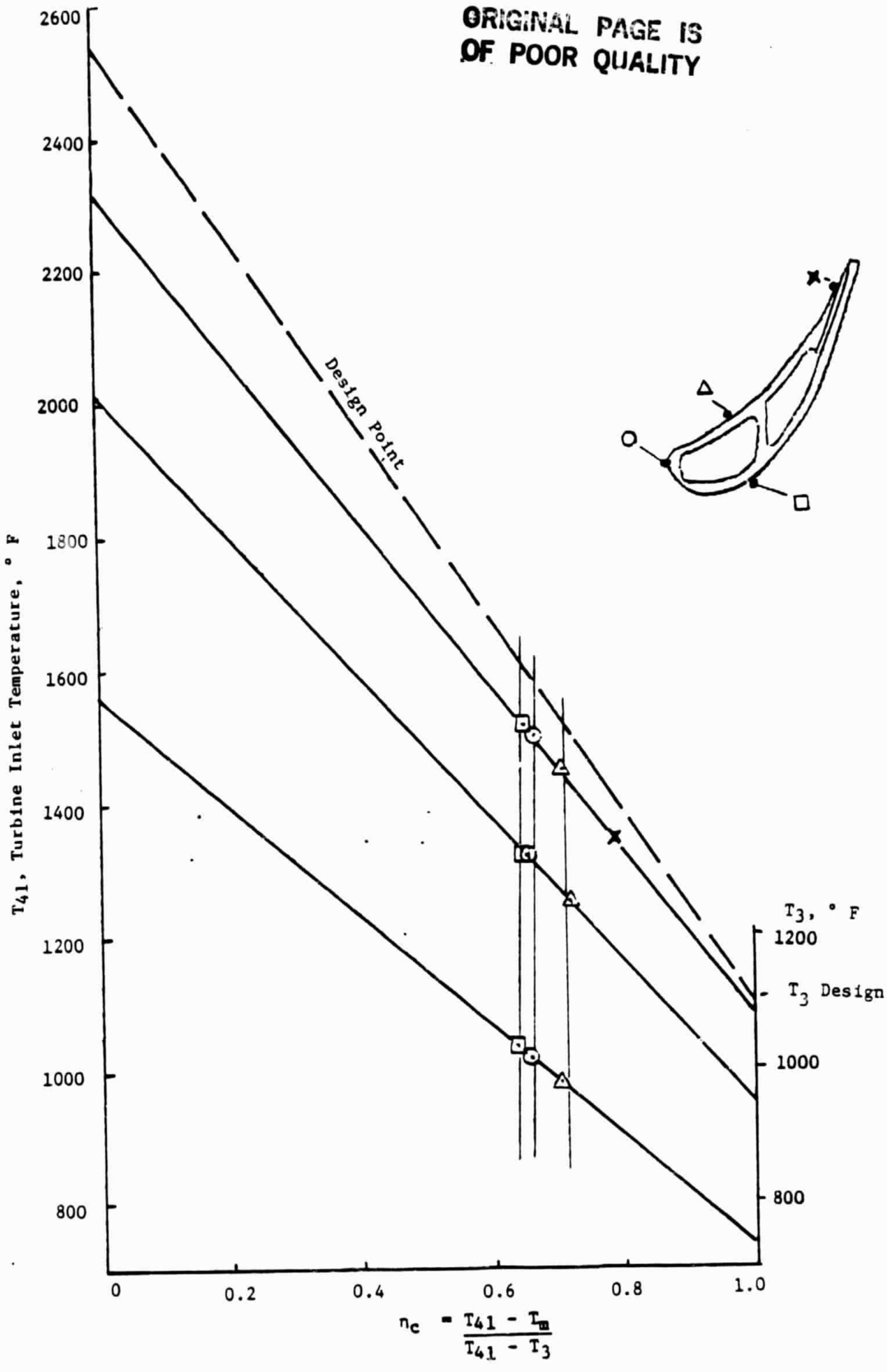

Figure 24. Field Plot of Generalized Turbine Blade Cooling Effectiveness at 15% Span.

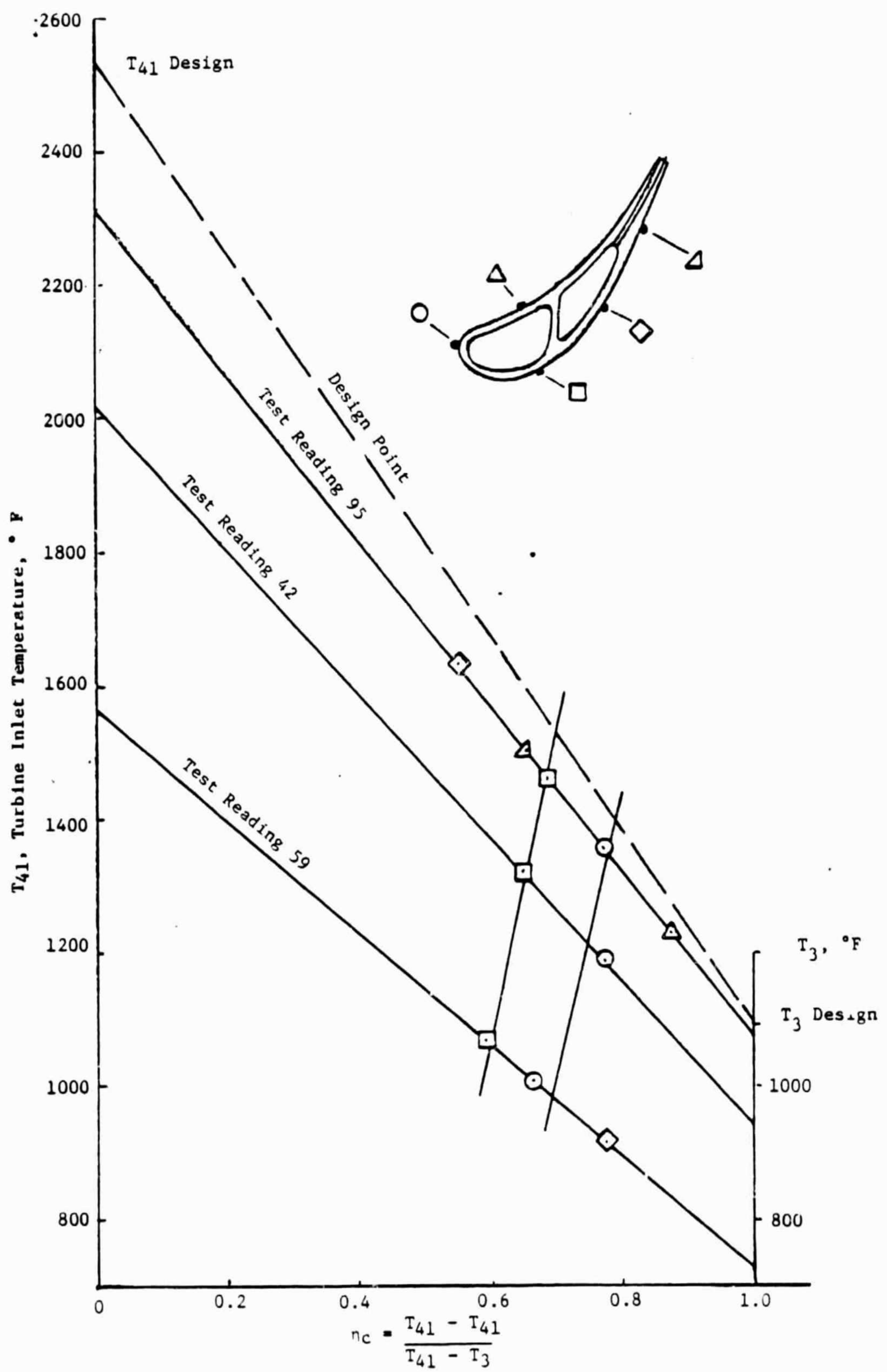

Figure 25. Field Plot of Generalized Turbine Vane Cooling Effectiveness at 50% Span.

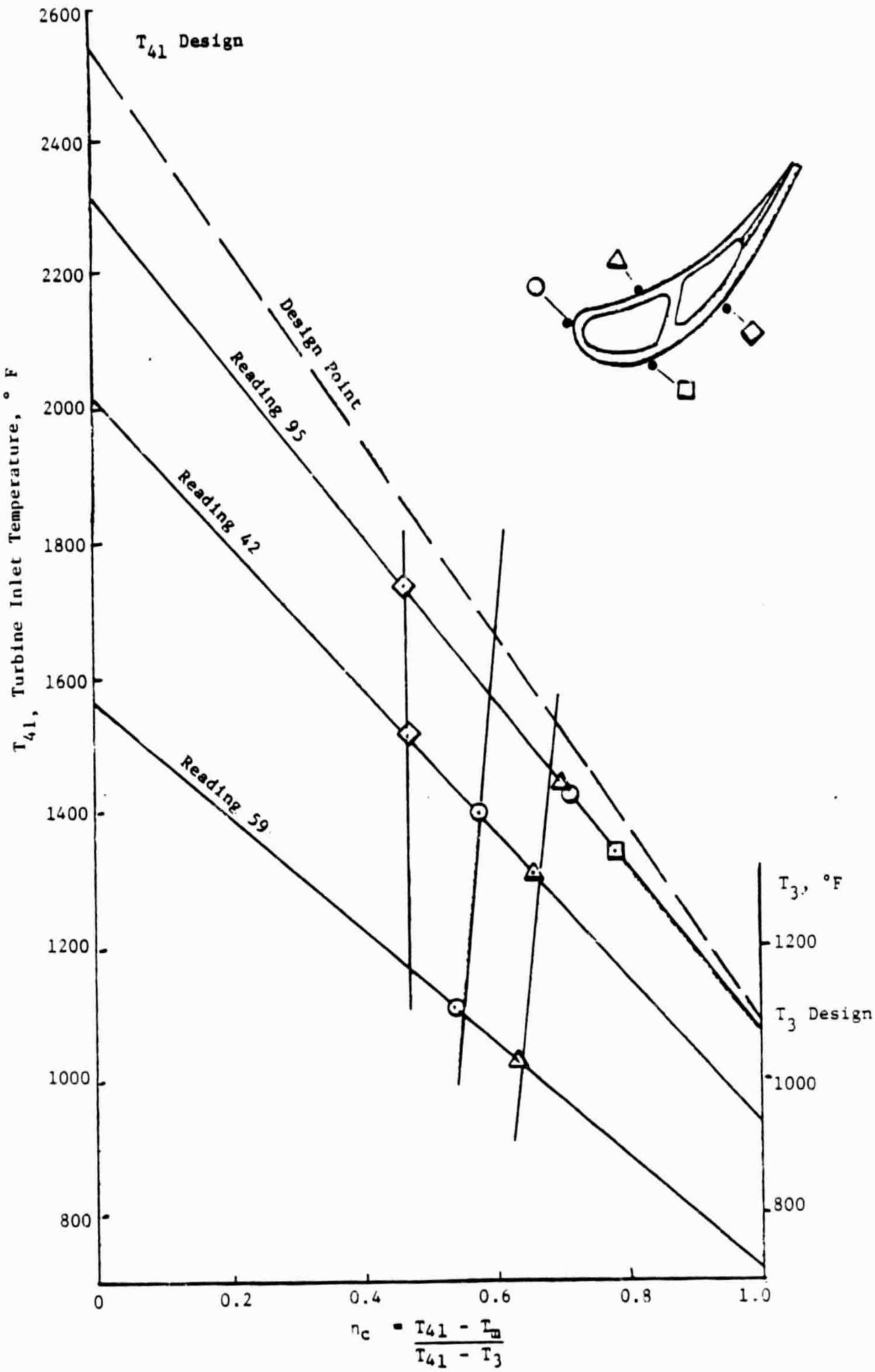

Figure 26. Field Plot of Generalized Turbine Vane Cooling Effectiveness at 85% Span.

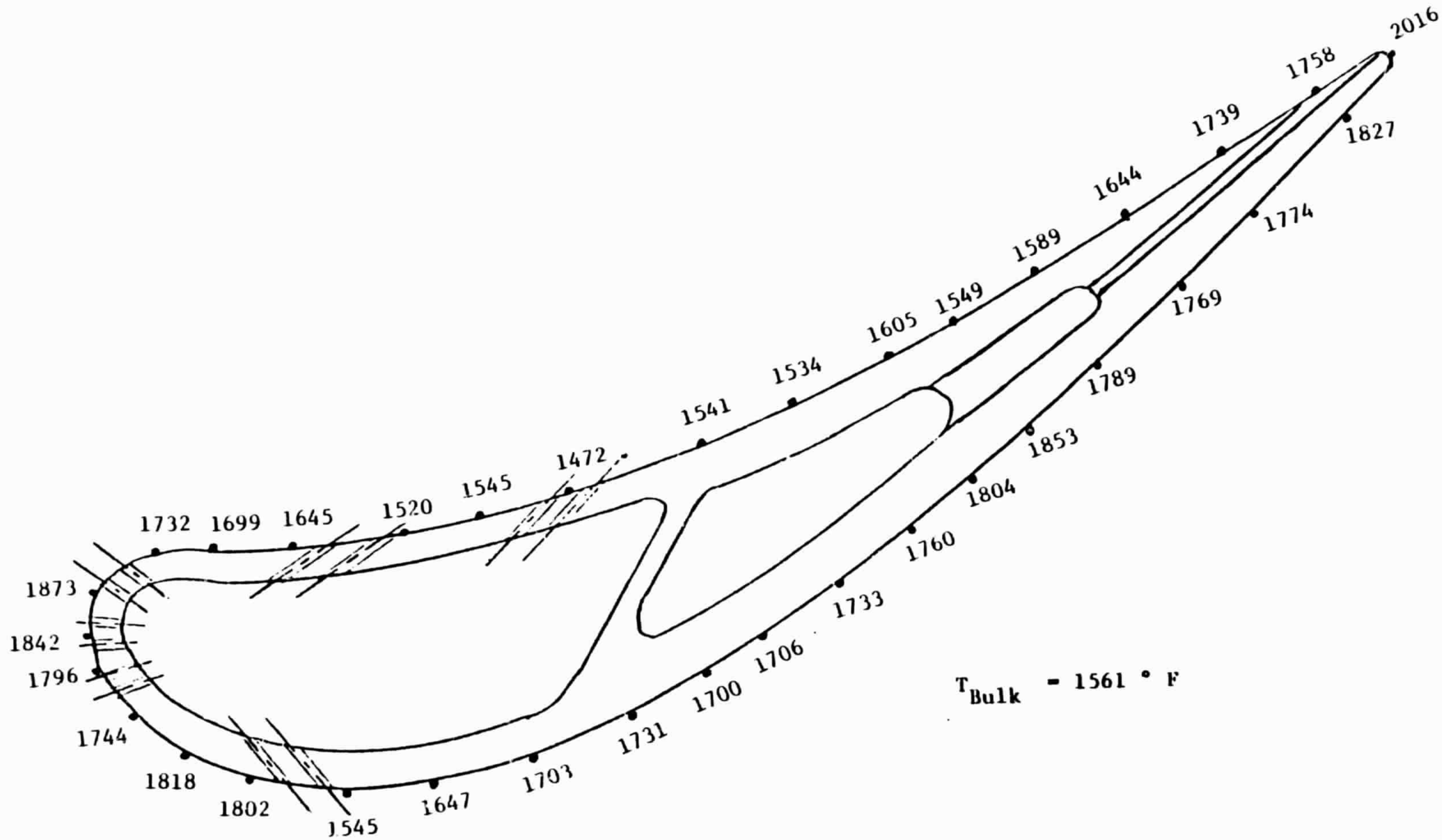

Figure 27. HPT Vane THTD-Predicted Surface Metal Temperatures (° F) Pitch Line at Design-Point Conditions.

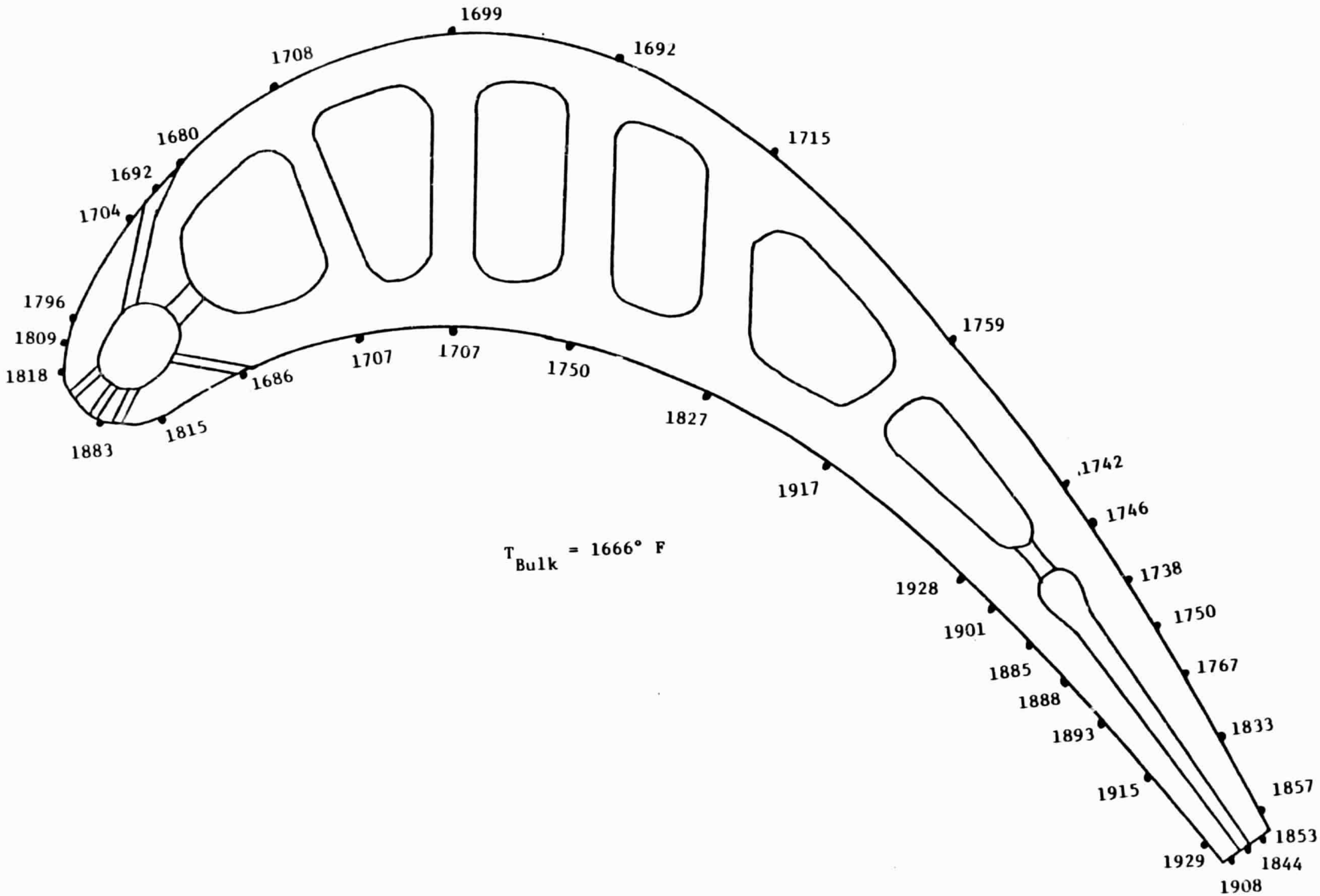

Figure 28. HPT Single-Shank Blade Pitch Line at Design Conditions, THTD-Predicted Surface Metal Temperatures (° F).

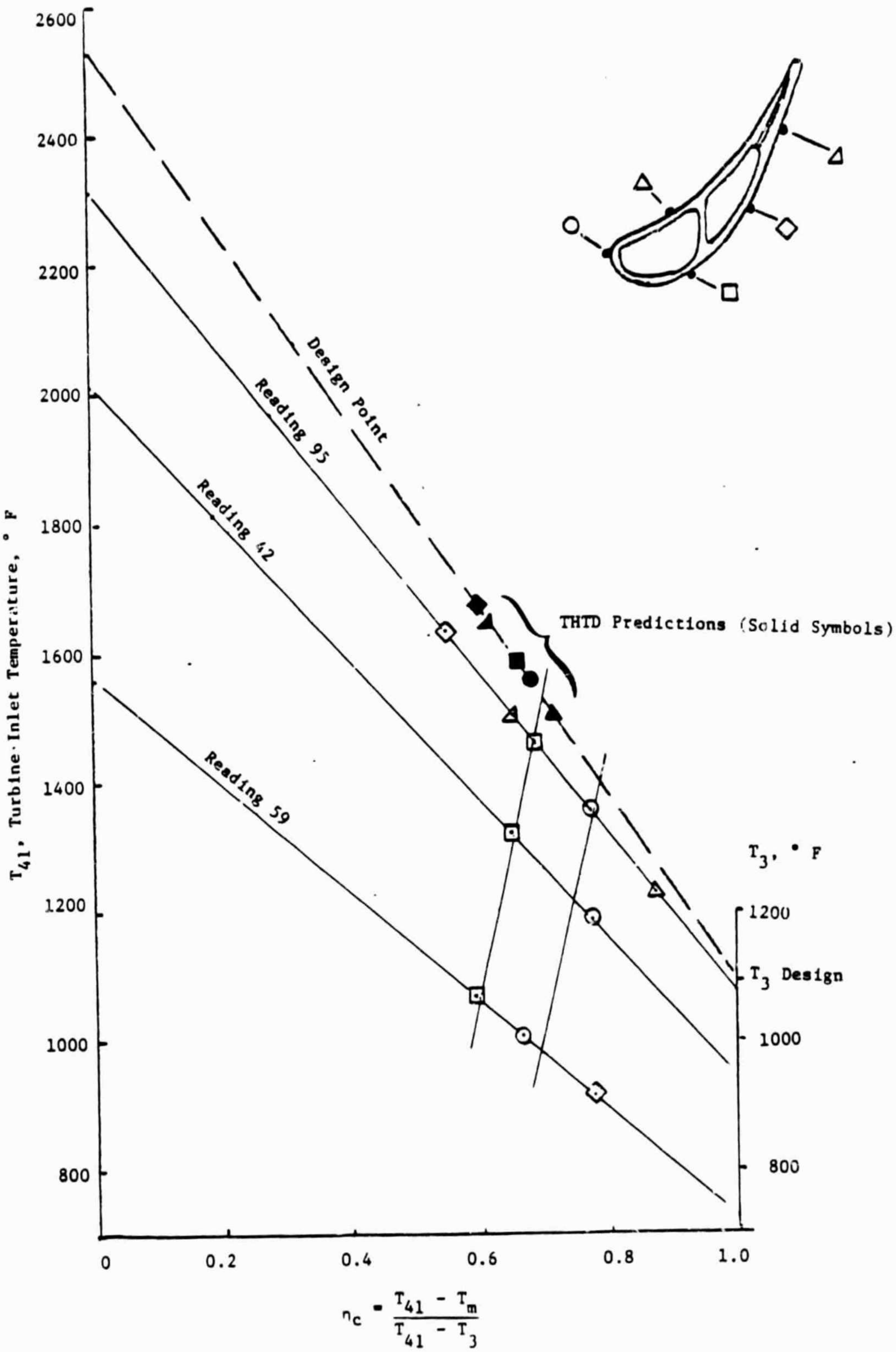

Figure 29. Stage 1 Vane Test Results at 50% Span.

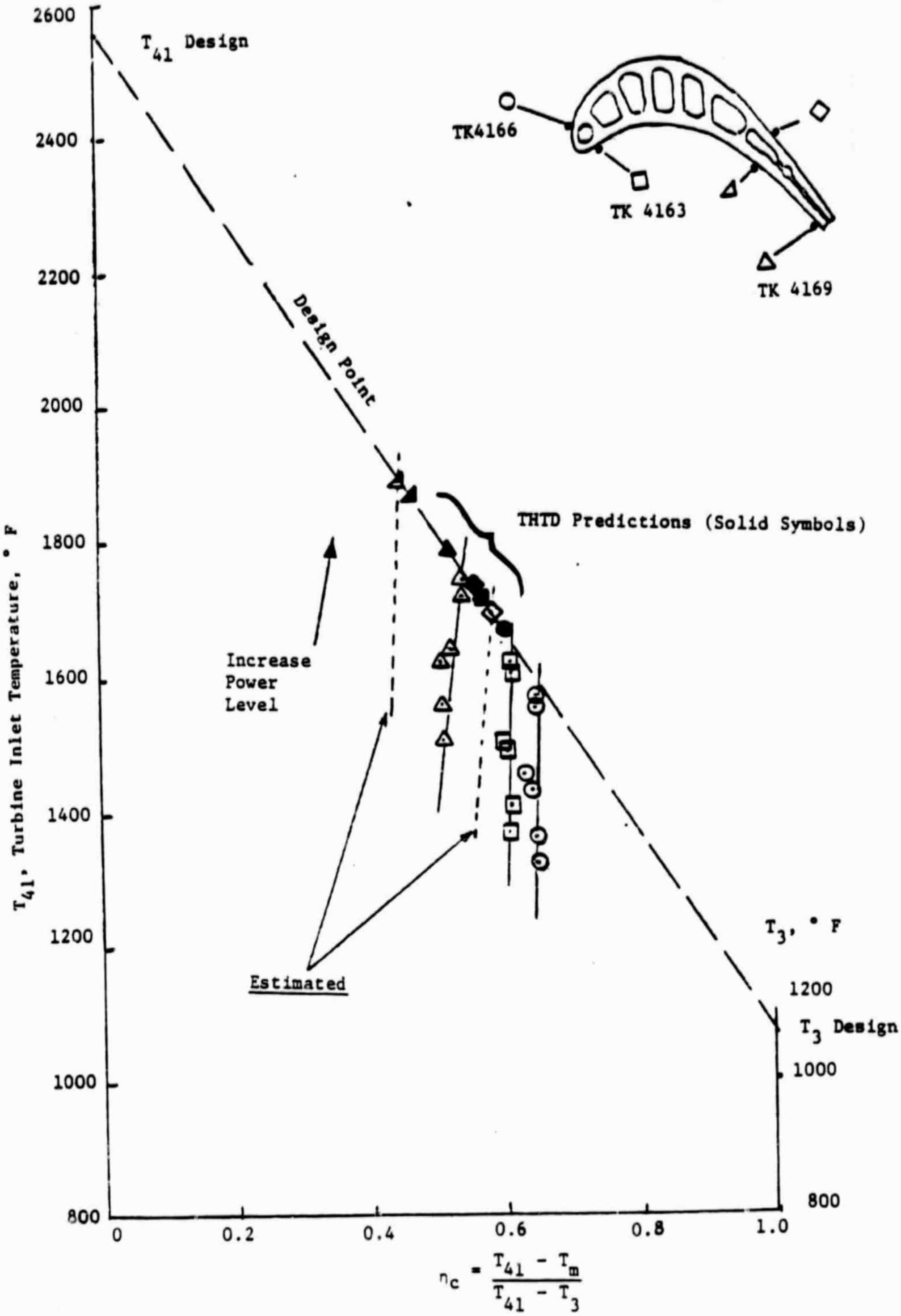

Figure 30. Stage 1 Blade Test Results.

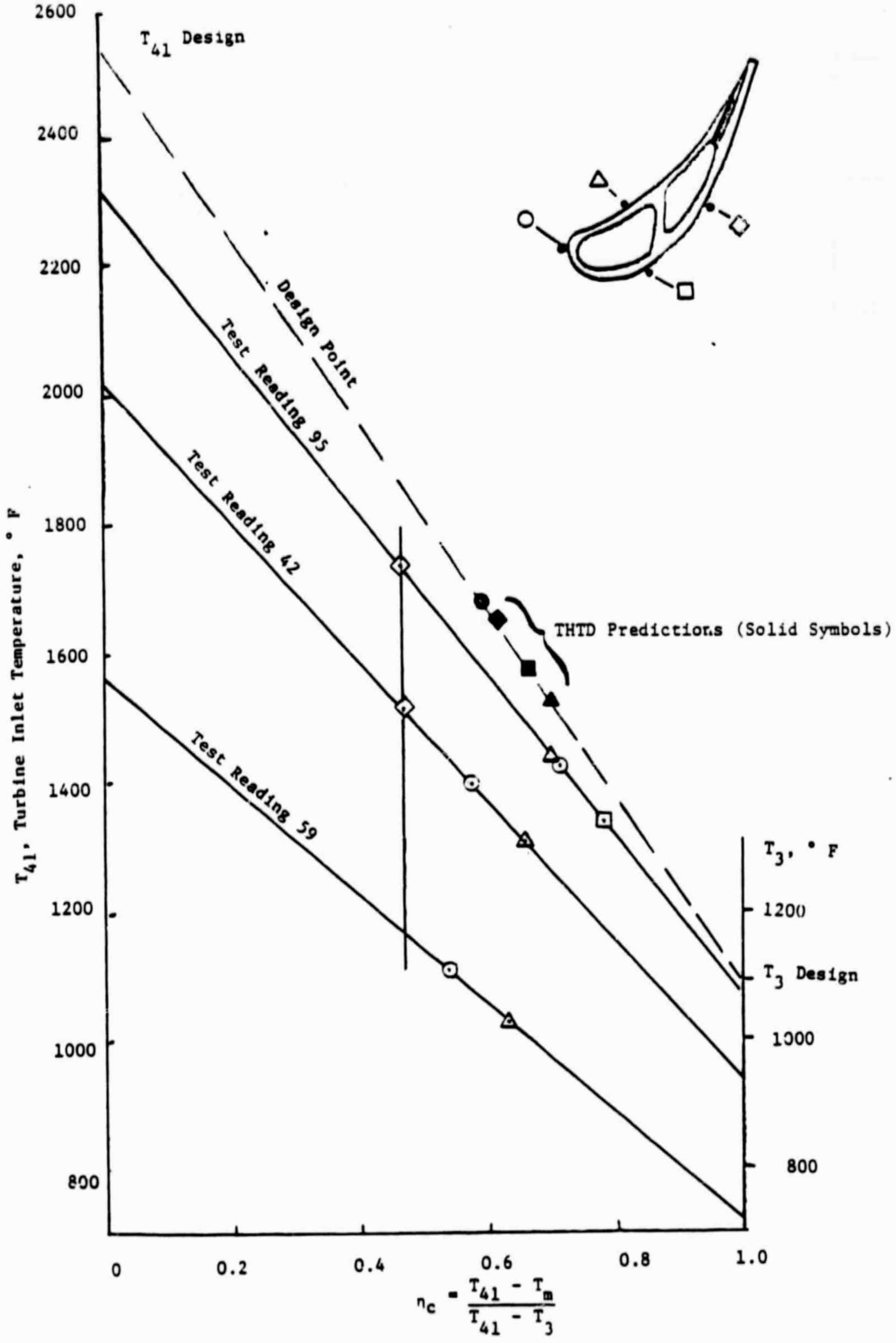

Figure 31. Stage 1 Vane Test Results at 15% Span.

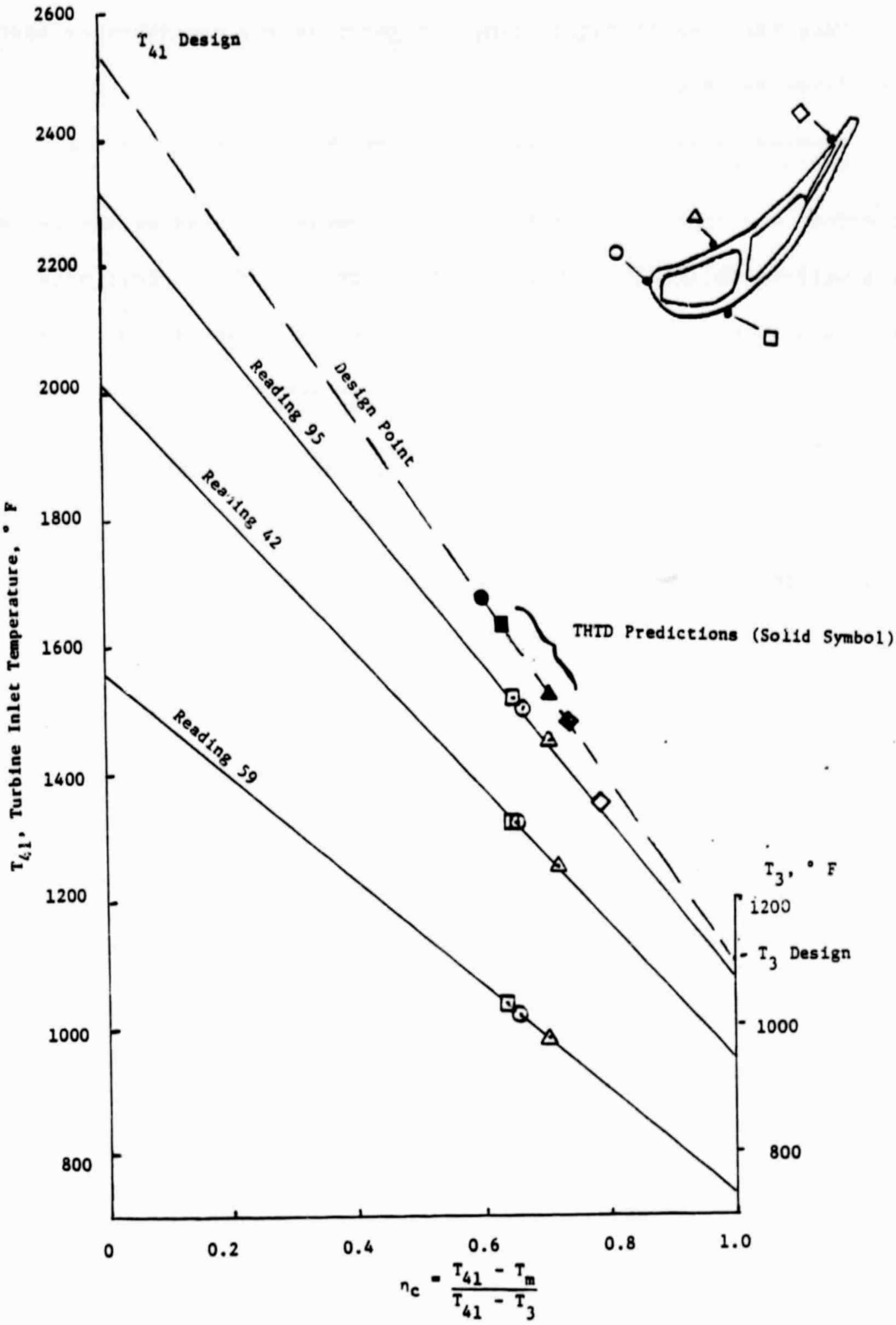

Figure 32. Stage 1 Vane Test Results at 85% Span.

- Uncertainties in calculating the gas-side and coolant-side heat transfer coefficients, the radiation heat flux, film cooling effectiveness, etc.

- Uncertainities in thermocouple measurements, flow checking measurements, etc.

No effort was spent to investigate these uncertainities or the design variable tolerance or to refine the test data matches for the vane and blade. THTD is a well-established analytical tool to predict the airfoil metal temperatures. Rather, our total effort was used to search the THTD predictions for blades and vanes at engine idle or intermediate power setting conditions.

To establish a general procedure to predict the static gas pressure distributions along the airfoil surface, typical design gas pressure distributions for the engine vane and blade were collected and plotted in Figures 33 and 34 respectively. These pressure distributions were assessed to develop the thermomechanical load model.

The final general procedure for predicting turbine vane and blade metal temperatures and their gas-side static pressure distributions throughout the engine operating range is as follows: local distributions of the generalized cooling effectiveness for the vane and blade are given in Figures 35 and 36, and were obtained from the THTD-predicted metal temperatures reported above. These cooling-effectiveness distributions are plotted against the normalized airfoil surface length S/L, and are shown in Figures 37 and 38. By specifying the engine cycle data T_3 and T_{41} and the airfoil suction and pressure-side surface lengths, the airfoil surface metal temperature distribution can be gotten from Figures 37 and 38 for the typical turbine vane and blade used in this study.

In a similar fashion, the normalized airfoil pressure distributions for turbine vane and blade are given in Figures 39 and 40. By specifying the engine cycle data (T_4 for the vane, P_{TB} for the blade and airfoil geometry), gas-side static pressure distributions along the airfoil surfaces can be seen in these figures.

The final method to gain a generalized cooling effectiveness from one-dimensional heat balance analysis yields the resulting equation:

$$\frac{\eta_c}{\eta_c^*} = \left(\frac{W_c/W_g}{W_c/W_g}\right)_* \left(\frac{P_T^{\ *}}{P_{Tg}}\right)^{0.2} \left(\frac{T_g}{T_g^*}\right)^{0.1} \left(\frac{K}{K^*}\right) \qquad (14)$$

where the * sign denotes the reference condition such as the THTD design point or the test data point, and

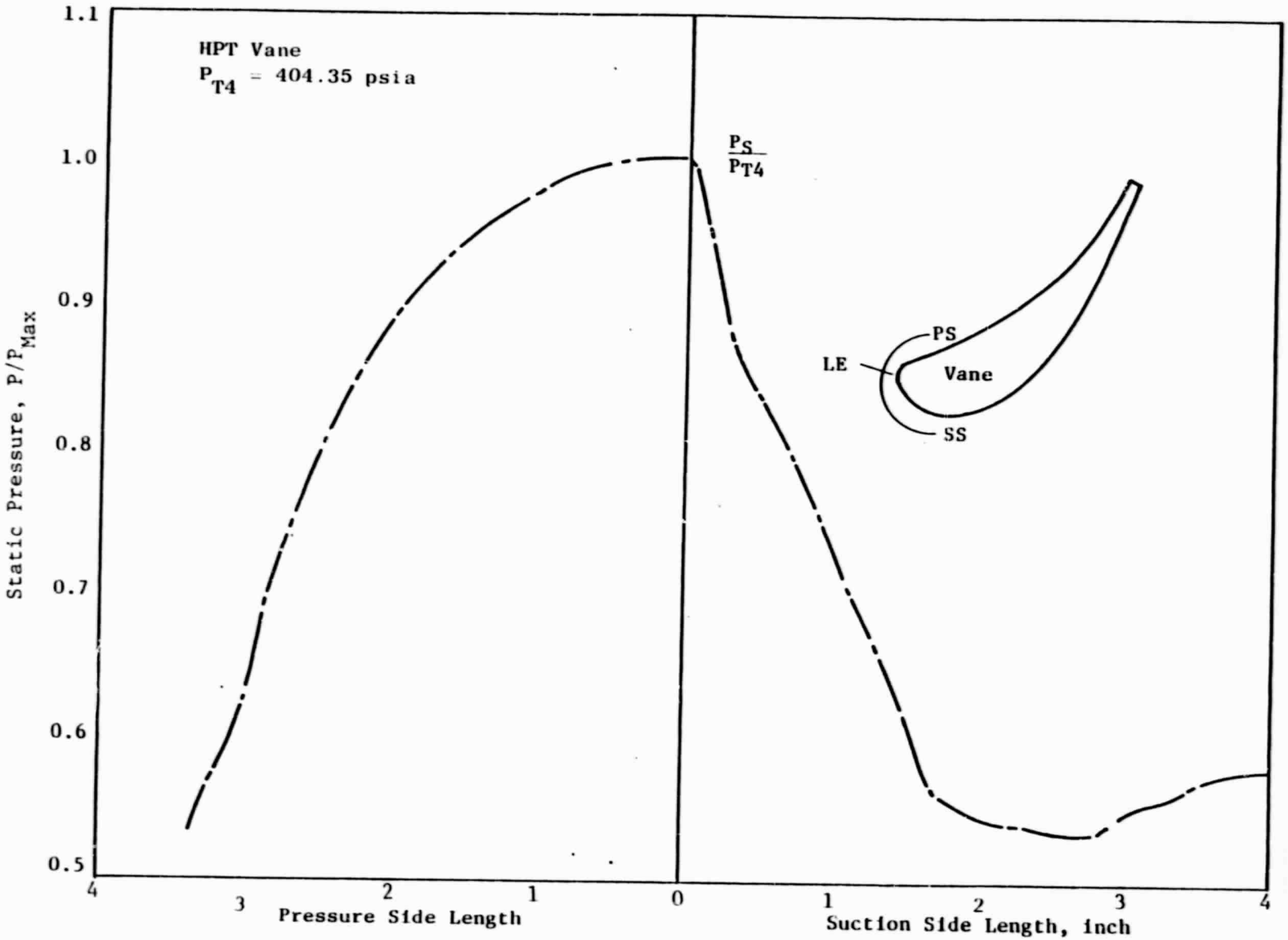

Figure 33. Gas Static Pressure Distribution Along Vane Surface.

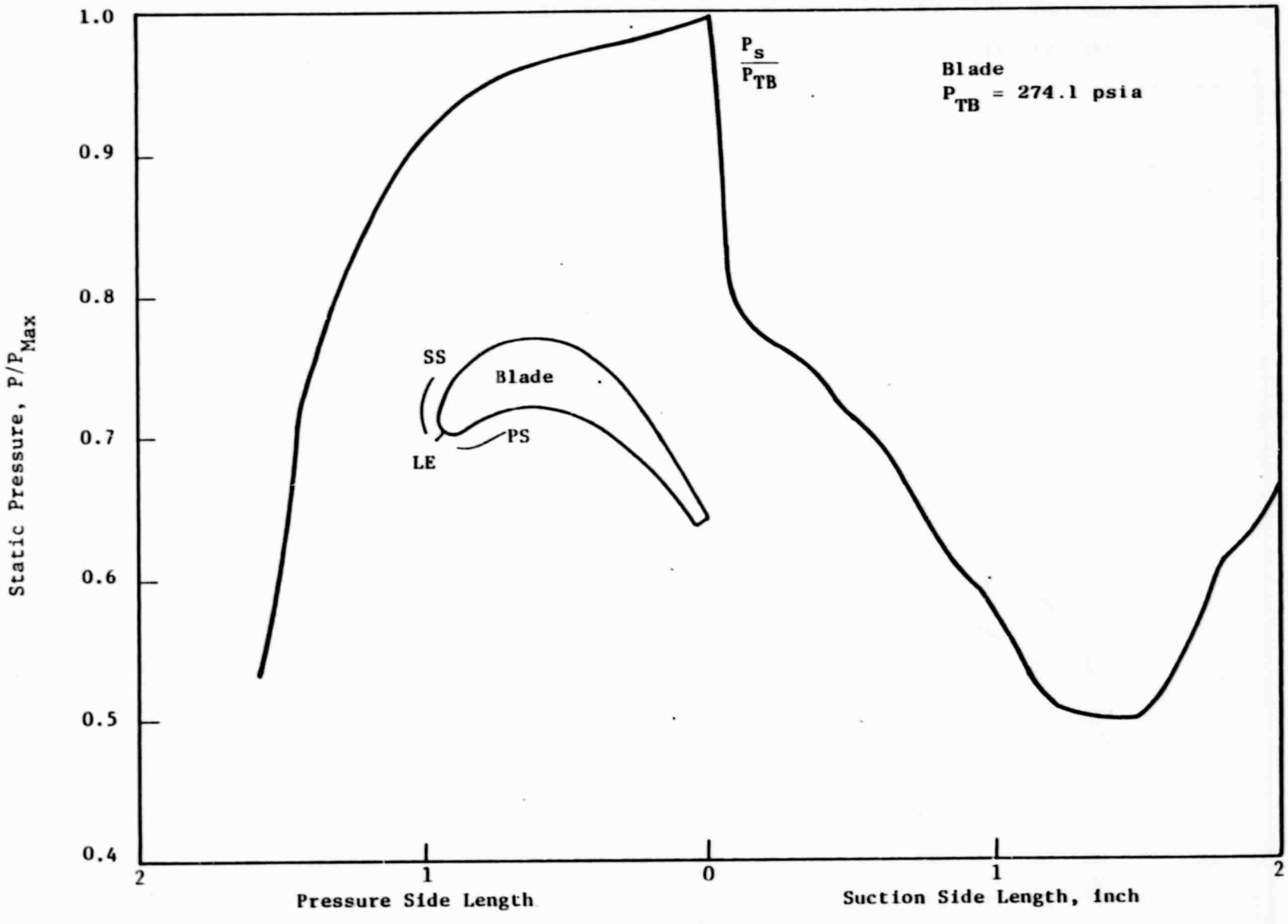

Figure 34. Gas Static Pressure Distribution Along Blade Surface.

η_c, Bulk = 0.592

at Pitch Line

$$\eta_c = \frac{T_{41} - T_m}{T_{41} - T_3}$$

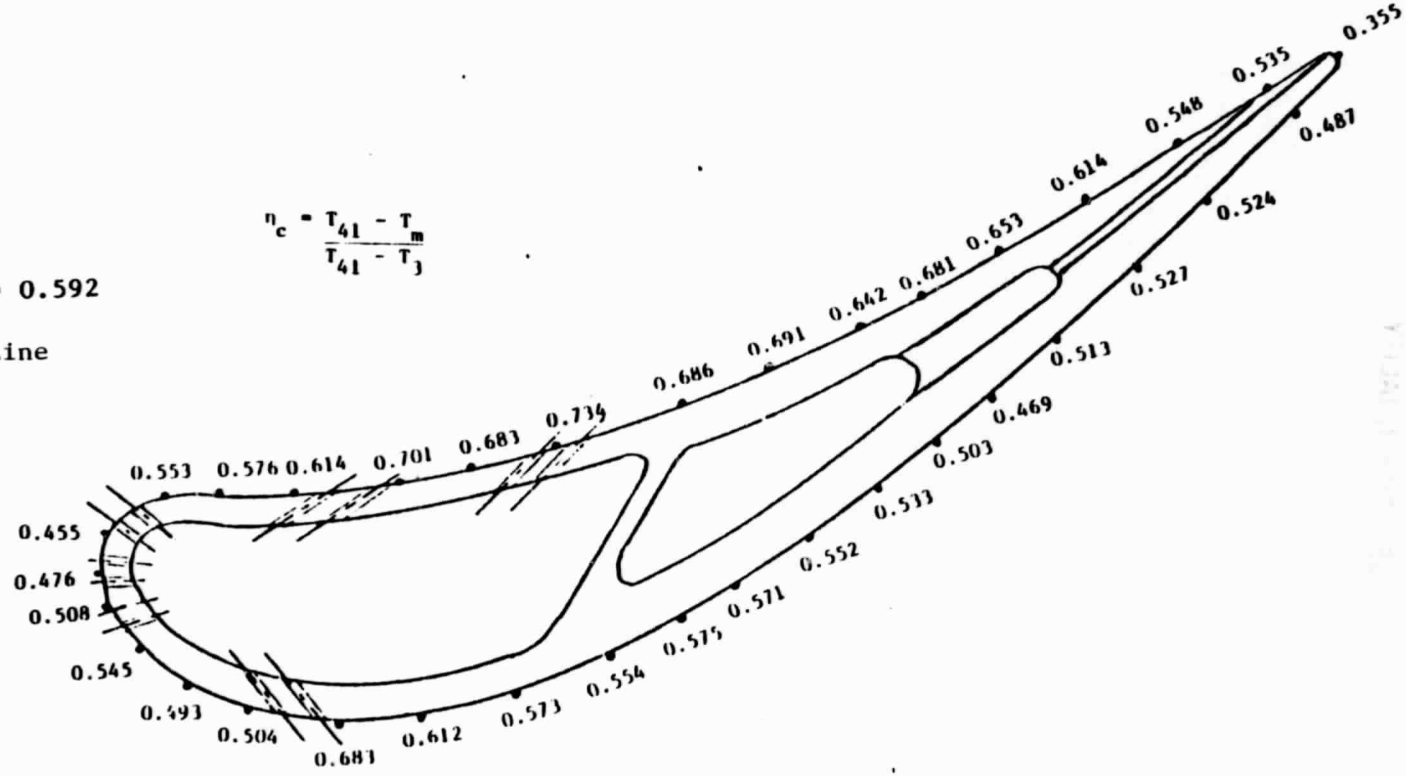

Figure 35. Distribution of Local Generalized Cooling Effectiveness (η_c) for Turbine Vane.

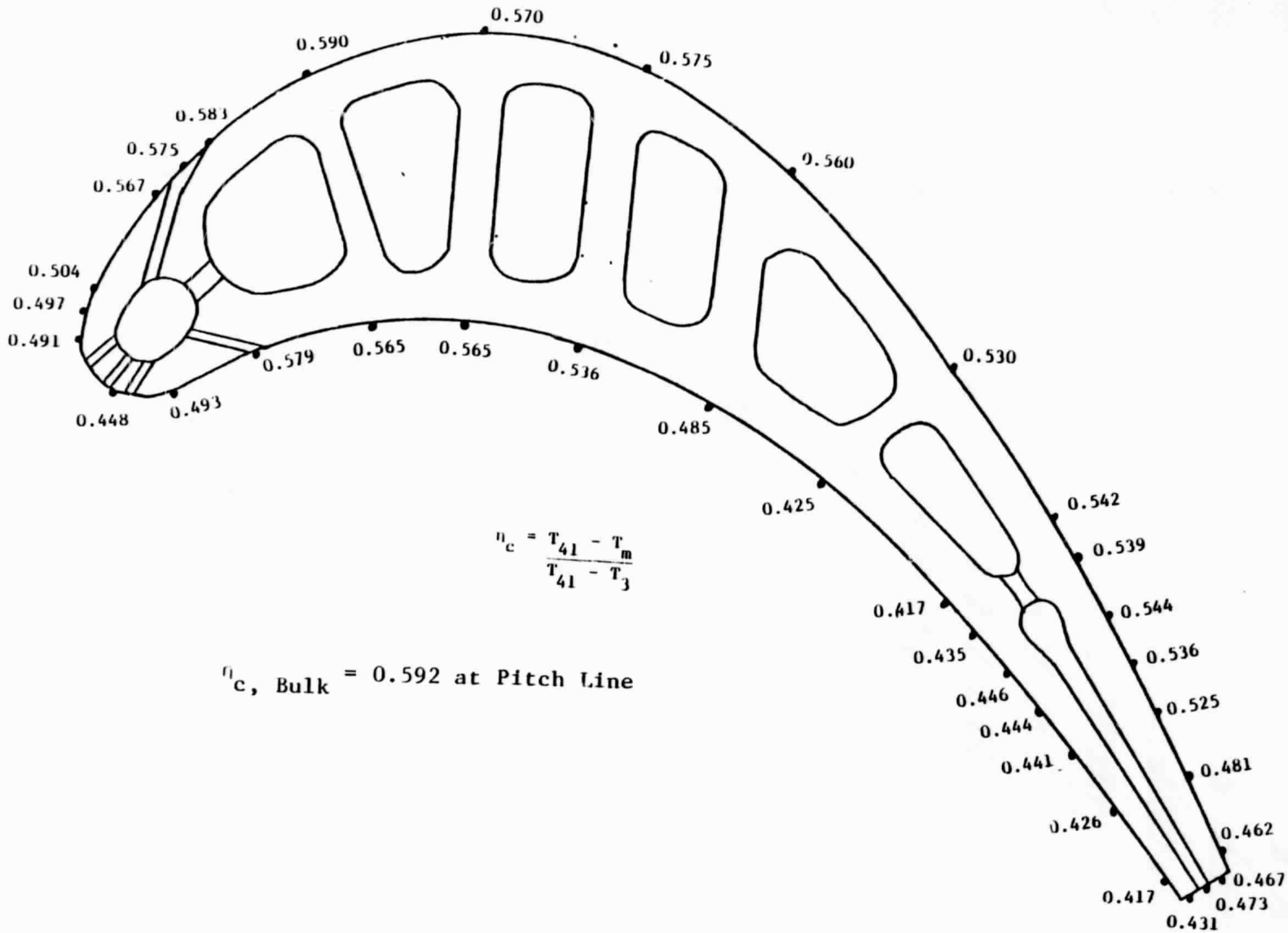

Figure 36. Distribution of Local Generalized Cooling Effectiveness (η_c) for Turbine Blade.

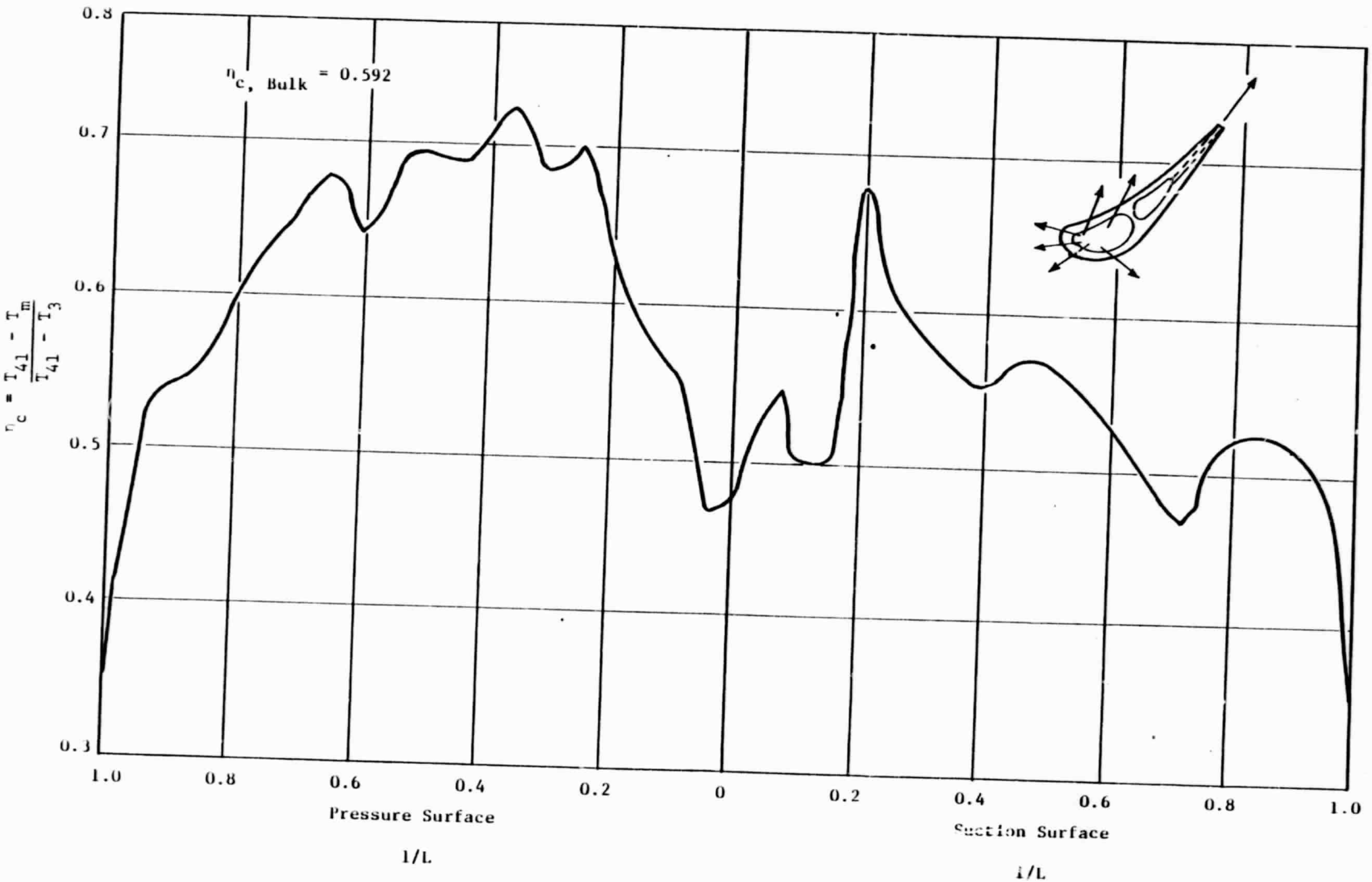

Figure 37. Turbine Vane Normalized Cooling Effectiveness Distribution at Pitch Line.

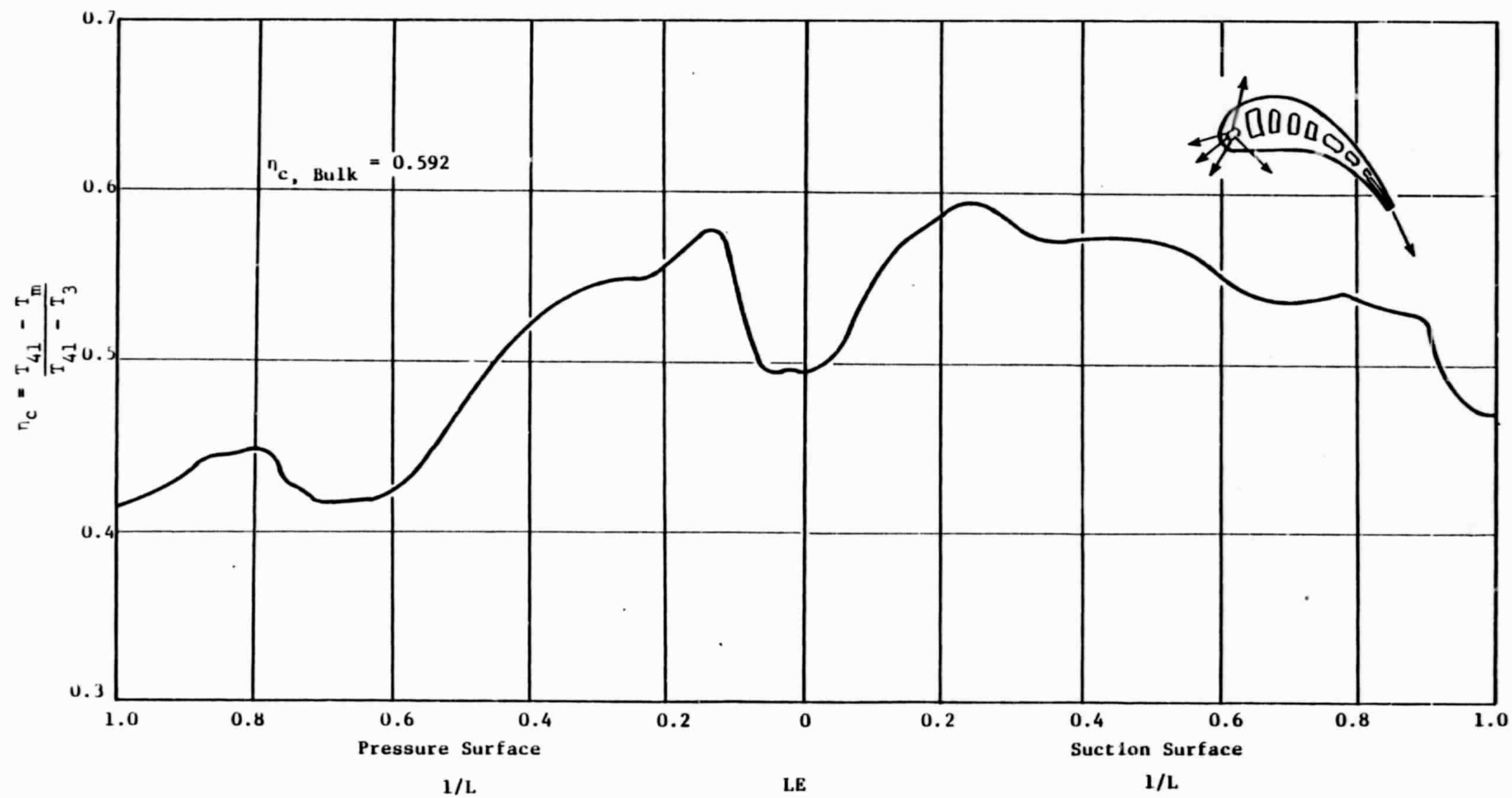

Figure 38. Turbine Blade Normalized Cooling Effectiveness Distribution at Pitch Line.

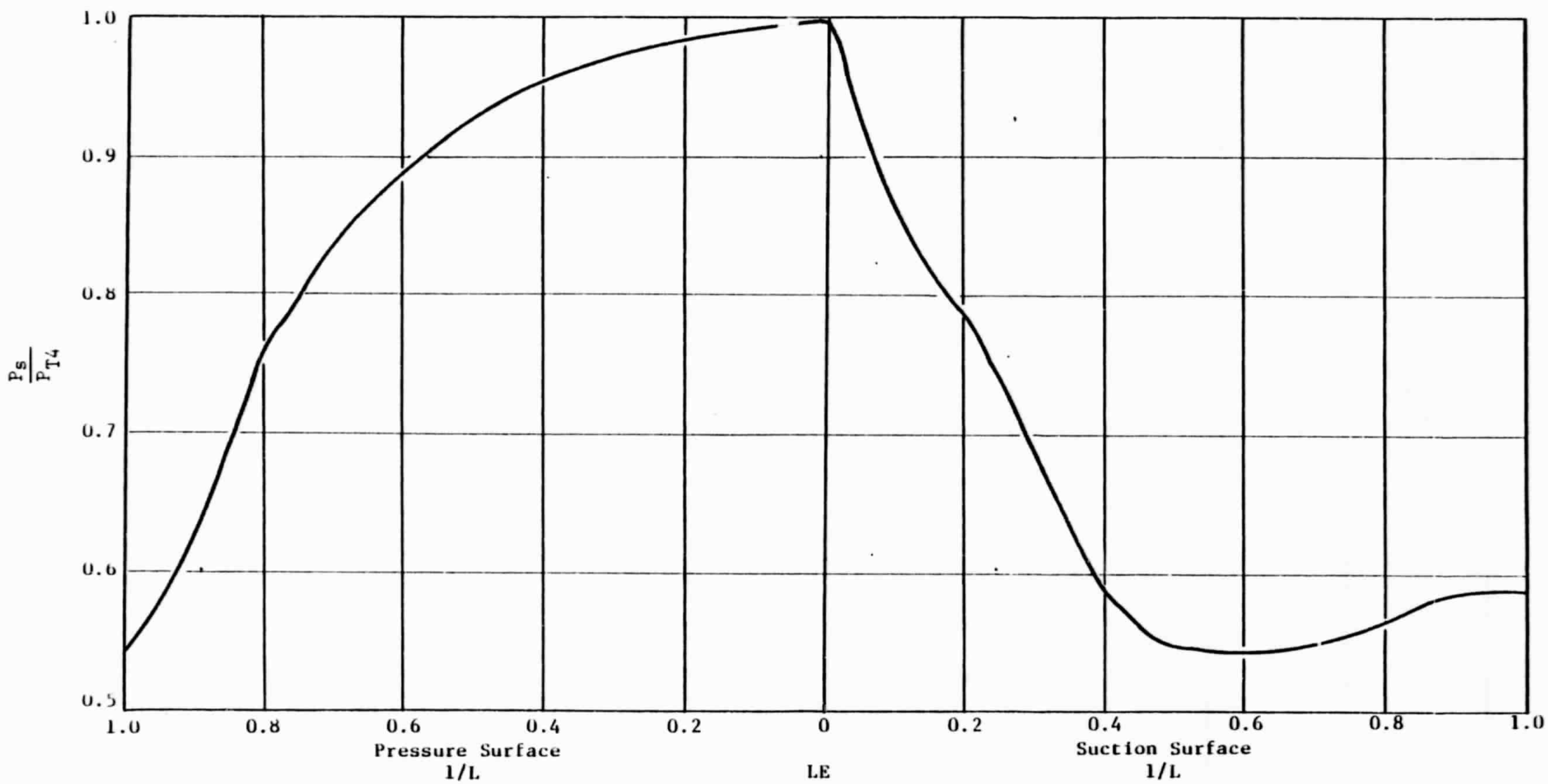

Figure 39. Turbine Vane Normalized Gas Static Pressure Distribution at Pitch Line.

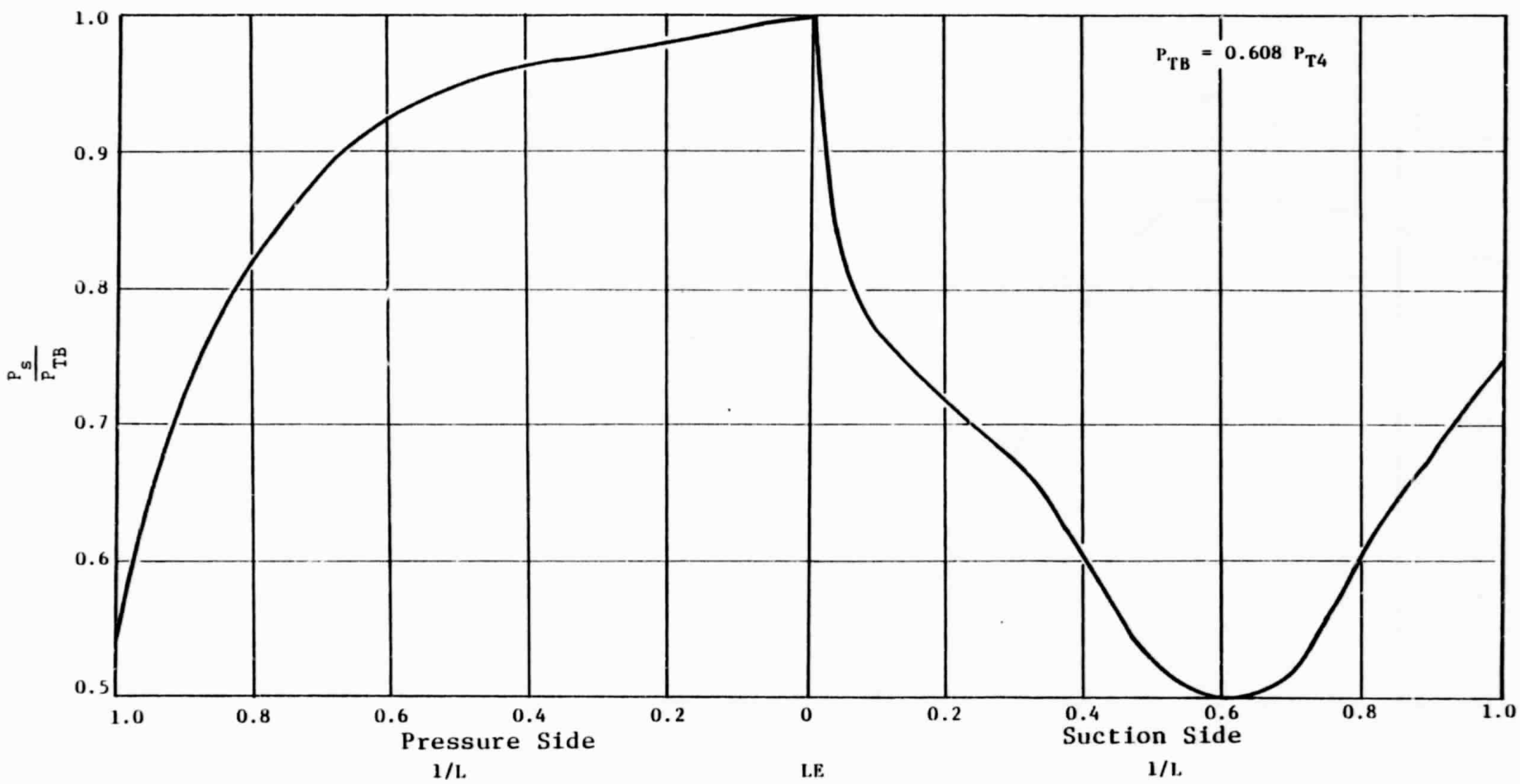

Figure 40. Turbine Blade Normalized Gas Static Pressure Distribution at Pitch Line.

$$\eta_c = \frac{T_g - T_m}{T_g - T_3}, \quad T_g = T_4 \text{ for vane} \quad = T_{41} \text{ for blade}$$

Wc/W_g = vane or blade cooling flow, % W_g

P_{T_g} = gas-side total pressure, P_{T4} or P_{T41}

T_g = gas-side temperature, T_4 or T_{41}

$$K = \frac{T_g + T_3}{T_g - T_3} - 1$$

Equation (14) can be used to predict the generalized cooling effectiveness η_c at any power setting from the referenced η_c^* and the stage variables T_g, T_3, and the cooling flow (Wc/W_g). The referenced η_c^* can either be gotten from THTD design prediction or test data or simply by the following equation through one-dimensional heat balance analysis,

$$\eta_c^* = \eta_f^* + \frac{W_c C_{pc}}{hgAg} \left[\frac{T_g + T_3}{T_g - T_3} - 1 \right] \tag{15}$$

where

η_f^* = film cooling effectiveness

C_{pc} = coolant specific heat

h_g = gas-side heat transfer coefficient

A_g = gas-side heat transfer area

Equation (11) can be restated as follows for local conditions:

$$\eta_{c,n} = \frac{T_g - T_{m,n}}{T_g - T_{c,i}} \tag{16}$$

where

T_g = Gas temperature relative to the surface, ° R

T_m = Metal temperature at a specific location, ° R

$T_{c,i}$ = Inlet coolant temperature, ° R

$\eta_{c,n}$ = Cooling effectiveness at location η

The value of $\eta_{c,n}$ has been shown to vary with power load in an approximately linear manner based on thermocouple temperature measurements. Some variances have also been noted between $\eta_{c,n}$ based on thermocouple temperature measurements and calculated temperatures from detailed 2D or 3D thermal analysis models. Such differences may result from any of the following causes - taken alone or in combination:

- Thermocouple variability and deterioration
- Calculated versus actual distribution of gas side heat transfer coefficients
- Unknown true temperature of the gas or coolant in the vicinity of the thermocouple
- Thermocouple is located in a high temperature gradient region
- 2D model versus 3D actual airfoil geometry

Use of the cooling effectiveness $\eta_{c,n}$ allows the calculation of a local metal temperature, $T_{m,n}$, when given the corresponding values of T_g, $T_{c,i}$, which are derived from cycle data and $\eta_{c,n}$ determined for the given airfoil design and operating conditions. The metal temperature is

$$T_{m,n} = T_g - \eta_{c,n} (T_g - T_{c,i}) \tag{17}$$

It would be convenient if expressions could be derived for predicting $\eta_{c,n}$ without running a detailed thermal analysis for each operating condition for stress analysis, as there can never be enough metal thermocouples to define $\eta_{c,n}$ for all locations needed by mechanical designers. But it is generally possible to install a few thermocouples on airfoils, sufficient to refine or verify procedures for calculating airfoil temperature distributions. The refinements result from matching the calculated temperatures at test point operating conditions which correspond to those for the measured temperature data.

The use of thermal analysis models, tuned up by temperature matching analyses, offers the wealth of detailed temperature distributions needed for stress analysis of cooled airfoils. However, it is inefficient and costly to run such detailed thermal analysis models for the many power and environmental conditions encountered in a flight mission. A cost-effective approach is to identify the regions in an airfoil where critical stresses occur. Temperatures at selected points in these stress regions can be converted to corresponding values of $\eta_{c,n}$ at other power or mission points of interest from those derived from a detailed thermal analysis model at a specified reference set of operating conditions. Such conditions are available at the design point and may be available at other conditions. In principle, $\eta_{c,n}$ can be obtained from Equation (18).

$$\eta_{c,n} = \left(\frac{\eta_{c,n}}{\eta_{c,n,Ref}}\right)\left(\eta_{c,n,Ref}\right) \quad \text{Based on a Detailed Thermo Analysis Mode} \tag{18}$$

where the subscript Ref stands for a specific set of reference conditions.

Previous work furnished some preliminary and approximate equations for $(\eta_{c,n}/\eta_{c,n,Ref})$. Further work was done in search of more appropriate approximate expressions. These expressions were based on the assumption of a series of one-dimensional heat exchangers, dominated by convective heat fluxes, to represent the surface of an airfoil. Some variances may result from using an approximate expression to relate η_c to operating parameters instead of running a complete thermal analysis mode. The relationship of $\eta_{c,n}$ to $\eta_{c,n,Ref}$ as determined from two detailed THTD runs of an engine high pressure turbine Stage 1 blade and vane at sea level takeoff and altitude cruise conditions was studied.

The approximate equation relating $\eta_{c,n}$ to $\eta_{c,n,Ref}$ can be tested by substituting turbine operating parameters for cruise and takeoff conditions and comparing the results with $\eta_{c,n}$ and $\eta_{c,n,Ref}$ based on the detailed THTD thermal models. The resulting first-order equation is

$$\frac{1-\eta_c}{1-\eta_{c,Ref}} = \frac{\left(\frac{P_{Tg}}{P_{Tc}}\right)^{0.8}\left(\frac{(FF)_g}{(FF)_c}\right)^{0.8}\left(\frac{T_{Tc}}{T_{Tg}}\right)^{0.4}\left(\frac{A_{f,g}}{A_{f,c}}\right)^{0.8}\left(\frac{T_{Tg}}{T_{Tc}}\right)^{0.36}}{\left[\left(\frac{P_{Tg}}{P_{Tc}}\right)^{0.8}\left(\frac{(FF)_g}{(FF)_c}\right)^{0.8}\left(\frac{T_{Tc}}{T_{Tg}}\right)^{0.4}\left(\frac{A_{f,g}}{A_{f,c}}\right)^{0.8}\left(\frac{T_{Tg}}{T_{Tc}}\right)^{0.36}\right]_{Ref}} \tag{17}$$

where

P_{Tg} = Average absolute total pressure of gas stream

P_{Tc} = Average absolute total pressure of coolant

$(FF)_g = \dfrac{W_g\sqrt{RT_{Tg}}}{A_{f,g}\,P_{Tg}}$ turbine flow function

$(FF)_c = \dfrac{W_c\sqrt{RT_{Tc}}}{A_{f,c}\,P_{Tc}}$ turbine flow function

T_{Tc} = Average absolute total temperature of coolant, °R

T_{Tg} = Average absolute total temperature of gas, °R

$A_{f,g}$ = Gas flow area

$A_{f,c}$ = Coolant supply, effective flow area for the same airfoil, turbine, and engine

$A_{f,g}/A_{f,c}$ = $(A_{f,g}/A_{f,c/Ref}$ and for normal operating ranges $(FF)_g/(FF)_{g,Ref}$ and $(FF)_c/(FF)_{c,Ref}$ are essentially constant. For convenience, T_{Tg} is sometimes replaced with related temperatures like $T_{4.1}$ and T_{TB} and T_{Tc} by T_3,

where

$T_{4.1}$ = Average absolute total temperature ahead of the turbine rotor, °R

T_{TB} = Gas temperature relative to the surface, °R

T_3 = Compressor discharge absolute average temperature, °R

The use of these engine cycle parameters in Equations (19) results in a single first-order expression for the nozzle vane and blade.

$$\frac{1 - \eta_c}{1 - \eta_{c,Ref}} = \left(\frac{T_3}{T_{3,Ref}}\right)^{0.04} \left(\frac{T_{4.1,Ref}}{T_{4.1}}\right)^{0.04}$$

For the CF6-50C high pressure turbine:

	T_3	$T_{4.1}$
Takeoff (Reference Conditions)	1555	3078
Cruise Conditions	1317	2446

from which,

$$\frac{1 - \eta_{c,\ cruise}}{1 - \eta_{c,\ T/O}} = 1.00255 \tag{21}$$

THTD 2D calculations of pitch-line vane and blade temperature distributions are listed in Table IV. The sea level takeoff data were used as the reference conditions. Similar altitude cruise data were used for the test cases.

Figure 41 compares $(\eta_{c,n})$ cruise $(\eta_{c,n})_{T/O}$ based on T_g and surface temperature. For the turbine Stage 1 vanes, the trend is similar for the 14 sampled temperatures identified in Figure 41. The same data are replotted in Figure 42 for comparison with the results of Equation (20). It can be seen that with the exclusion of three points in the leading edge region (Numbers 1, 2, and 14) the data group has about an average value of 0.92 as compared to a value of unity from Equation (21). Also note that $\eta_{c,n}$ cruise = $\eta_{c,n,T/O}$ when $(1 - \eta_{c,n})/(1 - \eta_{c,n,Ref}) = 1$.

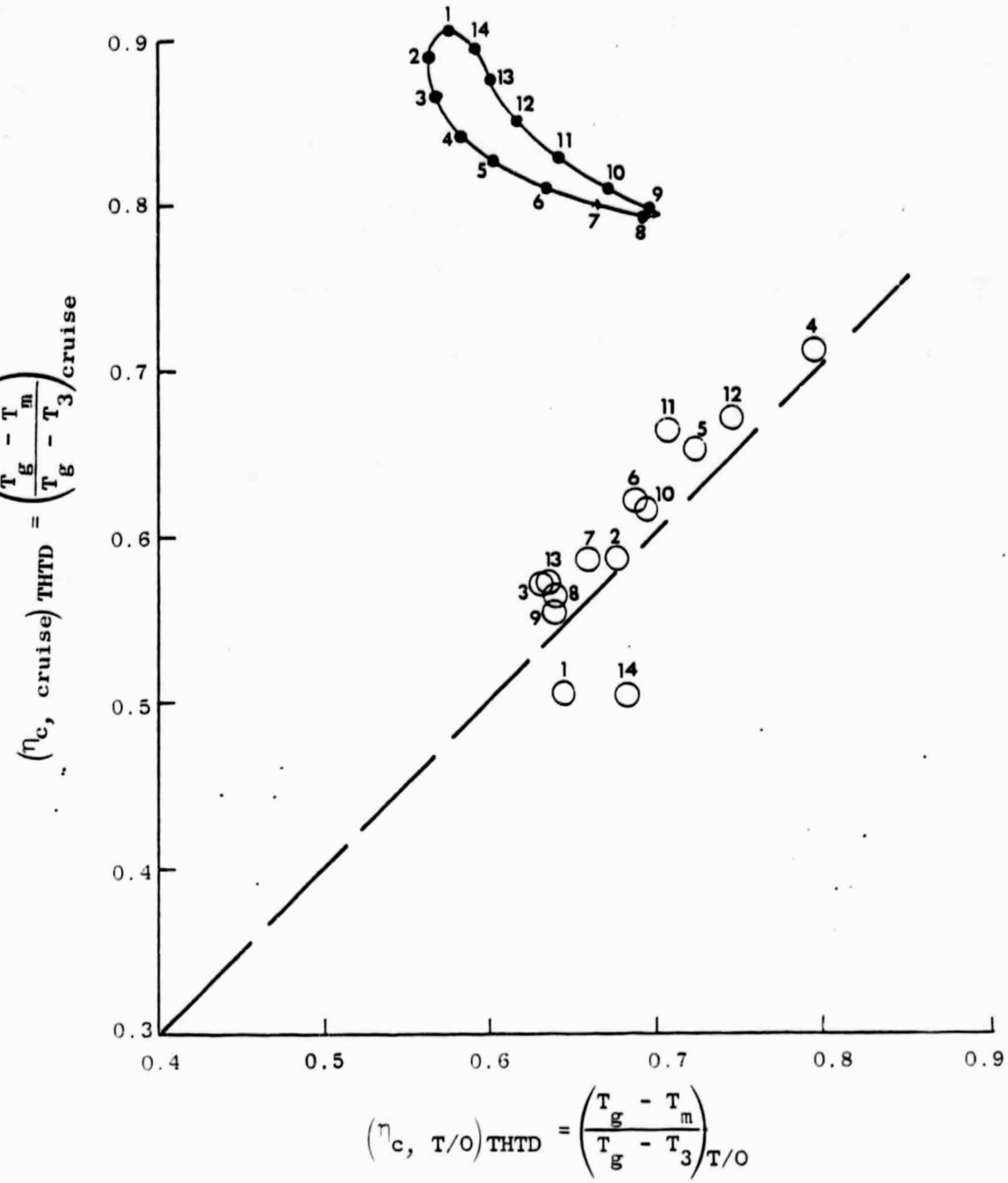

Figure 41. Comparison of Cruise and Sea Level Takeoff Cooling Effectiveness.

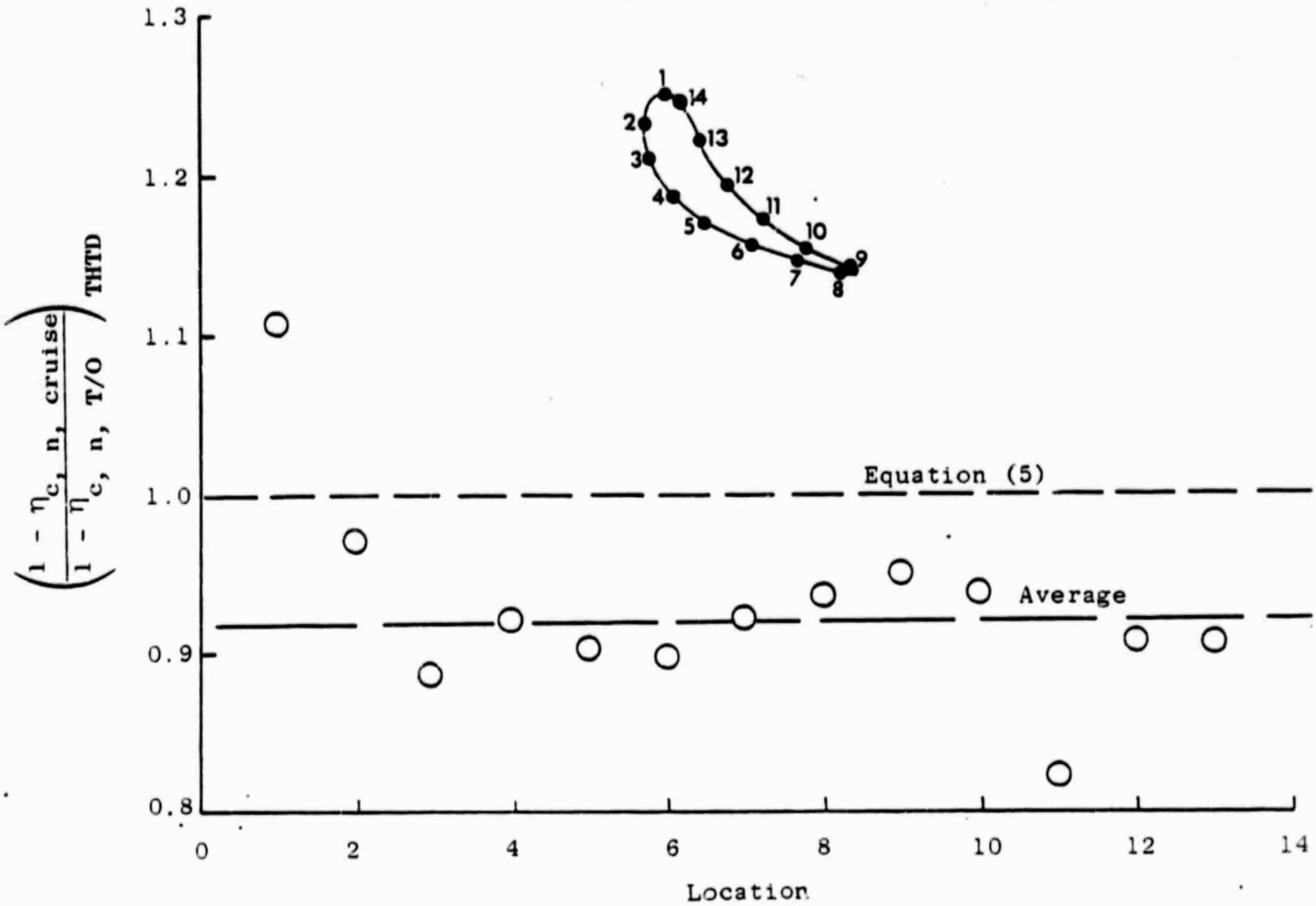

Figure 42. Prediction of Cooling Effectiveness Relationship at Cruise to Takeoff From the First Order Equation Versus Detailed THTD Results.

Table IV. High Pressure Turbine Stage 1 Vane and Blade Temperature Distribution.

- Sea Level T_3 = 1095° F $T4.1$ = 2618° F
- Cruise T_3 = 857° F $T4.1$ = 1986° F

Vane					Blade				
	Takeoff		Cruise			Takeoff		Cruise	
Location n	$T_{m,n}$ °F	$\eta_{c,n}$	$T_{m,n}$ °F	$\eta_{c,n}$	Location n	$T_{m,n}$ °F	$\eta_{c,n}$	$T_{m,n}$ °F	$\eta_{c,n}$
1	1850	0.647	1496	0.605	1	1897	0.473	1347	0.566
2	1785	0.677	1364	0.687	2	1857	0.500	1341	0.511
3	1884	0.631	1387	0.672	3	1863	0.496	1336	0.576
4	1529	0.797	1160	0.813	4	1913	0.463	1354	0.560
5	1683	0.725	1258	0.752	5	1917	0.460	1364	0.551
6	1759	0.689	1309	0.721	6	1923	0.456	1366	0.549
7	1822	0.66	1364	0.687	7	1884	0.482	1370	0.546
8	1862	0.641	1402	0.663	8	1975	0.422	1382	0.535
9	1865	0.639	1412	0.657	9	1912	0.464	1375	0.541
10	1745	0.696	1318	0.715	10	1797	0.539	1326	0.585
11	1718	0.708	1241	0.763	11	1805	0.534	1340	0.572
12	1633	0.748	1227	0.771	12	1821	0.523	1342	0.570
13	1866	0.639	1388	0.672	13	1809	0.531	1334	0.578
14	1778	0.681	1498	0.604	14	1811	0.530	1328	0.583
Bulk	1601	0.763	1237	0.765	15	1738	0.578	1312	0.597
					16	1846	0.507	1330	0.581
					Bulk	1759	0.564	1335	0.577
T_g, °F =	3233		2475		T_g, °F =	3233		2475	
$T_{4.1}$, °F =	2618		1986		$T_{4.1}$, °F =	2618		1986	
					T_{TB}, °F =	2560		1940	
T_3, °F =	1095		857		T_3, °F =	1095		857	

The foregoing results were anticipated because the vanes are hollow shells with impingement inserts. Therefore, the heat source and sink were essentially constant over the vane surfaces. Obviously, the simple flat plate heat exchanger model was better applied to the pressure and suction surfaces of the airfoil than to the "cylinder like" leading edge region.

Figure 43 compares $(\eta_{c,n})$ to $(\eta_{c,n})T/O$ based on T4.1 and surface temperatures for the HP turbine Stage 1 blade. The data for the 16 points around the airfoil lie in a band along a straight line. However, the cooling effectiveness shown for surface temperatures at cruise power is consistently higher

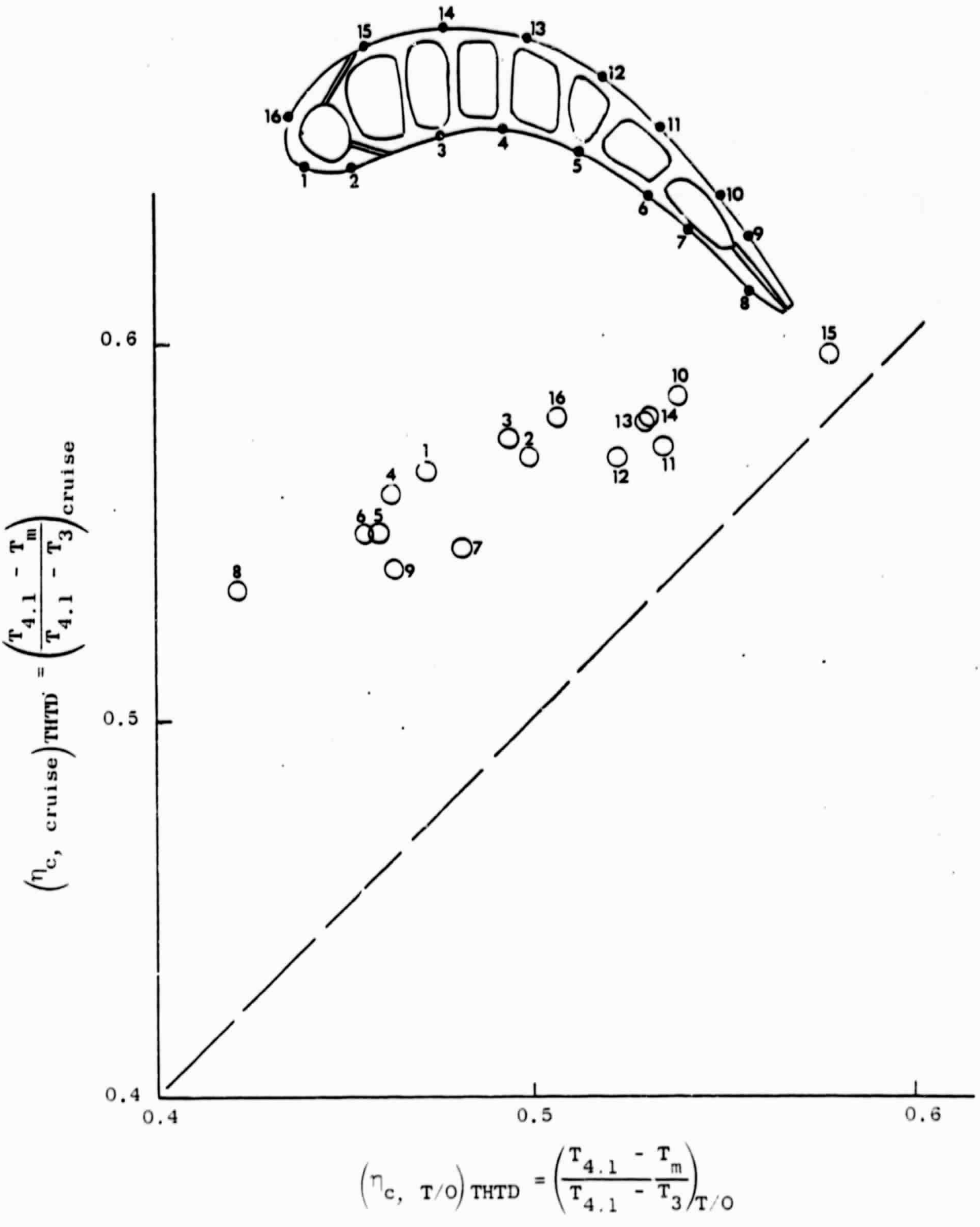

Figure 43. Comparison of Cruise and Sea Level Takeoff Cooling Effectiveness.

than at takeoff, with deviations up to 27% near the trailing edge. A somewhat better agreement would have been attained if local mean wall temperatures had been used. On closer examination, some of the 16 locations sampled are affected by 2D conduction in contrast to the 1D flat plate heat exchanger assumed in the derivation of Equation (4) and (5). The variances can also be due to local variation in coolant temperature as the air traverses through serpentine cooling passages, and to the variation in film cooling effectiveness. Hence, Figure 43 illustrates a fundamental problem in trying to derive a simple, but general, expression for predicting airfoil temperature distributions when the cooling system design is complex and several modes of heat transfer are combined. The data of Figure 43 constitute a correlation, but this is based on a detailed design analysis of the particular airfoil with cruise boundary conditions in the thermal model rather than a simple projection from the reference takeoff case. This problem is likely to be a common occurrence with sophisticated cooled airfoil designs. It is therefore planned to make a similar comparison of cruise and takeoff cooling effectiveness of another high pressure turbine blade design.

2.5.3 Stress-Strain Decomposition and Synthesis

The decomposition and synthesis of stresses, strains, and deformations is technically the most challenging portion of this program. It requires innovative methods to produce usable results for burner liners, turbine blades, and vanes. Thus, our goal under this task has been to compile a library of possible decomposition and synthesis techniques and to assess their validity. Among the techniques being considered are the following:

- Assume that the structure remains totally elastic at all stress levels and do the decomposition and synthesis based on an elastic "pseudostress."

- Assume that the structure is deformation-controlled (strain range invariance). The first level of decomposition and synthesis would be based on deformations (total strains). A second level of synthesis could then introduce the effects of plasticity and creep by using the material response characteristics to partition the total strain into elastic, plastic, and creep components.

- Assume that the structure is load-controlled (stress invariance). Decomposition and a first level of synthesis would be based on load terms reflecting the centrifugal loadings and the temperature and pressure distributions. A second level of synthesis could then introduce the effects of plasticity and creep by using the material response characteristics to determine the elastic, plastic, and creep strains that would be caused by the total load.

- Use simplified nonlinear finite element modeling to decompose and synthesize the stresses, strains, and deformations in terms of the set of analyzed mission components. These simplified models could be either one 2D or 3D element or a nonlinear substructure. These models could use boundary conditions from the detailed analysis or they could be run as an intimate part of the detailed analysis.

- Apply the method of superposition for the decomposition and synthesis of stresses, strains, and deformations. This method would be investigated based on the following hierarchy of calculated parameters:

  - deformations
  - strains
  - stresses

  We will determine to what degree these parameters can be decomposed and synthesized by superposing the results from individual loading functions (temperature, pressure, rpm).

- Use linear and nonlinear interpolation of the results of a detailed analysis for decomposing and synthesizing stresses, strains, and deformations. The interpolating parameters would be second-level predicted temperatures, pressures, and rpm's.

- Form look-up tables of deformations, stresses, and strains as functions of temperatures, pressures, and rpm's. These tables would then be used to decompose and synthesize the mission cycles.

- Finally, generate from test data an empirical model relating stresses, strains, and deformations to temperatures, pressures, and rpm's. With this model, mission cycles could be decomposed and new ones synthesized.

Our first step was to survey existing techniques for decomposition and synthesis. The best documented of these was used in combustor design. Combustor life is limited by (1) creep of the outer liner, (2) oxidation, (3) high cycle fatigue, and (4) low cycle thermal fatigue. Thermal fatigue is the most limiting on the CF6 family of engines. Life projections are made with a tool called CO-LIFE analysis. In this, thermal strains are computed as

$$\varepsilon_{\Delta T} = \alpha \Delta T$$

Metal temperatures are computed using a film effectiveness

$$\eta = \frac{T_{metal} - T_c}{T_{gas} - T_c}$$

The mechanical pressure strains are computed as a linear function of the pressure differential

$$\varepsilon_{\Delta P} = C \Delta P$$

The CO-LIFE analysis tool is used to predict installed life. As such, it must evaluate derate conditions and make factory to field life projections. To do this it utilizes actual engine parameters and actual test results to develop the necessary constants. The internal logic includes the following calculations:

$$\Delta\epsilon = (\epsilon_{\Delta} + \epsilon_{\Delta P})$$

$$\epsilon_{\Delta T} = K_1 (\epsilon_{HOT} - \epsilon_{COLD})$$

$$= K_2 (T_{HOT} - T_{COLD})$$

$$\epsilon_{\Delta P} = K_3 P_3$$

$$T_{HOT} = T_3 + \eta_c (T_{41} - T_3)$$

$$\Delta\epsilon = K N_f^{\alpha} + K_5 N_4^{\beta}$$

Laboratory 100-second hold time smooth bars test data are used to define the material life capability.

This calculation method was subsequently upgraded to the HOTSAM program by G. Weber, one of the COSMOS team. The following changes were made in the CO-LIFE logic.

- Use $(\epsilon_{HOT} - \epsilon_{COLD})$ instead of $(T_{HOT} - T_{COLD})$
- Assume K varies with metal stiffness so that

$$\epsilon_{\Delta T} = K_1 (\epsilon_{HOT} - \epsilon_{COLD}) \left(\frac{\epsilon_{HOT}}{\epsilon_{COLD}}\right)^{\alpha}$$

Our goal in COSMOS is to improve these techniques for decomposing and synthesizing the temperatures and pressures and the stress-strain response.

Two well-documented hot section problems are used as the tools in the initial efforts at decomposition and synthesis. The first of these is the uniaxial model from NASA CR-165268, "Turbine Blade Tip Durability Analysis." This model simulates the strain-temperature-time conditions occurring at a turbine blade squealer-tip cracking location. As a multiaxial tool we are using the problem reported in NASA CR-2271, "Multiaxial Cycle Thermoplasticity Analysis with Besseling's Subvolume Method." The problem analyzed in this paper is that of a shingled combustor segment with a hot spot. Table V gives the pertinent information for the critical location of the squealer tip problem.

The simplifying approach of assuming strain range invariance for this problem is obviously feasible and involves only a 2.8% error. However, the other individual parameters vary too much to make this approach acceptable by itself.

Table V. Results of Turbine Blade Tip Analyses, Inelastic.

	Elastic	Cycle 1	Cycle 2	Cycle 3
Maximum Total Strain, %	0.025	-0.05	-0.062	-0.0829
Minimum Total Strain, %	-0.2925	-0.3582	-0.371	0.3918
Total Strain Range, %	0.3175	0.3082	0.3090	0.3089
Mean Stress, ksi	-23.9	-1.9	4.9	11.7

Figure 44 shows the temperature-time cycle, and Figure 45 gives the total strain-time cycle, which are the imposed boundary conditions for the problem. Using the material properties as given in NASA CR-165268 and the classical constitutive equation embedded in CYANIDE, Figures 46, 47, and 48 show the results of the computer prediction. Figure 46 is the stress-time response, Figure 47 is the plastic strain-time response, and Figure 48 is the creep-time response. This will be used as the baseline against which decomposition/synthesis techniques will be measured.

Figure 49 shows the stress versus time prediction if the problem is considered totally elastic. Figure 50 shows the stress versus time response and Figure 51 shows the creep strain versus time response when plasticity is ignored.

Table VI is a comparison of the pertinent data for the three types of problem simulations. As can be seen, an elastic analysis (E) gives no meaningful data, whereas the approximation ignoring plasticity (EC) is useful. The mean stresses and stress ranges approximate reality.

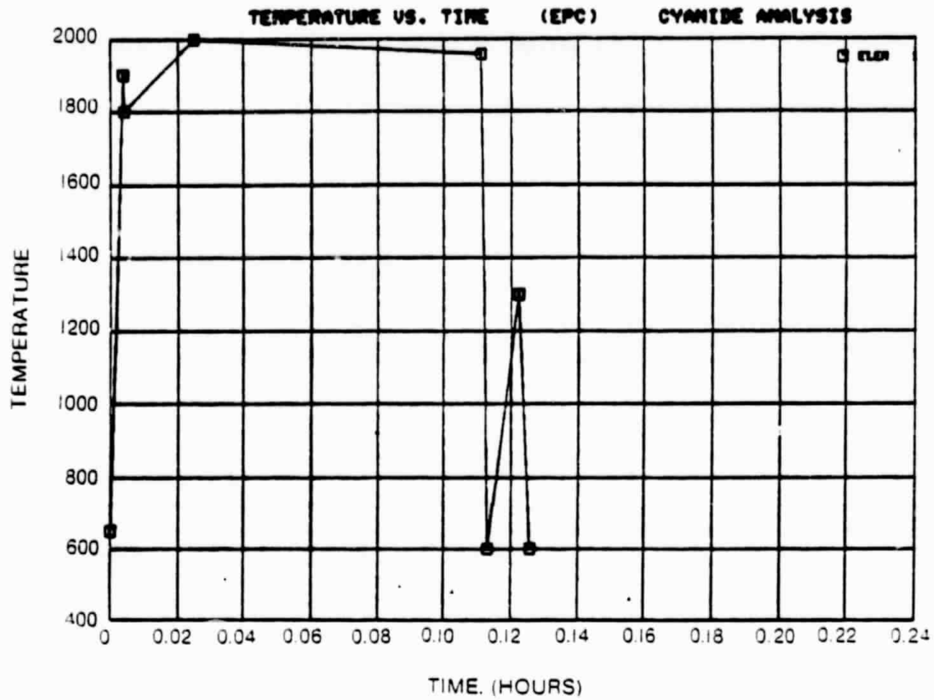

Figure 44. Temperature Versus Time Cycle.

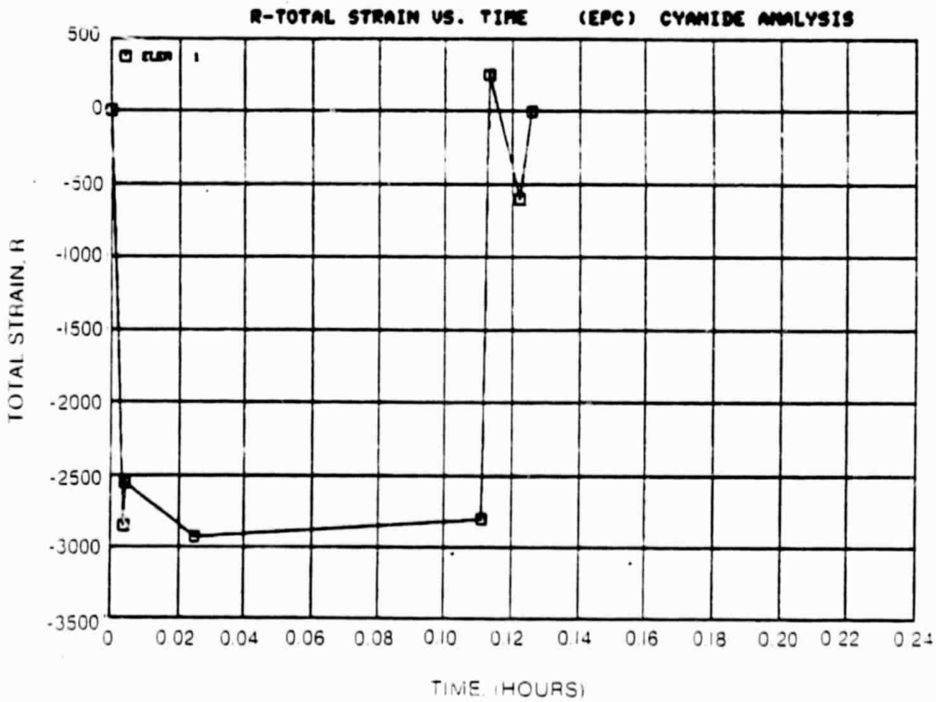

Figure 45. Total Strain Versus Time Cycle.

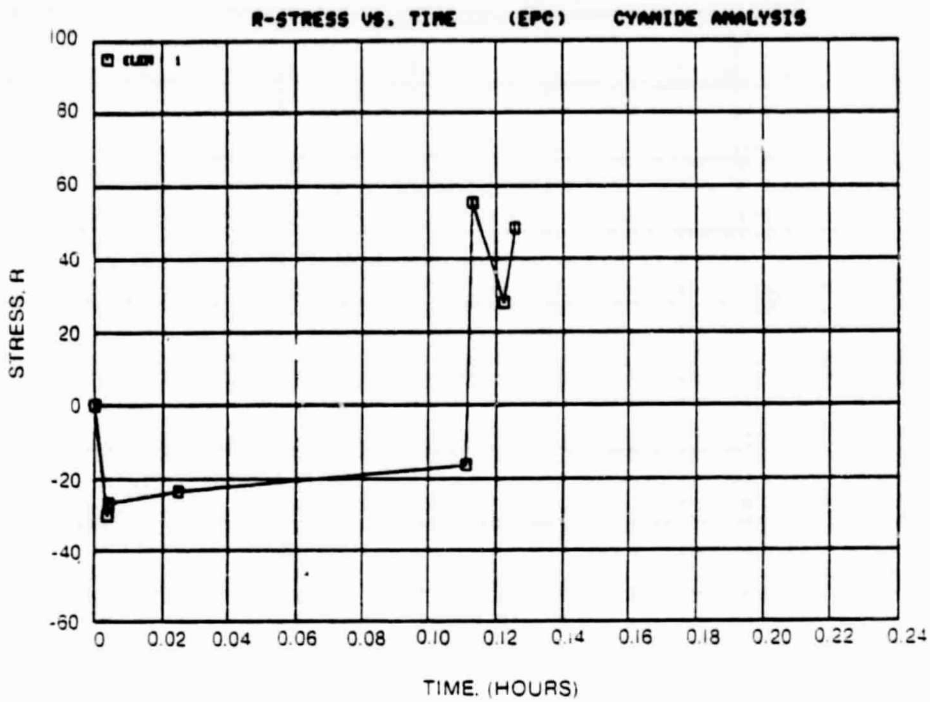

Figure 46. Stress Versus Time Response.

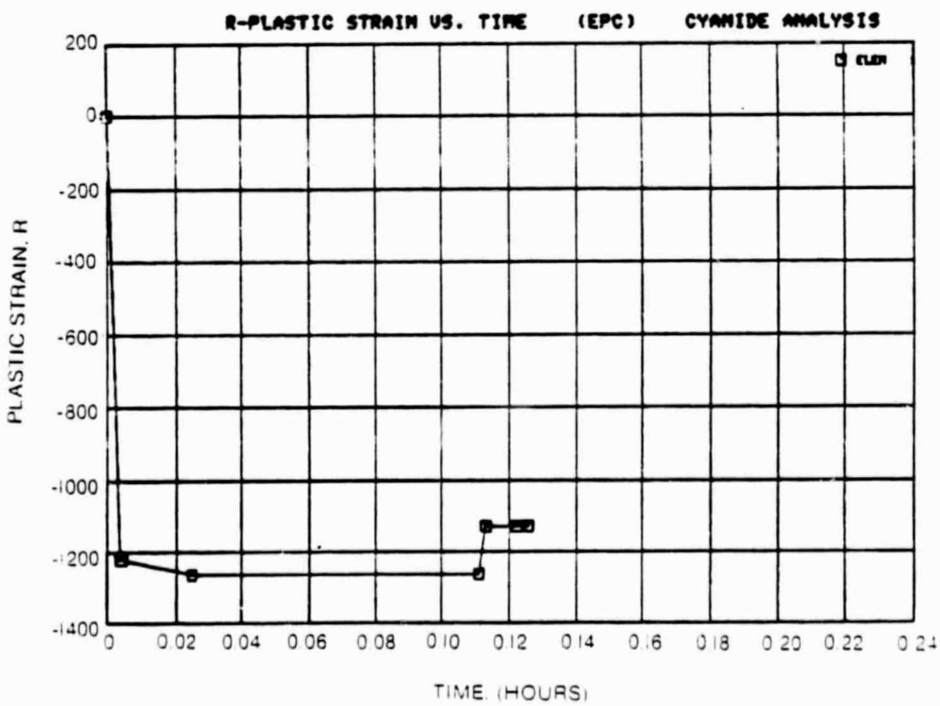

Figure 47. Plastic Strain-Time Response.

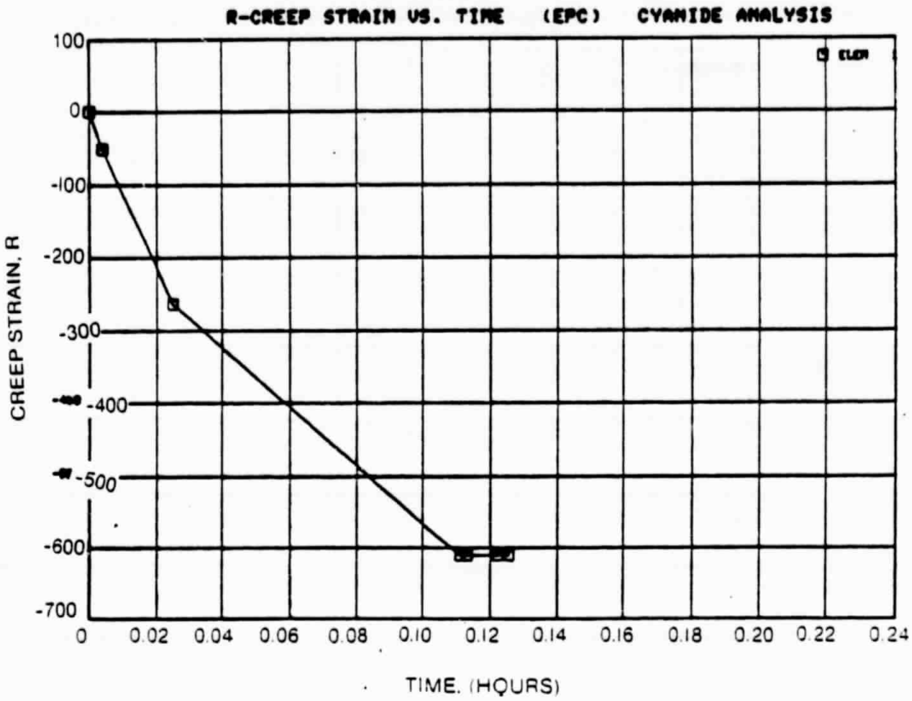

Figure 48. Creep Strain Versus Time Response.

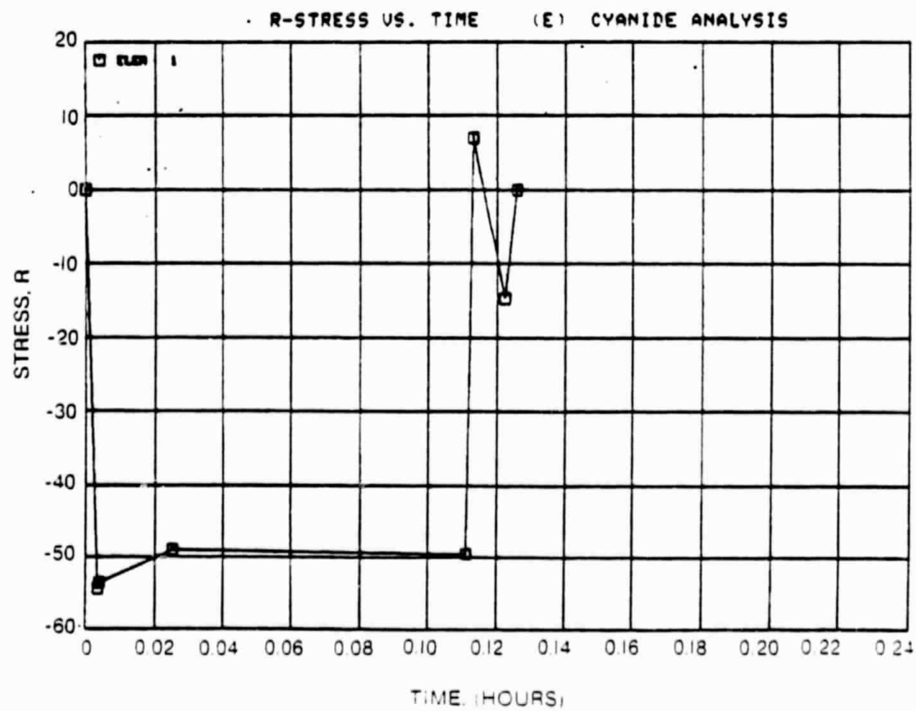

Figure 49. Stress Versus Time Response.

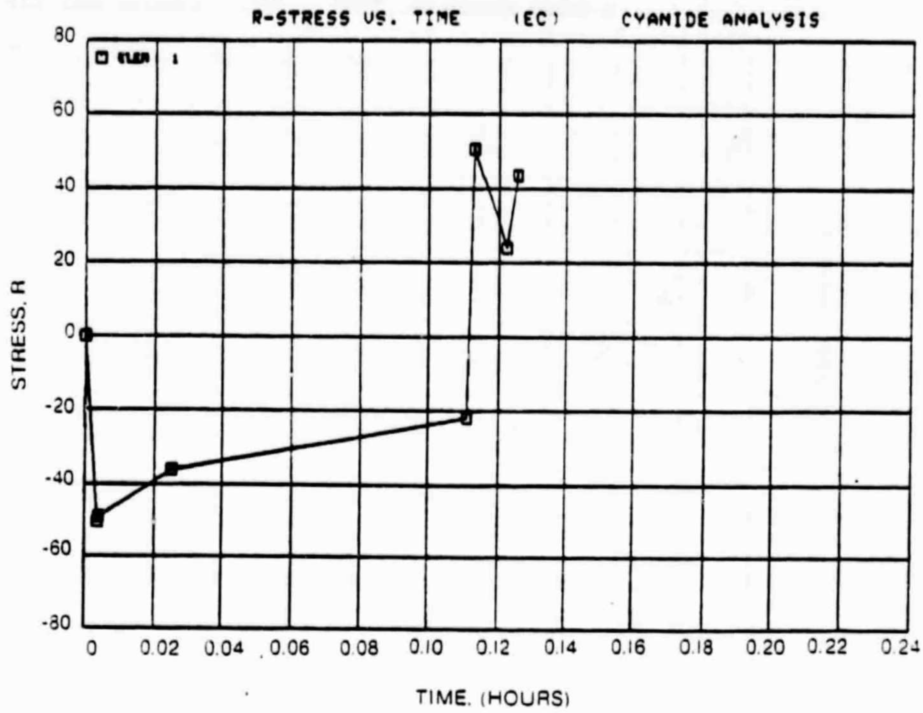

Figure 50. Stress Versus Time Response.

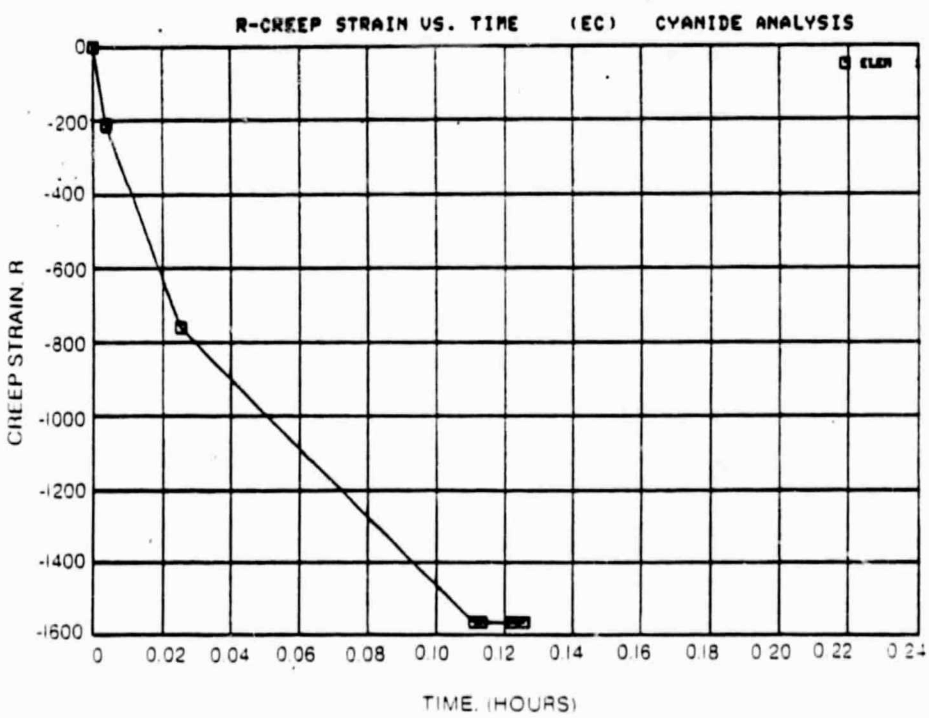

Figure 51. Creep Strain Versus Time Response
When Plasticity is Ignored.

Table VI. Comparison Data for Three Simulated Problems.

	Temperature, °F							
	1	2	3	4	5	6	7	8
E	650	1900	1800	2000	1960	600	1300	600
EC	650	1900	1800	2000	1960	600	1300	600
EPC	650	1900	1800	2000	1960	600	1300	600
• R - Total Strain (in./in.)								
E	0.0	-2850	-2550	-2925	-2800	250	-600	0.0
EC	0.0	-2850	-2550	-2925	-2800	250	-600	0.0
EPC	0.0	-2850	-2550	-2925	-2800	250	-600	0.0
• R - Stress (ksi)								
E	0.0	-54.4	-53.5	-49.0	-49.5	7.0	-14.8	0.0
EC	0.0	-50.4	-49.0	-36.2	-21.8	50.6	23.9	43.6
EPC	0.0	-30.1	-26.8	-23.4	-16.4	55.4	28.1	48.4
• R - Plastic Strain (in./in.)								
E	0.0	0.0	0.0	0.0	0.0	0.0	0.0	0.0
EC	0.0	0.0	0.0	0.0	0.0	0.0	0.0	0.0
EPC	0.0	-1222	-1222	-1262	-1262	-1129	-1129	-1129
• R - Creep Strain (in./in.)								
E	0.0	0.0	0.0	0.0	0.0	0.0	0.0	0.0
EC	0.0	-211	-217	-762	-1568	-1568	-1568	-1568
EPC	0.0	-51	-52	-265	-611	-611	-611	-611

Legend

E = Elastic only
EC = Elastic and Creep
EPC = Elastic, Plastic, and Creep

Next, the turbine blade tip durability model was exercised with a simplified thermal cycle. Reference is made to Figures 44 and 45 for the original complex cycle being investigated. To assess the effect and utility, the temperature cycle was revised as shown in Figure 52. Table VII shows the 2D CYANIDE results for this revised cycle. These values compared to those in Table VI show this approximation to be very good.

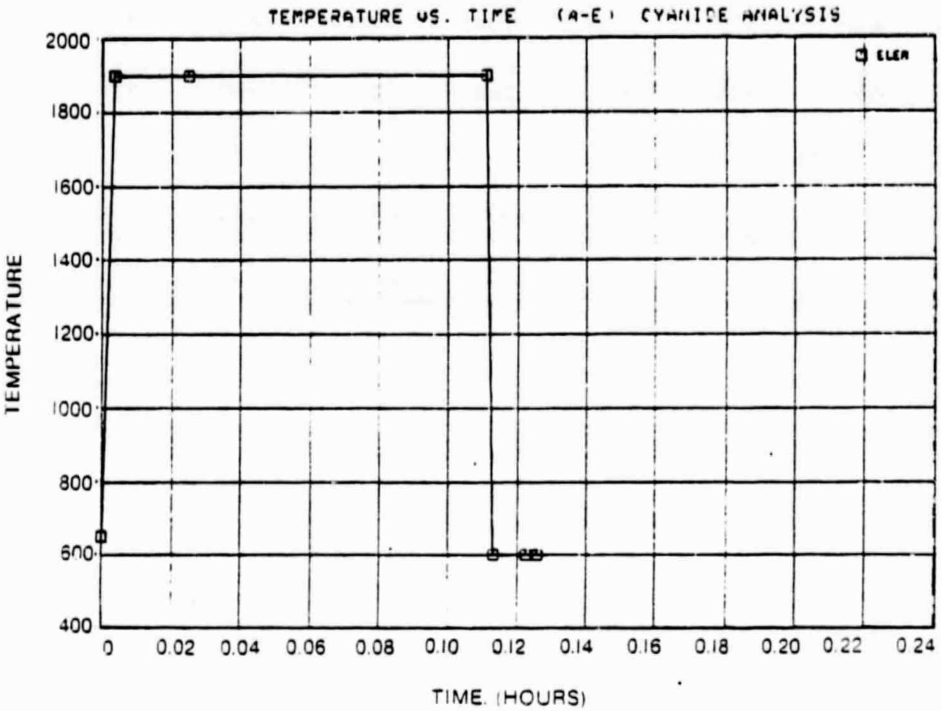

Figure 52. Simplified Temperature Cycle.

Table VII. Simplified Temperature Cycle Results.

	Temperature, °F							
	1	2	3	4	5	6	7	8
E	650	1900	1900	1900	1900	600	600	600
EC	650	1900	1900	1900	1900	600	600	600
EP	650	1900	1900	1900	1900	600	600	600
EPC	650	1900	1900	1900	1900	600	600	600
• R - Total Strain								
E	0.0	-2856	-2550	-2925	-2800	256	-600	0.0
EC	0.0	-2850	-2550	-2925	-2800	250	-600	0.0
EP	0.0	-2850	-2550	-2925	-2800	250	-600	0.0
EPC	0.0	-2850	-2550	-2925	-2800	250	-600	0.0
• R - Stress								
E	0	-54.4	-48.7	-55.9	-53.5	7.0	-16.7	0.0
EC	0	-50.4	-44.6	-39.1	-23.1	51.3	27.6	44.3
EP	0	-31.1	-25.4	-31.6	-29.2	42.4	18.7	35.5
EPC	0	-30.1	-24.4	-27.2	-18.6	55.0	31.4	48.1
• R - Plastic Strain								
E	0	0	0	0	0	0	0	0
EC	0	0	0	0	0	0	0	0
EP	0	-1222	-1222	-1273	-1273	-1273	-1273	-1273
EPC	0	-1222	-1222	-1238	-1238	-1136	-1136	-1136
• R - Creep Strain								
E	0	0	0	0	0	0	0	0
EC	0	-211	-215	-877	-1591	-1591	-1591	-1591
EP	0	0	0	0	0	0	0	0
EPC	0	-51	-52	-263	-590	-590	-590	-590

In the multiaxial work, the model under analysis is a single shingle combustor segment analyzed as a flat plate in a condition of plane stress. The shingle segment is shown in Figure 53 and modeled as illustrated in Figure 54. The combustor shingle model was chosen because of its multiaxial nature and the complex thermal cycle. The thermal condition of the combustor shingle at peak temperature is shown in Figure 55. Figure 56 defines the thermal cycle at the center of the hot spot.

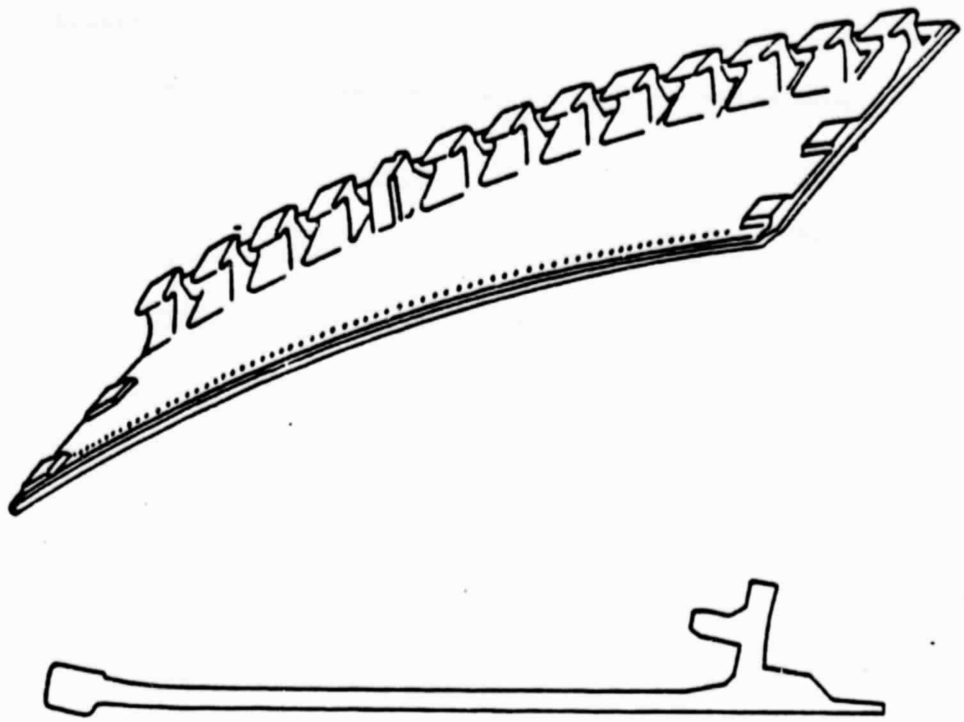

Figure 53. Shingle Segment.

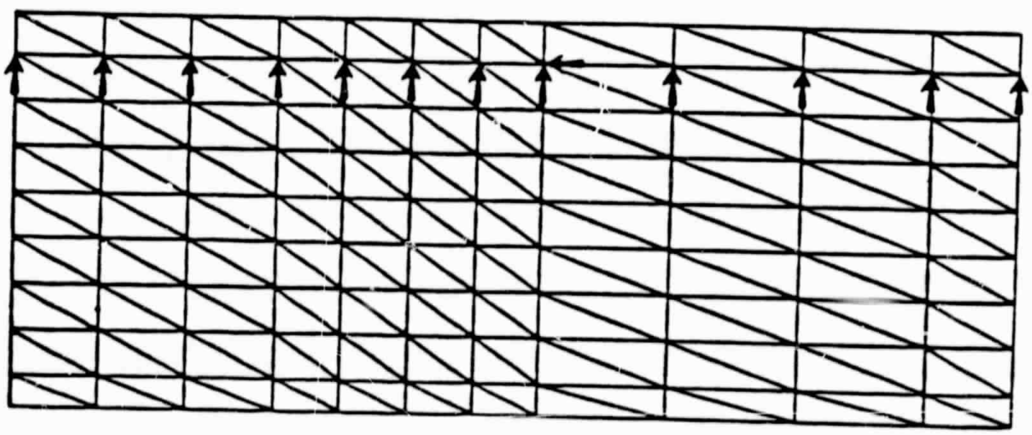

Figure 54. CYANIDE Model.

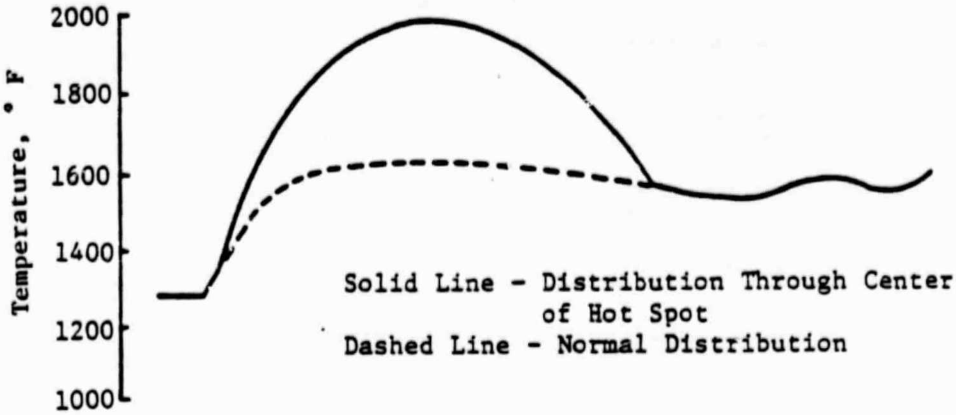

(a)

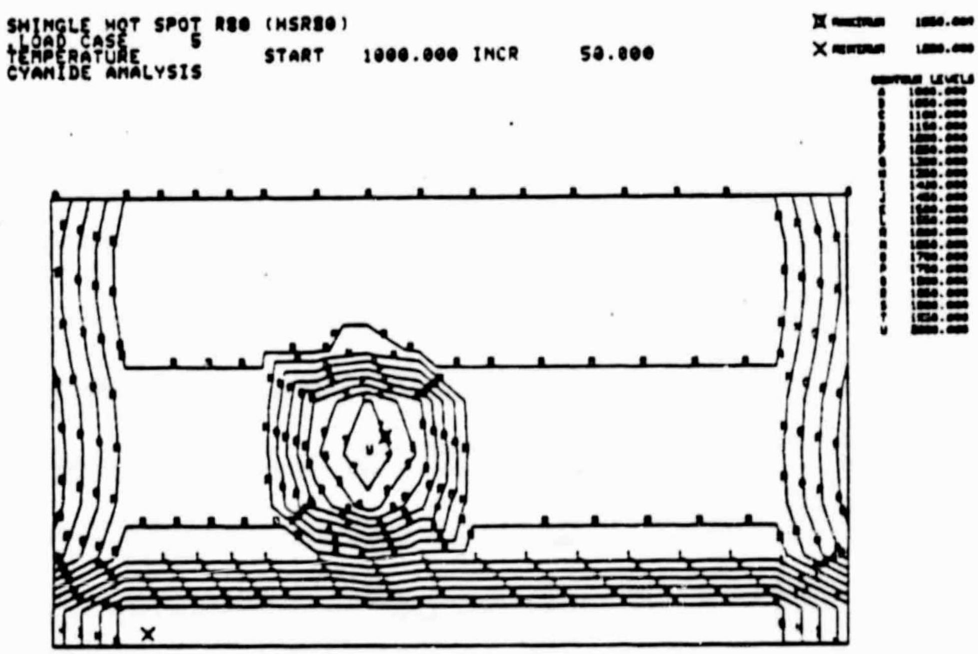

(b)

Figure 55. Temperature Distribution on Shingle at Peak Condition.

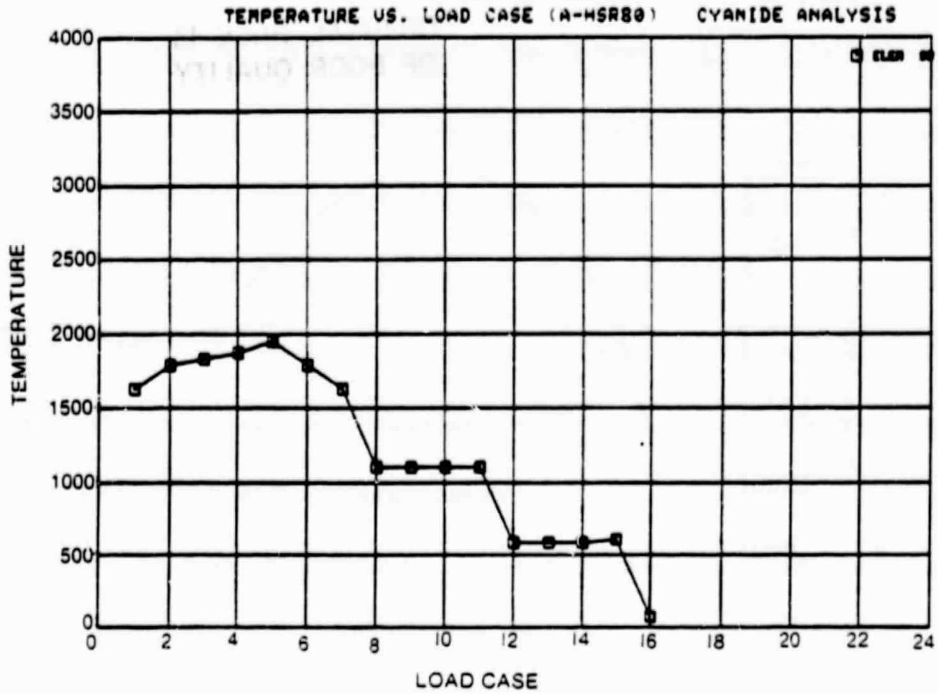

Figure 56. Thermal Cycle at Center of Hot Spot.

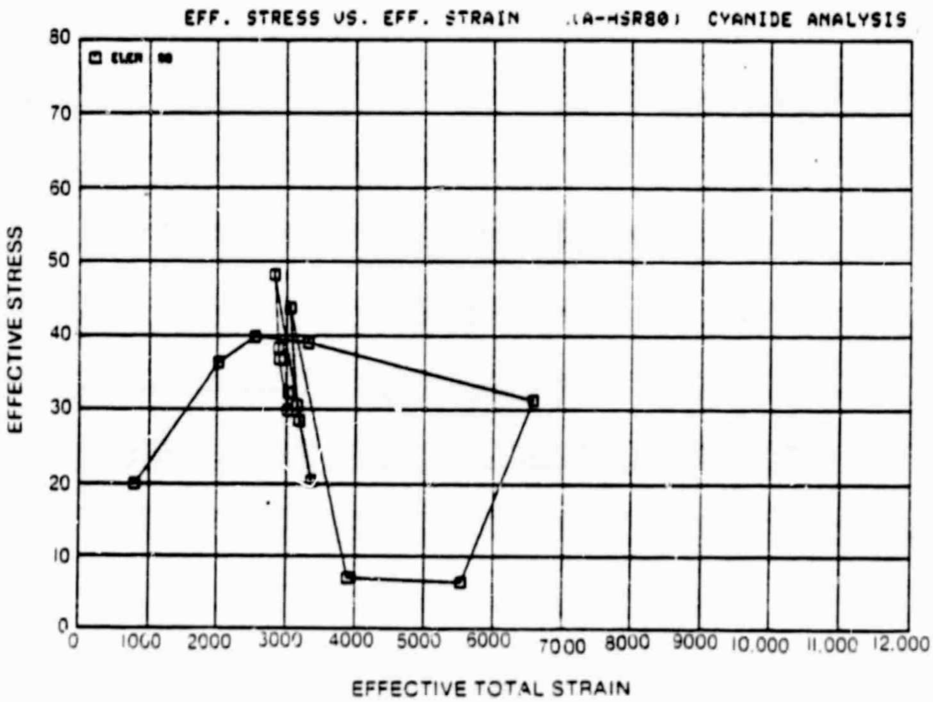

Figure 57. Effective Stress Versus Effective Strain at Center of Hot Spot for Base Case (1).

The combustor model was run under four separate analysis conditions to enable the effects of creep and plasticity to be separated. The analysis conditions were as follows:

- Elastic/Plastic/Creep (HSR80)
- Elastic/Plastic (HSR80-B)
- Elastic/Creep (HSR80-C)
- Elastic only (HSR80-D)

Figures 57 through 71 give pertinent information concerning the state of stress for the element at the center of the hot spot.

2.6 TASK VIII - COMPONENT SPECIFIC MODEL DEVELOPMENT

2.6.1 Geometric Modeling

The geometric modeling of these three specific components will dovetail with and make use of the modeling capability being developed in the ESMOSS contract. At the end of the ESMOSS contract, the personnel involved will be joining this program, bringing with them the new modeling capability. Meanwhile, all of the necessary hooks to other parts of this computer system are now being generated.

2.6.2 Remeshing and Mesh Refinement

This area and the next, Self-Adaptive Solution strategies, touch on each other synergistically. What is sought in this program is the best combination of both. This involves two major areas of investigation: the method to be used to refine, upgrade, and rearrange the mesh, and the criteria to be used to activate this process.

There are a number of ways to refine a mesh to get a better answer: (1) one way is to progressively subdivide a coarse mesh, always retaining all previous meshes within the finer mesh; (2) a second family of techniques totally realigns the mesh based on some criteria such as strain energy density; (3) a third method is to leave the mesh unchanged but upgrade the order of the elements.

The first method, progressive subdivision, has certain theoretical and computational advantages. If the finite element interpolating functions used meet the requirements for completeness and continuity, convergence is mathematically guaranteed when we refine the mesh by progressive subdivision. The computational process of remeshing by progressive subdivision is straightforward; however, it guarantees a larger problem to solve.

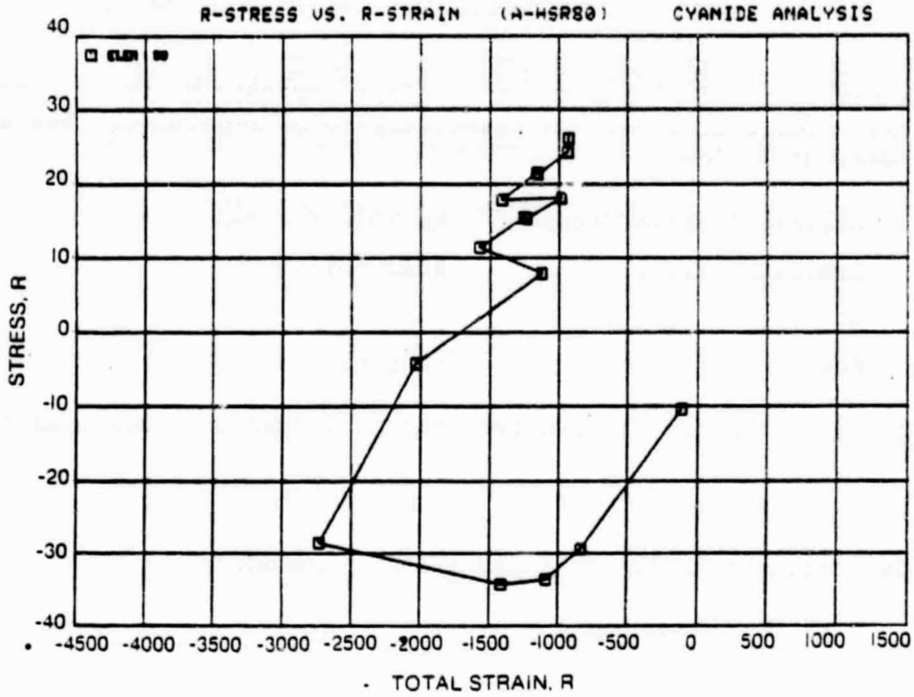

Figure 58. R-Direction Stress-Strain Cycle at Center of Hot Spot for Base Case (1).

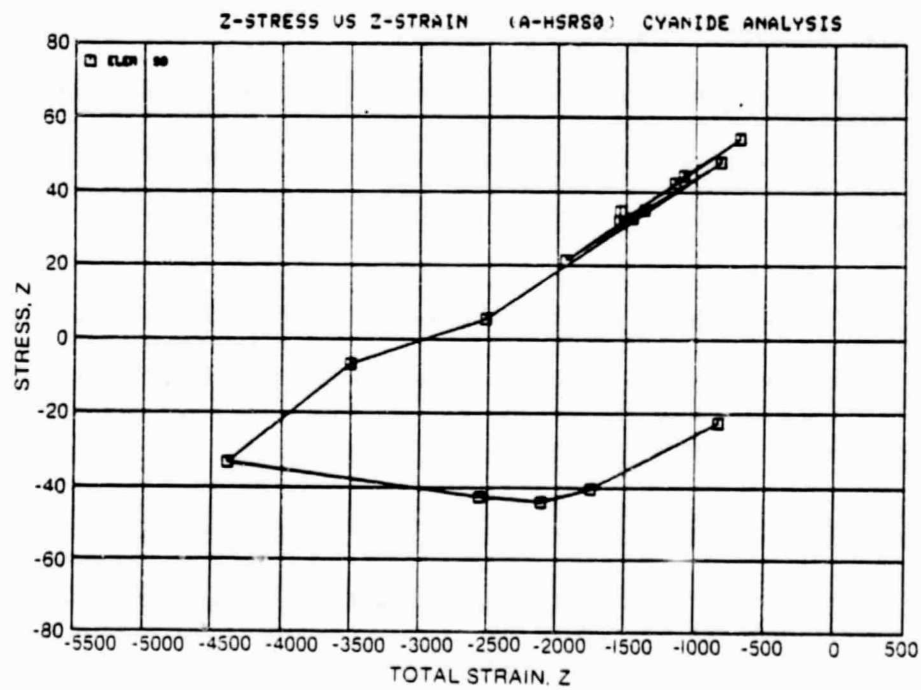

Figure 59. Z-Direction Stress-Strain Cycle at Center of Hot Spot for Base Case (1).

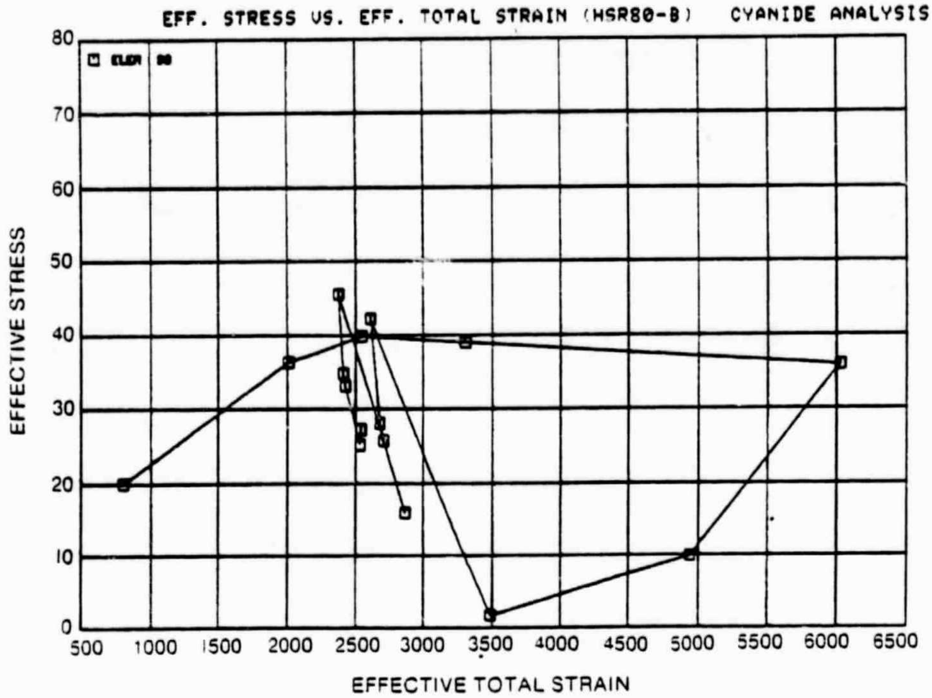

Figure 60. Effective Stress Versus Effective Strain at Center of Hot Spot for Case 2.

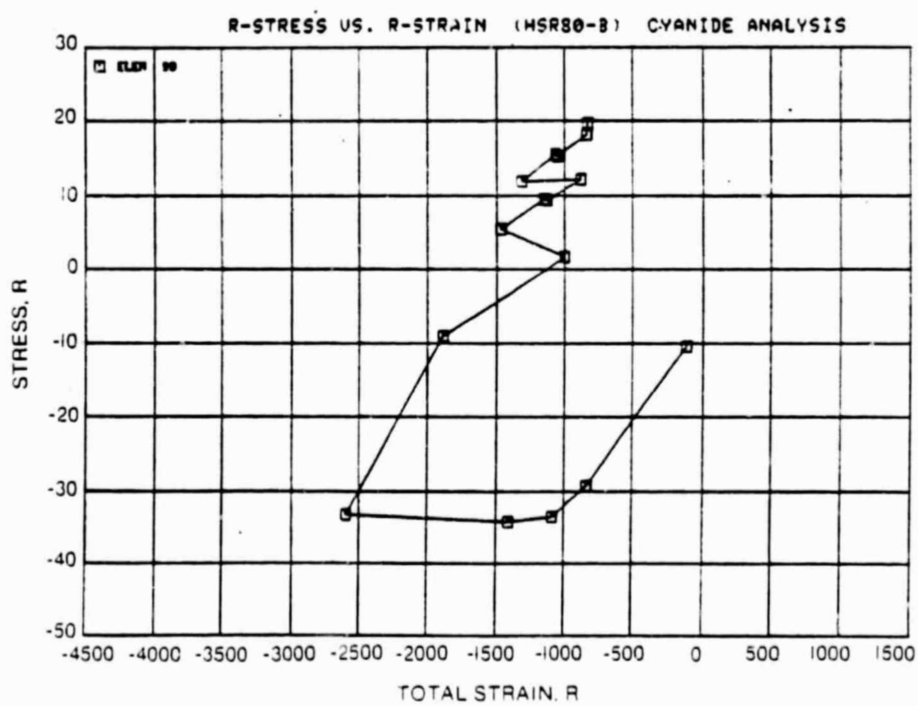

Figure 61. R-Direction Stress-Strain Cycle at Center of Hot Spot for Case 2.

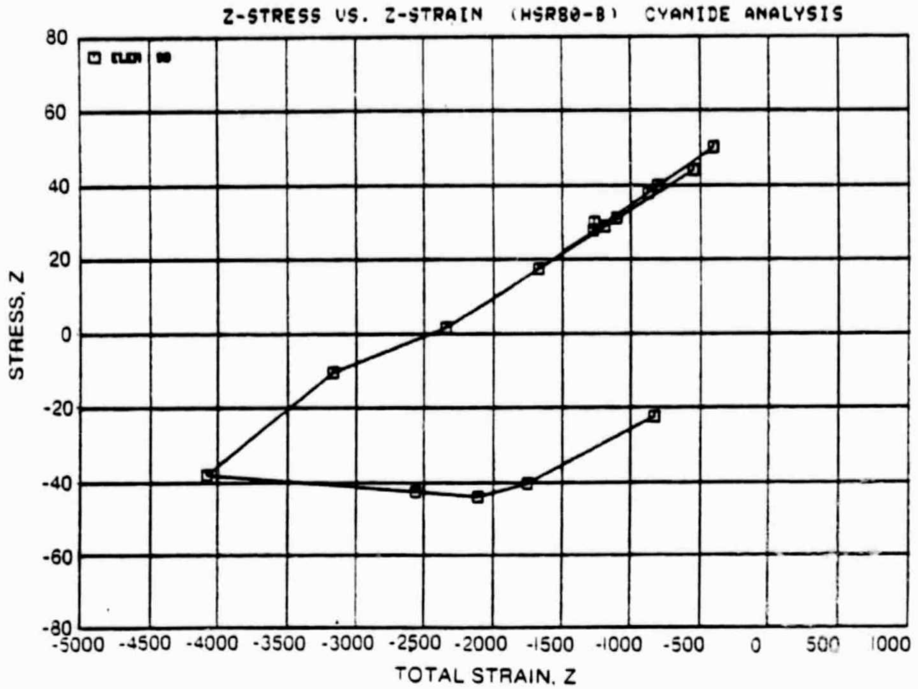

Figure 62. Z-Direction Stress-Strain Cycle for Center of Hot Spot for Case 2.

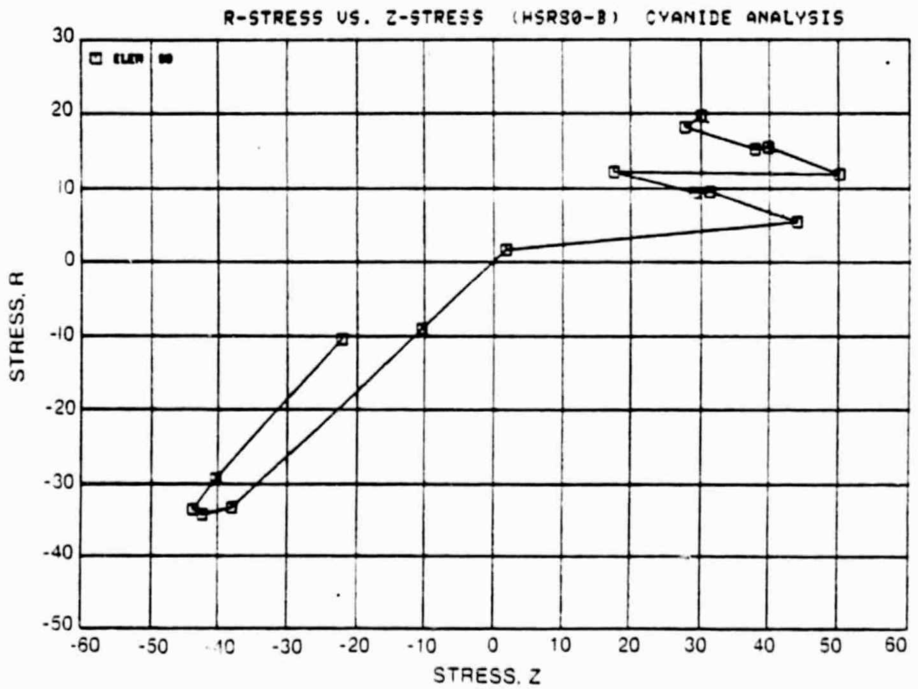

Figure 63. R-Direction Stress Versus Z-Direction Stress at Center of Hot Spot for Case 2.

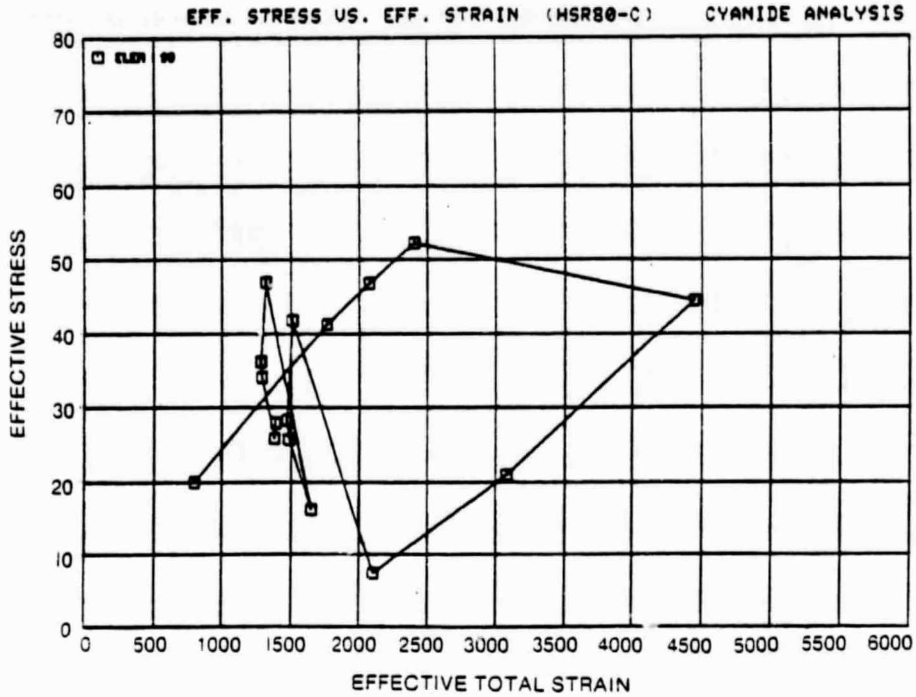

Figure 64. Effective Stress Versus Effective Strain at Center of Hot Spot for Case 3.

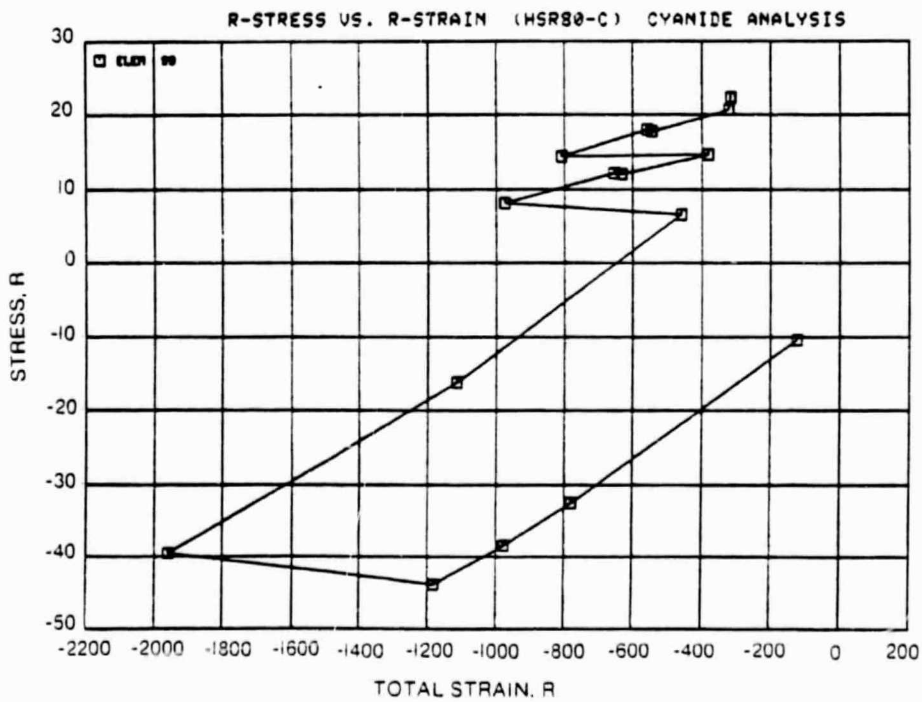

Figure 65. R-Direction Stress-Strain Cycle at Center of Hot Spot for Case 3.

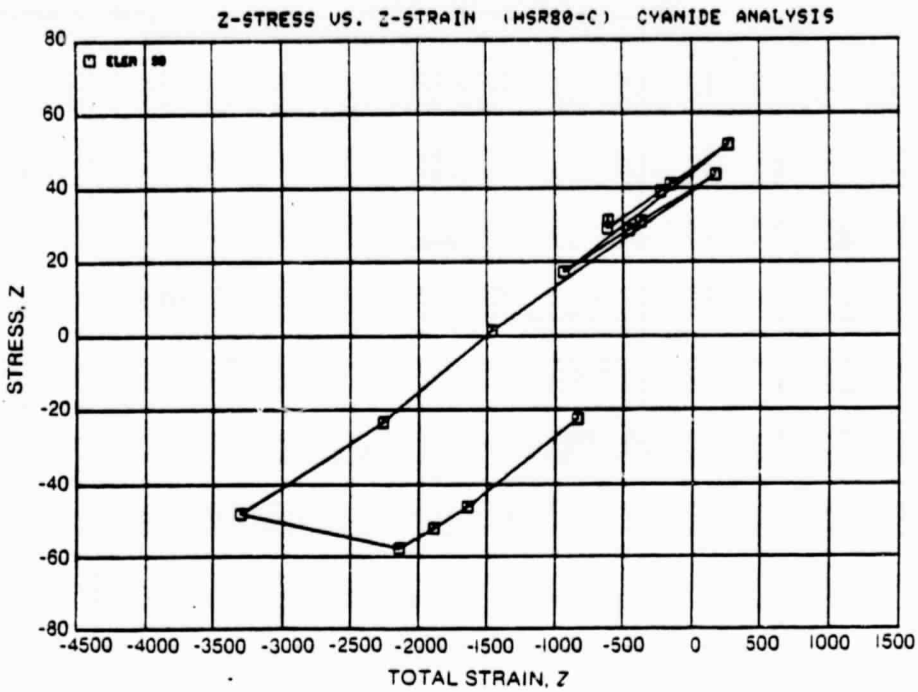

Figure 66. Z-Direction Stress-Strain Cycle at Center of Hot Spot for Case 3.

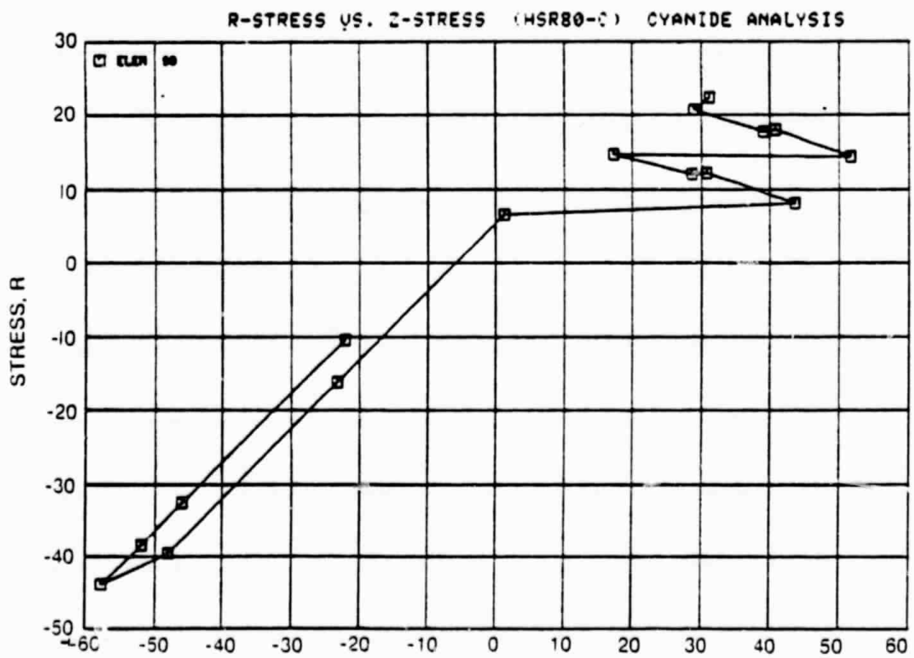

Figure 67. R-Direction Stress Versus Z-Direction Stress at Center of Hot Spot for Case 3.

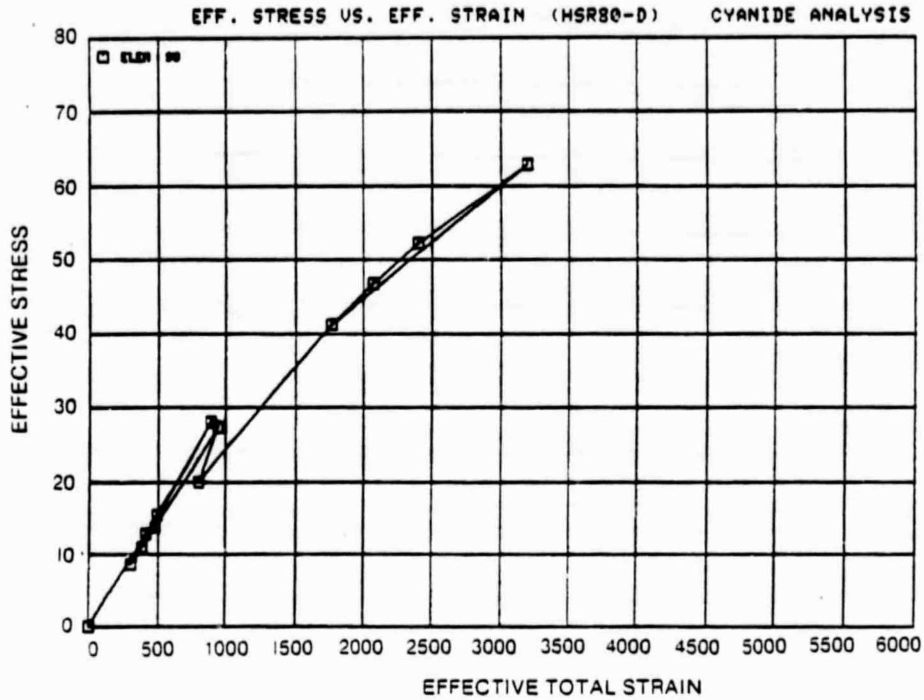

Figure 68. Effective Stress Versus Effective Strain at Center of Hot Spot for Case 4.

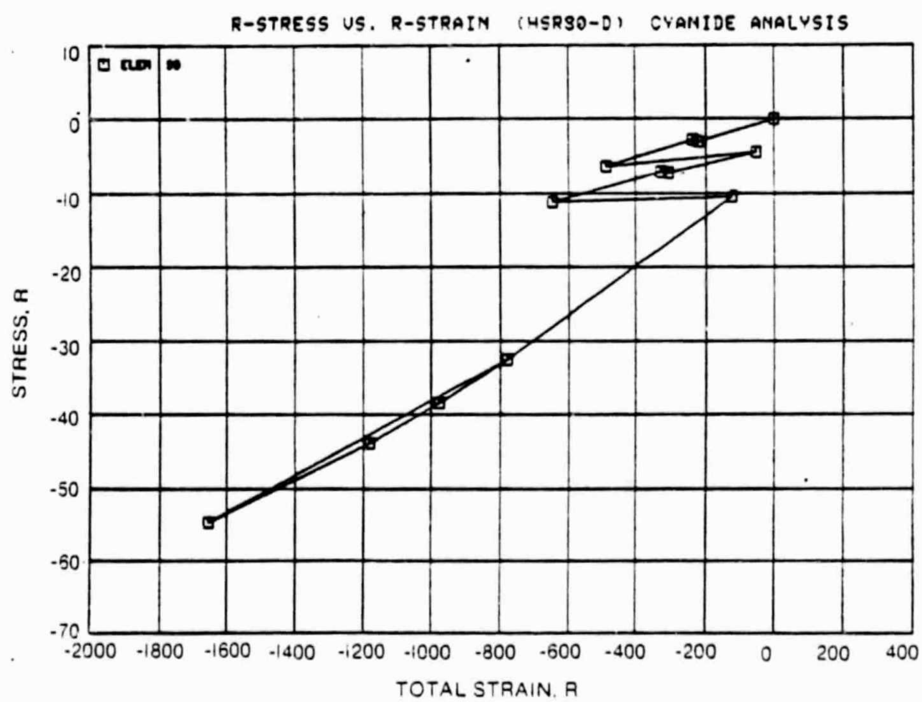

Figure 69. R-Direction Stress-Strain Cycle at Center of Hot Spot for Case 4.

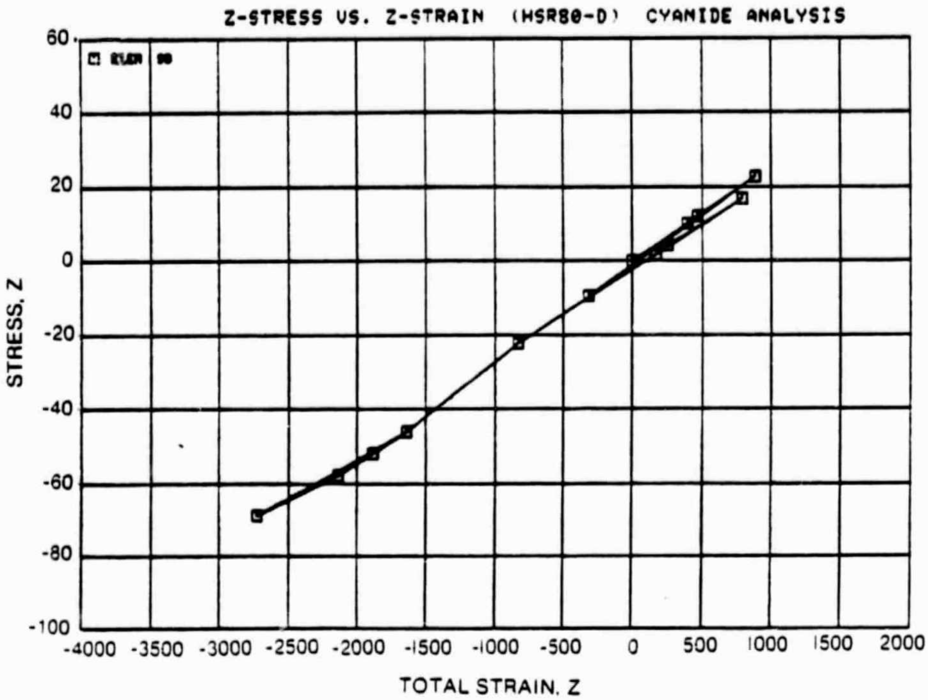

Figure 70. Z-Direction Stress-Strain Cycle at Center of Hot Spot for Case 4.

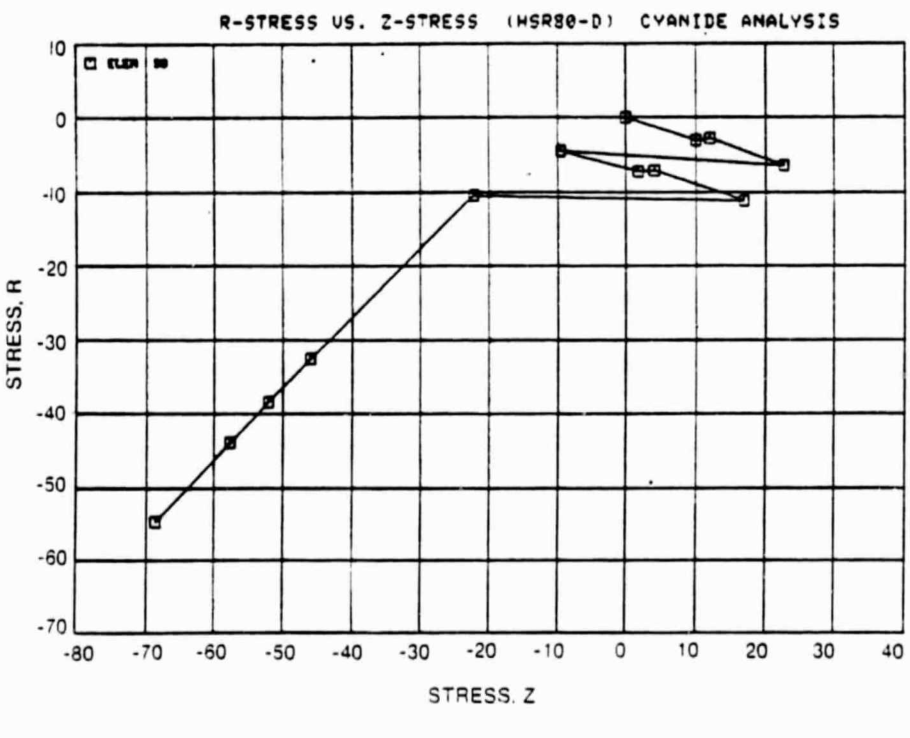

Figure 71. R-Direction Stress Versus Z-Direction Stress at Center of Hot Spot for Case 4.

For a solution of the finite element system of equations:

$$[K]\ \{\delta\} = \{F\}$$

suppose there is a numerical solution for the displacement, $\{\delta^*\}$. Then the equilibrium or residual force vector is generated:

$$\{R\} = \{F\} - [K]\ \{w^*\}$$

A perfect solution would result in this vector containing all zeros. Given the finite numerical accuracy of the computer, this is impossible. Therefore, a measure of the numerical "goodness" of the solution is to be found in how much this vector deviates from zero. Decisions on whether to re-solve or redefine the problem can be based on the total and local deviations from zero. If a few local degrees of freedom are out of equilibrium, this might suggest a local remeshing. If the total equilibrium is deficient, this will require remeshing and/or re-solving with greater numerical accuracy.

The decision tree for this is as follows

1. $\left\{\begin{array}{l}\text{If } \Sigma R_i < C_R \\ \text{and all } R_i < C_{R_{iL}}\end{array}\right\}$ the solution is good

2. If $\Sigma R_i > C_R$
   and [Number of nodes with $C_{R_{iL}} < R_i < C_{R_{iu}}$] $> C_s$
   then re-solve

3. If $\Sigma R_i > C_R$
   and [Number of nodes with $R_i > C_{R_{iu}}$] $< C_s$
   then remesh and re-solve

4. If $R_i < C_R$
   but some $R_i > C_{R_{iu}}$
   then remesh and re-solve

where:

R_i = i^{th} residual-free vector

C_R = Maximum allowable sum of R_i

$C_{R_{iL}}$ = Lower bound for Ri for possible remeshing

$C_{R_{iu}}$ = Maximum allowable upper bound for R_i

Once an acceptable displacement solution has been reached, proceed to the element level. If, at the elastic level, stresses and strains are linearly connected, only one of these two needs to be evaluated. Strain will be checked. The total strain at each calculation point in an element is made up of an elastic strain and a thermal strain:

$$\epsilon_i = \epsilon_i^e + \epsilon_i^\tau$$

One aspect of this program is the establishment of acceptable strain gradients for different element types. Between adjacent strain calculation points in one element, and probably over the entire element, a strain gradient would not be chosen that could encompass an elastic-plastic-elastic or a plastic-elastic-plastic variation. Therefore,

if

$$\epsilon_i^e - \epsilon_j^e \geq | 2\epsilon_{yield} |,$$

remesh this element.

Additionally, there will be a change in sign. Therefore,

if

$$\frac{\epsilon_i^\tau}{\epsilon_j^\tau} < 0$$

remesh this element.

Once the nonlinear solution has been entered, the element level checks become more complex and more important. The total strain is now made up of the elastic strain, thermal strain, plastic strain, and creep strain:

$$\epsilon_i = \epsilon_i^e + \epsilon_i^t + \epsilon_i^\rho + \epsilon_i^c$$

Now stress and strain are no longer linearly connected; stress is a function of elastic strain only. Once again, between any two adjacent calculation points within one element, an elastic strain gradient greater than the allowable material elastic gradient is not desirable. Thus,

if

$$\epsilon_i^e - \epsilon_j^e \geq | 2\epsilon_{yield} |,$$

remesh this element. The limit on the thermal strain would still be retained.

If

$$\frac{\varepsilon^{\tau}_{i}}{\varepsilon^{\tau}_{j}} < 0 \quad \text{, remesh this element.}$$

The next check is on the computed plastic and creep strain. No sign changes in either of these are allowed. In addition, a maximum gradient is set.

if

$$\frac{\varepsilon^{\rho}_{i}}{\varepsilon^{\rho}_{j}} < 0$$

or

$$\frac{\varepsilon^{c}_{i}}{\varepsilon^{c}_{j}} < 0$$

or

$$| \varepsilon^{\rho}_{i} - \varepsilon^{\rho}_{j} | > C_{P}$$

or

$$| \varepsilon^{c}_{i} - \varepsilon^{c}_{j} | > C_{C},$$

remesh this element.

Next, proceed to the interelement level check. These are of the same nature as the above, but now involve adjacent calculation points in adjacent elements.

2.6.3 Self-Adaptive Solution Strategies

In the development of basic self-adaptive solution strategies, we are using the work of Edward T. Wilson of the University of California at Berkeley, and Joseph Padovan and Surapong Tovichakehaikul of the University of Akron.

Wilson's efforts are directed toward an overall solution strategy, while Padovan's and Tovichakchaikul's work is on load incrementing and time-stepping for geometrical and material nonlinear solutions.

Wilson's philosophy on internal program organization for SAP-80 computer programs is applicable to the Component-Specific Modeling Program, with some extensions. He suggests that the basic internal organization of a computer program for structural analysis depends strongly on the method used to form and solve linear equations, with the frontal and profile (or active column) methods most often used. Both have the exact same economy so that the choice must be based on other factors.

In the frontal method, element stiffnesses and solutions of equations are formulated in a joint sequence manner. Therefore, all element stiffness subroutines, the equation solver, and the front of the stiffness matrix must be in core storage (or rolled in and out) during the reduction of the stiffness matrix. For the profile approach, the formation of all element stiffnesses for a particular type of element can be accomplished by a single call to one program segment. The formation of the total stiffness is a separate program segment in which the element stiffnesses are read in sequence from secondary storage and the total stiffness matrix is formed in active column blocks. In this case, the actual solution phase is another separate program link. Evaluation of substructure stiffnesses, calculations of mode shapes and frequencies, and evaluations of reactions and member forces are all separate links. This clear uncoupling of different phases of the program gives the profile approach a clear advantage in modularity and adaptive solution techniques. Also, the profile approach has no significant disadvantages when compared to the frontal method.

Padovan and his coworkers at the University of Akron have been developing "Self-Adaptive Incremental Newton-Raphson Algorithms" for nonlinear problems. They use a three-level approach. In the first level, incremental Newton-Raphson operators are used to "tunnel" into the problem solution space. The second level involves the constant monitoring of the different stages of solution through various quality/convergence/nonlinearity tests. The third level works with the results of the second level. The violation of any of the quality/convergences/nonlinearity tests triggers various scenarios for modifying the incremental Newton-Raphson strategy. The self-adaptive modifications triggered by the third level fall into one of three categories: global stiffness reformation; preferential, local reformation; or load increment adjustment. Recently, they have developed constrained, self-adaptive solution procedures for structures subject to high temperature elastic/plastic/creep effects. In this, they used closed, piecewise, continuous least-upper-bounding constraint surfaces that control the size of successive dependent variable excursions arising out of the time-stepping process.

A list of parameters to be controlled by the self-adaptive solution strategies has been generated. The parameters defined to date are listed below.

Parameters to be Controlled

1. Element Type(s)
2. Type(s) of Integration
3. Order(s) of Numerical Quadrature
4. Maximum Number of Iterations
5. Tolerance(s) on Convergence
6. Constitutive Equation(s)
7. Yield Criterion (Criteria)
8. Load Increments
9. Time Increments
10. Nonlinear Solution Algorithm(s)

Experience with the in-house programs has given us a good basis for developing the necessary tolerances on convergence. First, convergence is evaluated locally, not globally; that is, it is evaluated at each element or each numerical integration point. Second, for numerical conditioning, limits should be set below which inelastic strains are considered to be zero. Third, for time-dependent effects, both temperature and stress cutoffs should be established below which time dependent inelastic strain is considered to be zero. Then the local convergence criteria for incremental analysis are the following.

Time Independent

If

$$Ep < PCUTOFF, \ \epsilon p \equiv 0.0$$

then

$$\Delta\epsilon p_I < TOL = CONVERGENCE$$

or

$$\frac{\Delta\epsilon p_I - \Delta\epsilon p\ (I-1)}{\Delta\epsilon p_I} < TOL = CONVERGENCE$$

Time Dependent

If

$$TEMP < TOLC, \ \epsilon_c \equiv 0.0$$

and/or

$$\sigma_e < \sigma_c, \ \epsilon_c \equiv 0.0$$

then

$$\Delta\sigma_{eI} < \text{CTOL} = \text{CONVERGENCE}$$

or

$$\frac{\Delta\sigma_{EI} \ \Delta\sigma_{E(I-1)}}{\Delta\sigma_{EI}} < \text{CTOL} = \text{CONVERGENCE}$$

The different convergence criteria are dictated by the wide material strength levels encountered in nonlinear analysis. We have also discovered that it is advantageous to be able to change these criteria during the course of an incremental analysis.

One approach taken in nonlinear computer codes is the right-hand-side technique, in which the plasticity is accounted for by adding an additional force vector to the right-hand side of the system of equations

$$[K]\ \{d\} = \{F\} + \{f_p\}$$

The basic logic is as follows:

1. Solve for displacements from

$$[K]\ \{d\} = \{F\} + \{f_p\}$$

2. Using the displacements and the constitutive equations, determine elastic and plastic strains for each element.

3. Check convergence.

4. Make an estimate of plastic strains that will satisfy the constitutive equations, equilibrium, and compatibility.

5. Based on the estimate of plastic strains from Step 4, form a new plastic load vector and go back to Step 1.

This iteration scheme continues until the convergence criteria are satisfied.

The plastic iteration accounts for a considerable portion of the total computer cost in running a nonlinear finite element code. Substantial improvements have been made in accelerating the convergence of plastic iteration by improving the estimate of the solution in Step 4. Three options are now available.

The first of these schemes is the simplest, and uses the current calculation of plastic strain from the constitutive equations as the estimate of the solution. This is the usual method on right-hand-side iteration schemes.

The second scheme is a modification of the original iteration scheme, and is essentially a successive-over-relaxation (SOR) scheme. The estimate of the solution is given by:

$$\hat{\epsilon}_p^i = \epsilon_p^{i-1} + \alpha \left(\epsilon_p^i - \epsilon_p^{i-1} \right)$$

$\hat{\epsilon}_p^i$ = current estimate of solution

ϵ_p^{i-1} = previous calculation of plastic strain from constitutive equations

ϵ_p^i = current calculation of plastic strain from constitutive equations

α = current acceleration factor

α = 1.5 is used.

This estimation procedure continues until $\epsilon_p^i < \epsilon_p^{i-1}$, then the following is used:

$$\epsilon^i = \epsilon^{i-1} + 0.5 \left(\epsilon_p^i - \epsilon^{i-1} \right)$$

The third scheme is based on an Aitken's extrapolation formula for a fixed-point iteration. Although we are not really doing a fixed-point iteration, the finite element equations behave in much the same way. The equation used in estimating the solution is:

$$\hat{\epsilon}_p^i = \epsilon_p^{i-2} - \frac{\left(\epsilon_p^{i-1} - \epsilon_p^{i-2} \right)^2}{\epsilon_p^i + 2\epsilon_p^{i-1} + \epsilon_p^{1-2}}$$

Where the symbols are as before and ϵ_p^{i-2} = calculation of plastic strain from the constitutive equations two iterations ago.

The Aitken's extrapolation works best when performed every third iteration. In between Aitken's extrapolations

$$\hat{\epsilon}_p^i = \epsilon_p^i$$

C.2

is used. This equation is also used when the denominator in the Aitken's equation approaches zero.

Test cases using the bolthole model of Figure 72 loaded in tension have been run. Comparisons of the number of iterations needed are shown in Figure 73 for the various iteration schemes.

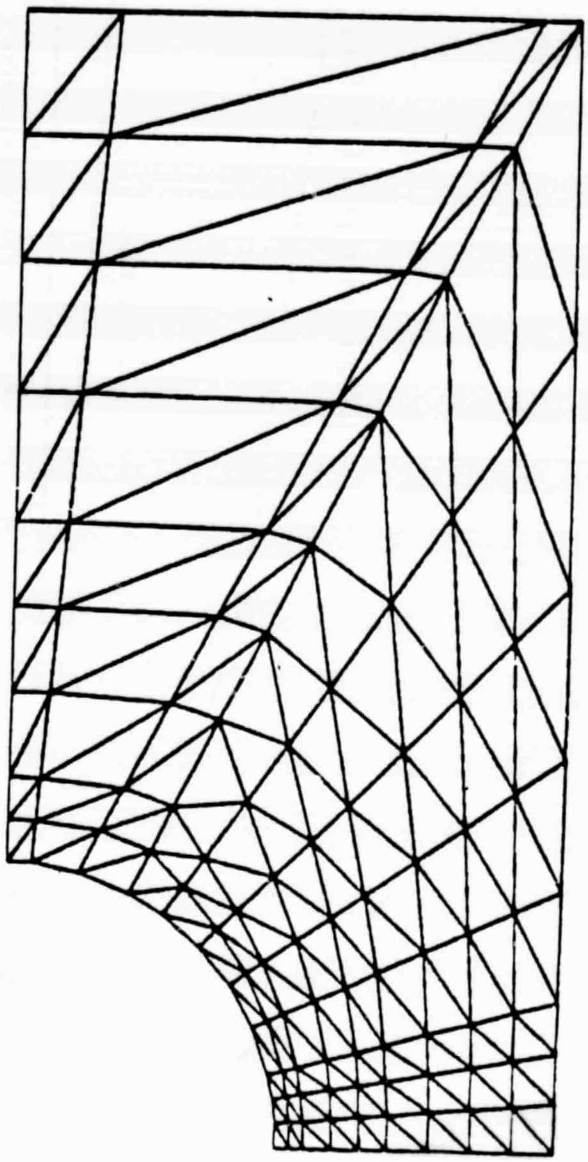

Figure 72. Iteration Test Case.

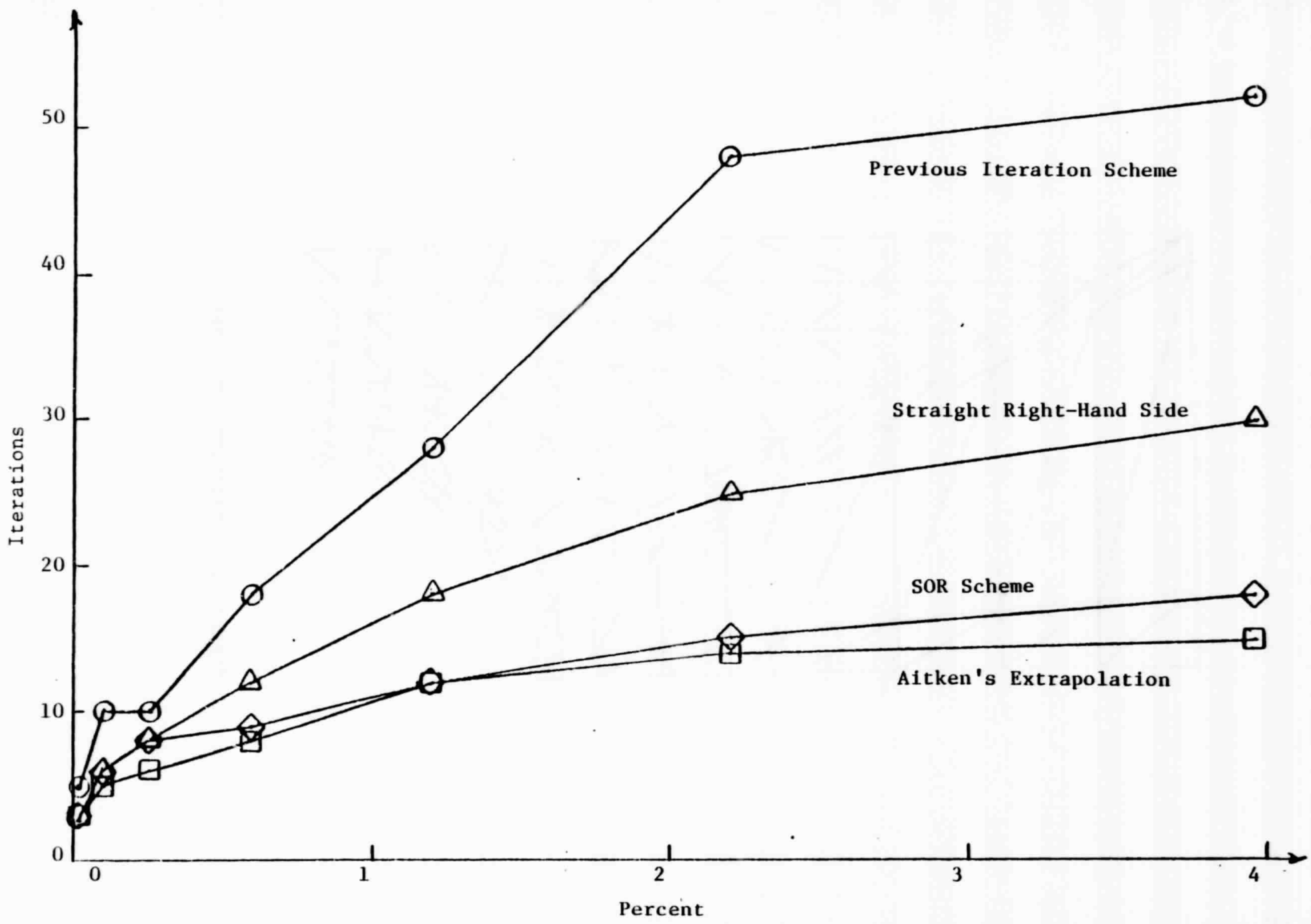

Figure 73. Effective Plastic Strain in Percent Radius.

APPENDIX A

LITERATURE IN HAND

APPENDIX A

LITERATURE IN HAND

1. Padovan, J. and Tovichakchaikul, S., "Self-Adaptive Predictor-Corrector Algorithms for Static Non-Linear Structural Analysis," Computer Structures 15, 365-377 (1982).

2. Padovan, J. and Tovichakchaikul, S., "On The Solution of Creep Induced Buckling in General Structure," Computer Structures 15, 379-392 (1982.)

3. Liw, W.K. and Belytschko, T., "Mixed-Time Implicit-Explicit Finite Elements for Transient Analysis," Computer Structures 15, 445-450 (1982).

4. Zhang, L. and Owen, D.R.J., "A Modified Secant Newton Method for Non-Linear Problems," Computer Structures 15, 543-547 (1982).

5. Zienkiewicz, O.C. and Parekh, C.J., "Transient Field Problems: Two-Dimensional and Three-Dimensional Analysis by Isoparametric Finite Elements," Int. J. Num. Metho. Engrg. 2, 61-71 (1970).

6. Stricklin, J.A. and Haider, W.E., "Formulations and Solution Procedures for Nonlinear Structural Analysis," Computer Structures 7, 125-136 (1977).

7. Barsoum, R.S., "A Convergent Method for Cyclic Plasticity Analysis with Application to Nuclear Components," Int. J. Num. Meth. Engr. 6, 227-236 (1973).

8. Powell, G. and Simons J., "Improved Iteration Strategy for Nonlinear Structures," Int. J. Num. Meth. Engrg. 17, 1455-1467 (1981).

9. Levy, A. and Pifko, A.B., "On Computational Strategies for Problems Involving Plasticity and Creep," Int. J. Num. Meth. Engrg. 17, 747-771 (1981).

10. Tsybenko, A.S., Vashchenko, N.G., Krishchuk, N.G., and Kulakooskii, V.N., "Automatic Formulation of Triangular-Element Grid for Arbitrary Plane Regions," Translated from Problems Prochnosti, 12, 84-89 (1980).

11. Sobreszczanski, A., Sobieski, J., and Hajela, R., "Accuracy of an Approximate Static Structural Analysis Technique Based on Stiffness Matrix Eigenmodes," AIAA Paper No. 79-0748.

12. Bergan, P.G., Horrigmoe, G., Krikeland, B., and Soreide, T.H., "Solution Techniques for Nonlinear Finite Element Problems," Int. J. Num. Meth. Engrg. 12, 1677-1696 (1978).

13. Jirousek, J. and Teodorescu P., "Large Finite Elements Method for the Solution of Problems in the Theory of Elasticity," Computer Structures 15, 575-587 (1982).

LITERATURE IN HAND

14. Sorek, S. and Blech, J.J., "Finite-Element Technique for Solving Problems Formulated by Hamilton's Principle," Computer Structures 15, 533-541 (1982).

15. Bausha, I. and Rheinboldt, W.C., "Adaptive Approaches and Reliability Estimations in Finite Element Analysis," Computer Meth. Appl. Mech. Engrg. 17/18, 519-540 (1979).

16. Boyle, E.T. and Jennings, A., "Accelerating The Convergence of Elastic-Plastic Stress Analysis," Int. J. Num. Meth. Engr. 7, 232-235 (1973).

17. Morjaria, M., Sarihan, V., and Mukherjz, S., "Comparison of Boundary Element and Finite Element Methods In Two-Dimensional Inelastic Analysis," DOE Report No. COO-2733-22 (1979).

18. Rzasnicki, W., Mendelson, A., Albers, L.U., and Raftoponlos, D.D., "Application of Boundary Integral Method to Elastoplastic Analysis of V-Notched Beams," NASA TN D-7637 (1974).

19. Katz, C. and Werner, H., "Implementation of Nonlinear Boundary Conditions in Finite Element Analysis," Computer Structures 15, 299-304 (1982).

20. Tong, P., Maw, S.T., and Pian, T.H.H., "Derivation of Geometric Stiffness and Mass Matrices for Finite Element Hybrid Models," Int. J. Solids Structures 10, 919-932 (1974).

21. Olderson, R.G., Tani, M.A., Tree, D.J., and Hill, R.J., "A Three-Dimensional Approach to the Optimization of a Gas Turbine Disk and Blade Attachment," AIAA Paper No. 75-1312 (1975).

22. Rice, J.R., "On the Structure of Stress-Strain Relations for Time-Dependent Plastic Deformation in Metals," Journal Appl. Mech. 728-737 (1970).

23. Ponter, A.R.S. and Leckie, F.A., "Constitutive Relationships for the Time-Dependent Deformation of Metals," J. Engrg. Mat. Tech. 47-51 (1976).

24. Gittus, J.H., "Dislocation-Creep Under Cyclic Stressing: Physical Model and Theoretical Equations," Acta Metal. 26, 305-317 (1978).

25. Allen, J.M., "Effect of Temperature Dependent Mechanical Properties on Thermal Stress in Cooled Turbine Blades," Journal Engrg. Power 1-5 (1981).

26. Kaufman, A. and Gaugler, R., "Cyclic Structural Analyses of Air-Cooled Gas Turbine Blades and Vanes," SAE Paper No. 760918 (1976).

APPENDIX A (Continued)

LITERATURE IN HAND

27. Peterson, M.R., Alderson, R.G., Stockton, R.J., and Tree, D.J. "Three-Dimensional Finite-Element Techniques for Gas Turbine Blade Life Prediction."

28. Allen, J.M. and Erickson, L.B., "NASTRAN Analysis of a Turbine Blade and Comparison with Test and Field Data," ASME Paper No. 75-GT-77 (1975).

29. Wolf, D.S., "Stress Analysis of a First Turbine Vane Using a Three-Dimensional Model with Nonlinear Material Behavior Subjected to Transient Temperatures," AIAA 81-1437 (1981).

30. Kaufman, A. and Gangler, R.E., "Thermal-Structural Mission Analyses of Air-Cooled Gas Turbine Blades," ASME Paper No. 79-GT-19 (1979).

31. Requicha, A.A.G. and Voelcker, H.B., "Solid Modeling: A Historical Summary and Contemporary Assessment," IEEE CG&A, March 1982.

32. Boyse, J.W. and Gelchrist, J.E., "GM Solid: Interactive Modeling for Design and Analysis of Solids," IEEE CG&A, March 1982.

33. Hillyard, R., "The Build Group of Solid Modelers," IEEE CG&A, March 1982.

34. Brown, C.M., "PADL-2: A Technical Summary," IEEE CG&A, March 1982.

35. Klein, S. and Trujillo, D.M., "An Unconditionally Stable Finite Element Analysis for Nonlinear Structures," Computer Structures 16, 187-197 (1983).

36. Padovan, J. and Tovichakchaikul, S., "On The Solution of Elastic - Static and Dynamic Postbuckling Collapse of General Structure," Computer Structures 16, 199-205 (1983).

37. Ghabrial, M.A.E. and Wellford, L.C., Jr., "An Averaged LaGrangian-Finite Element Technique for the Solution of Nonlinear Vibration Problems," Computer Structures 16, 207-214 (1983).

38. LeMaster, R.A., "A Theoretical and Numerical Comparison of Three Finite Strain Finite Element Formulations for Elastic-Viscoplastic Materials," Computer Structures, 16, 215-222 (1983).

39. Allen, D.H., "Computational Aspects of the Nonisothermal Classical Plasticity," Computer Structures 15, 589-599 (1982).

LITERATURE IN HAND

40. Backlund, J. and Wennerstrom, H., "Finite Element Analysis of Elasto-Plastic Shells," Int. J. Num. Meth. Engrg. 8, 415-424 (1974).

41. Knothe, K. and Muller, W., "Some Remarks on the Elastic-Plastic Limit Load Analysis of a Plane V-Notched Specimen," Int. J. Mech. Sci. 22, 167-172 (1980).

42. Hunsaker, B., Jr., Vaughan, D.K., Stricklin, J.A., and Haisler, W.E., "A Comparison of Current Work-Hardening Models Used in the Analysis of Plastic Deformation," Texas A&M University, TEES-RPT-2926-73-3 (1973).

43. Owen, D.R.J., Prakash, A., and Zienkiewicz, O.C., "Finite Element Analysis of Nonlinear Composite Materials By Use of Overlay Systems," Computer Structures 4, 1251-1267 (1974).

44. Montogue, P. and Horne, M.R., "Elastic-Plastic Axisymmetric Analysis of a Thin-Walled Cylindrical Shell Subjected to a Radial Pressure Difference," J. Appl. Mech. Paper No. 68-APM-AA (1968).

45. Berman, I., Rao, M.S.M., and Gupta, G.D., "Full Life Elastic-Plastic-Creep Analysis and Comparison to Tests of Axially Cycled Pressurized Tubular Specimens," ASME 82-PVP-72 (1982).

46. Rao, M.S.M., Naryanan, T.V., and Gupta, G.D., "Inelastic Analysis of Non-axisymmetrically Heated Thick Cylindrical Shells," J. Pres. Ves. Tech. 101, 234-241 (1979).

47. Jhansale, H.R. and Sharma, G.K., "Inelastic Behavior of Structural Metals Under Complex Cyclic Loadings," AIAA/ASME Paper No. 77-366 (1977).

48. Iwan, W.D., "On a Class of Models for the Yielding Behavior of Continuous and Composite Systems," J. Appl. Mech. 612-617 (1917).

49. Drucker, D.C. and Palgen, L., "On Stress-Strain Relations Suitable for Cyclic and Other Loading," J. Appl. Mech. 48, 479-485 (1981).

50. Besseling, J.F., "A Theory of Plastic Flow for Anisotropic Hardening in Plastic Deformation of an Initially Isotropic Material," Nat. Aero. Res. Inst. Report 5.410 (1953).

51. Wroz, Z., "An Attempt to Describe the Behavior of Metals Under Cyclic Loads Using a More General Work Hardening Model," Acta Mechanica 7, 199-212 (1969).

52. DeKoning, A.U., "A Continuum Theory of Time Independent Plasticity Based on a Volume Fractions Model," NLR The Netherlands, NLR MP 77017 U (1978).

APPENDIX A (Continued)

LITERATURE IN HAND

53. Williams, J.F. and Svensson, N.L., "A Rationally Based Yield Criterion for Work Hardening Materials," Mechanica 6, 104-114 (1971).

54. Baladi, G.Y., "Numerical Implementation of a Transverse-Isotropic Inelastic, Work-Hardening Constitutive Model," Nuc. Engrg. Design 46, 263-272 (1978).

55. Wells, C.H., "An Analysis of the Bauschinger Effect in Some Engineering Alloys," ASME Paper No. 47-WA (Met-1) (1967).

56. Radomski, M. and White, D.J., "Some Theoretical Considerations Relating to Strain Concentration in Elastic-Plastic Bending of Beams," J. Strain Analysis 3, 304-312 (1968).

57. White, D.J. and Radomski, M., "Strain Concentration in Beams Under Cyclic Plastic Straining," J. Strain Analysis 3, 313-324 (1968).

58. Malinin, N.N. and Niquin, A.A., "The Influence of Stress Concentration on Creep Rupture at Nonstationary Loading," Int. J. Mech. Sci. 19, 521-531 (1977).

59. Kiselev, V.A. and Semishkin V.P., "Stress State Kinetics Near Stress Raisers Under High-Temperature Creep Conditions," Problemy Prochnostic 2, (1981).

60. Goldman, A. Ya and Tsygavkoo, S.A., "Model of a Physically Nonlinear Viscoelastic Medium for Describing the Creep of Polymers in a Complex Stress State," Problemy Prochnosti 2, 14-18 (1981).

61. Pospishil, B., "Relation Between Creep Equation Coefficients and Damage Accumulation," Problemy Prochnosti 2, 19-22 (1981).

62. Nikutenko, A.F., "Effect of Prior Creep Strain on Instantaneous Elastoplastic Deformation of a Material," Problemy Prochnosti 2, 23-26 (1981).

63. Hayhurst, D.R., "Creep Rupture Under Multi-Axial States of Stress," Journal Mech. Phys. Solids 20, 381-390 (1972).

64. Bui-Qnoc, T., "An Engineering Approach for Cumulative Damage in Metals Under Creep Loading," Journal Engrg. Mat. Tech. 101, 337-343 (1979).

65. Ponter, A.R.S. and Walter, M.H., "A Theoretical and Experimental Investigation of Creep Problems With Variable Temperature," Journal Appl. Mech. 639-644 (1976).

LITERATURE IN HAND

66. White, J.L., "Finite Elements In Linear Viscoelasticity," AFFDL-TR-18-150 (1967).

67. Gattaso, M. and Abel, J.F., "Interactive-Adaptive, Large Displacement Analysis With Real-Time Computer Graphics," Computer Structures 16, 141-152 (1983).

68. Nour-Omid, B., Parlett, B.N., and Taylor R.K., "A Newton-Lanczos Method for Solution of Nonlinear Finite Element Equations," Computer Structures 16, 241-252 (1983).

69. Weingarten, V.I., Ramanathan, R.K., and Chen, C.N., "Lanczos Eigenvalue Algorithm for Large Structures on a Minicomputer," Comput. Structures 16, 253-257 (1983).

70. Wilson, E.L. and Itoh, T., "An Eigensolution Strategy for Large Systems," Computer Structures 16, 259-265 (1983).

71. Kirsch, U. and Toledano, G., "Approximate Reanalysis for Modifications of Structural Geometry," Computer Structures 16, 269-277 (1983).

72. Rooney, M.F. and Smith, S.E., "Artificial Intelligence in Engineering Design," Computer Structures 16, 279-288 (1983).

73. Lam, H.L., Choi, K.K., and Hang, E.J. "A Sparse Matrix Finite Element Technique for Iterative Structural Optimization," Computer Structures 16, 289-295 (1983).

74. Lewis, D.J. and Hellen, T.K., "Analysis Techniques for Elevated Temperature Applications," Creep and Fatigue in Elevated Temperature Applications 1, 233.1-233.17, Institute of Mechanical Engineering, 1974.

75. Carpenter, W.C. and Gell, P.A.T., "Creep Analysis for a Material Having an Elastoplastic Response," Creep and Fatigue in Elevated Temperature Applications 1, 237.1-237.10, I. Mech. Eng. 1974.

76. Cook, R.D., "Loubigac's Iterative Method In Finite Element Elastostatics," Int. Journal Num. Methods Engineering 18, 67-75 (1982).

77. Allen, J.M., "Effect of Temperature Dependent Mechanical Properties on Thermal Stress in Cooled Turbine Blades," ASME 81-GT-105, 1981.

78. Brown, K.W. and Krabula, J.L., "Linear-Nonlinear Interface for Finite Element Impact Analysis," ASME 81-GT-39, 1981.

79. Gersch, H., "NASA Gas Turbine Stator Vane Ring," ASME 81-GT-208, 1981.

APPENDIX A (Concluded)

LITERATURE IN HAND

80. Sabla, P.E., Taylor, J.R., and Gauntner, D.J., "Design and Development of the Combustor Inlet Diffuser for the NASA/GE Energy Efficient Engine," ASME 81-GT-129, 1981.

81. Downs, B., "The Effect of Substantial Pretwist on the Stiffness Properties of Thin Beams of Cambered Section," J. Appl. Mech. 46, 341-344 (1979).

82. Haber, R. and Abel, J.F., "Discrete Transfinite Mappings for the Description and Meshing of Three-Dimensional Surfaces Using Interactive Computer Graphics, " Int. Journal Num. Methods Engineering 18, 41-66 (1982).

83. Stricklin, J.A. and Haisler, W.E., "Formulations and Solution Procedures For Nonlinear Structural Analysis," Computer Structures 7, 125-136 (1977).

84. Dupuis, G.A., Hibbit, H.D., McNamara, S.F., and Marcal, P.V., "Nonlinear Material and Geometric Behavior of Shell Structures," Computer Structures 1, 233-239 (1971).

85. Haisler, W.E., Stricklin, J.A., and Stebbins, F.J., "Development and Evaluation of Solution Procedures for Geometrically Nonlinear Structural Analyses," AIAA J. 1- , 264-272 (1972).

APPENDIX B

SOFTWARE ARCHITECTURE
FUNCTIONAL ANALYSIS

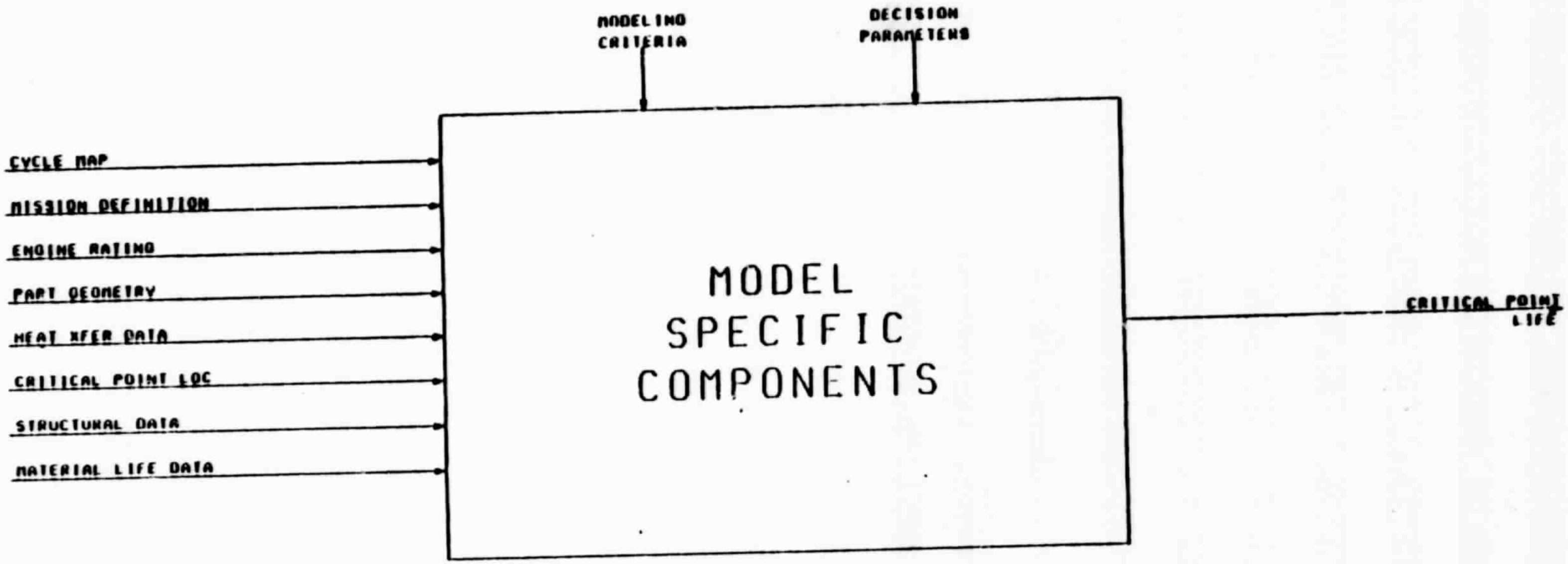

COSMOS - CONTEXT

A-0
REVISION-4

8-10-83

ORIGINAL PAGE IS
OF POOR QUALITY

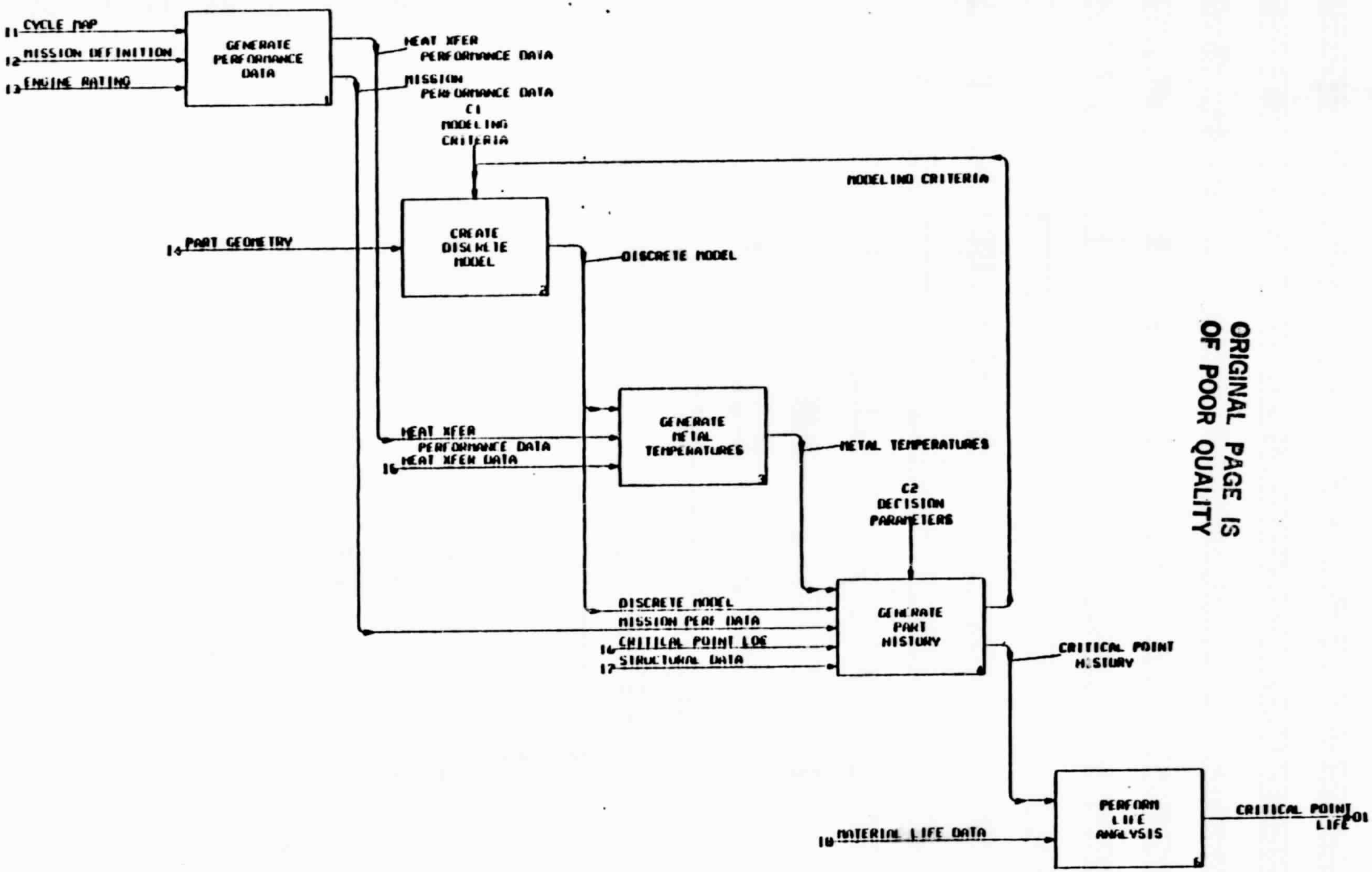

MODEL SPECIFIC COMPONENTS

A0

REVISION- 4

8-10-83

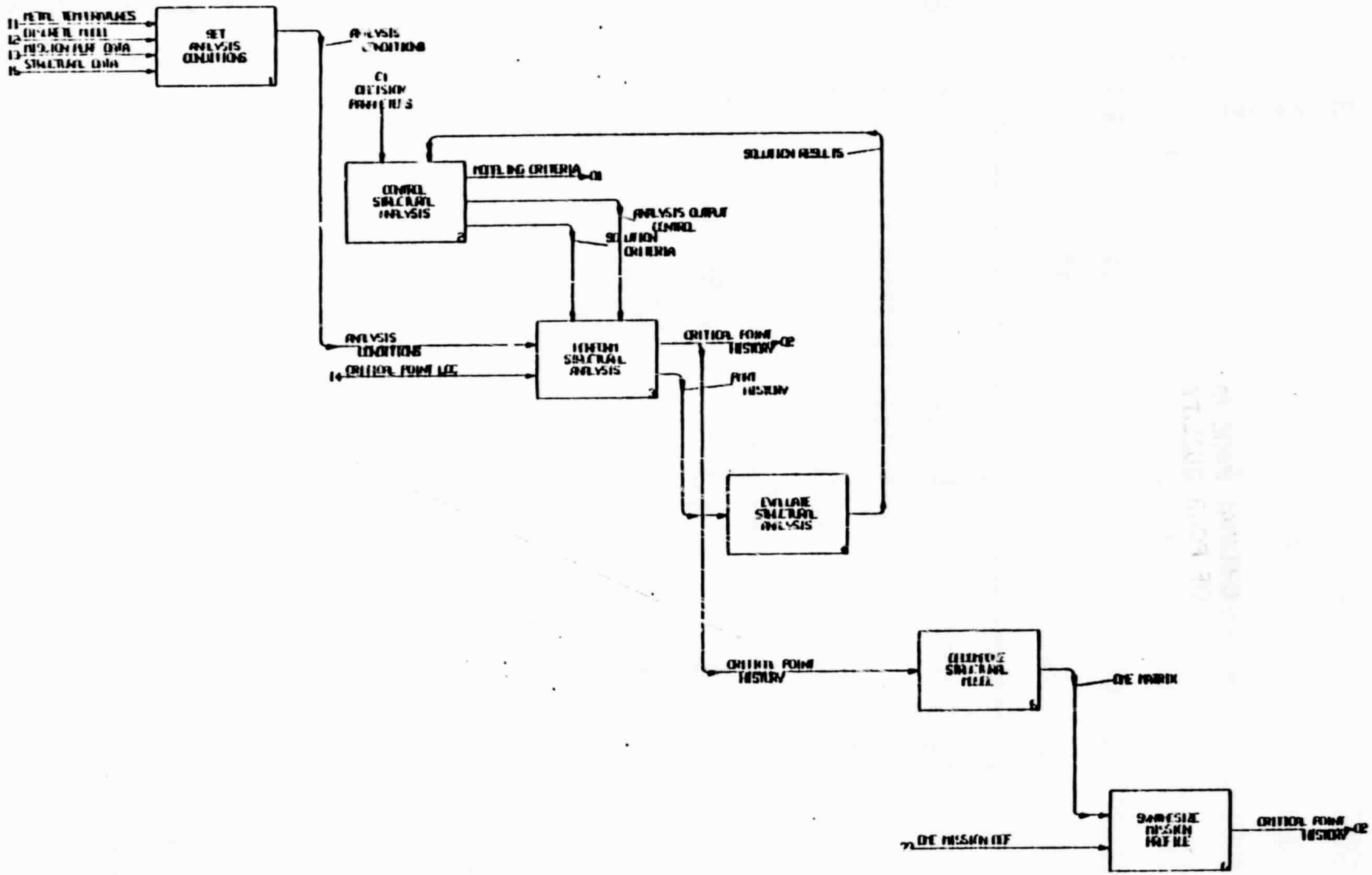

GENERATE PART HISTORY

A4

REVISION- 1

7-22-83

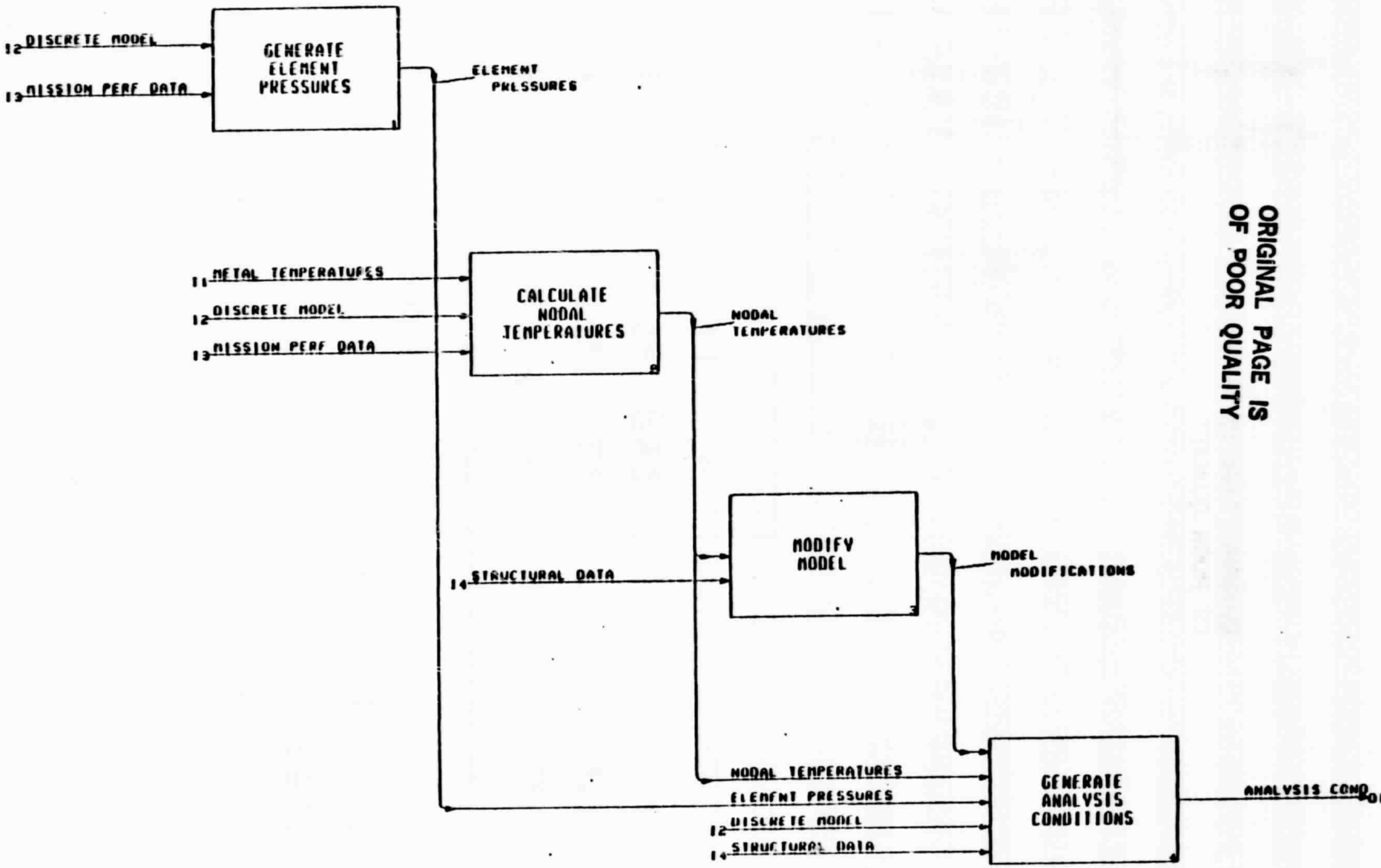

SET ANALYSIS CONDITIONS

A4.1

REVISION- 1

8-10-83

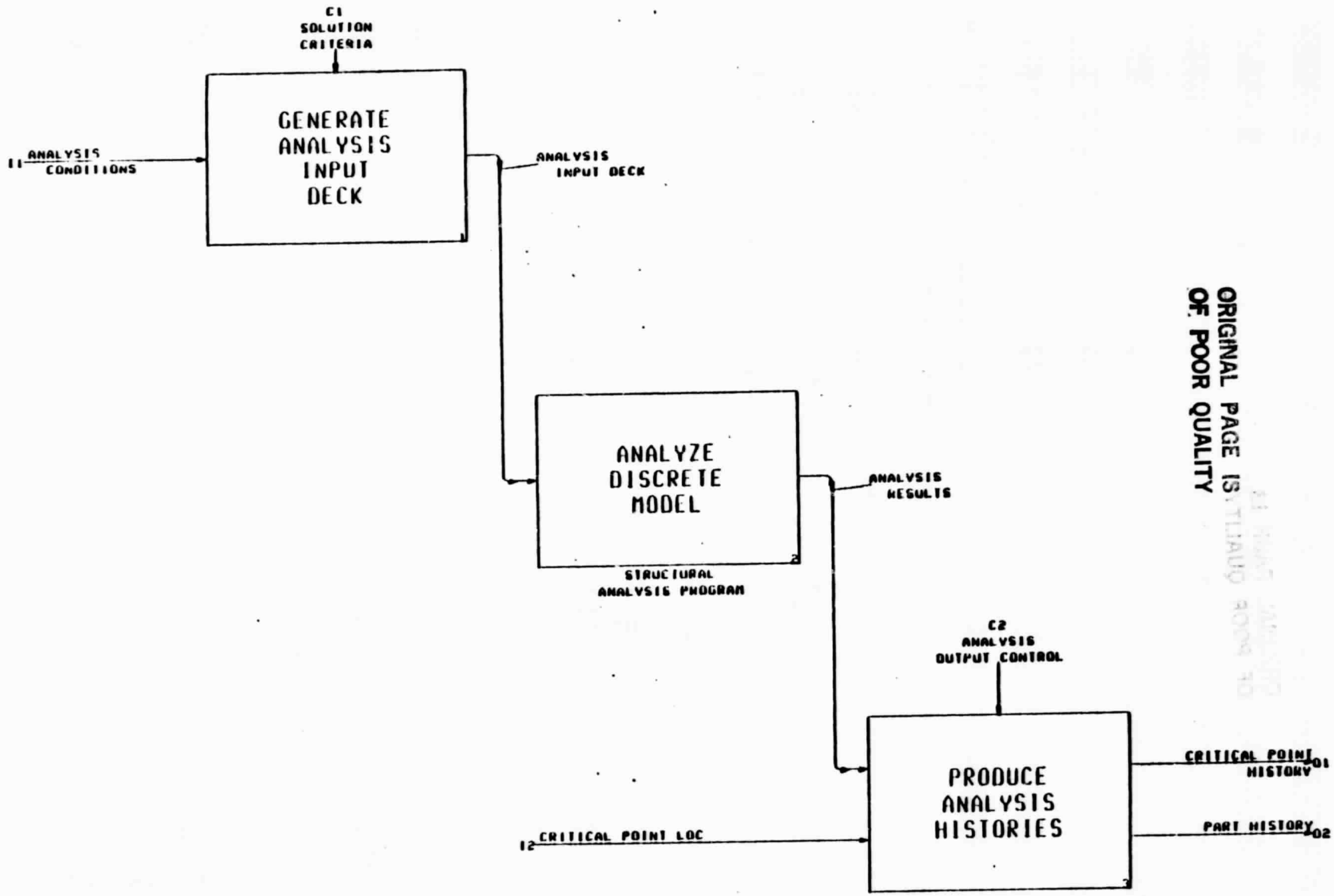

PERFORM STRUCTURAL ANALYSIS

A4.3

REVISION- 1

8-10-83

***** COSMOS DATA DICTIONARY SUMMARY *****

DATE	REV	NAME
08/16/83	A2	ANALYSIS CONDITIONS
08/15/83	A0	ANALYSIS INPUT DECK
08/16/83	A1	ANALYSIS OUTPUT CONTROL
08/15/83	A0	ANALYSIS RESULTS
08/16/83	A2	CONFIGURATION DETAIL GEOMETRY
06/20/83	A5	CRITICAL POINT HISTORY
06/10/83	A0	CRITICAL POINT LIFE
06/20/83	A1	CRITICAL POINT LOCATION
06/07/83	A1	CYCLE MAP
08/16/83	A2	DECISION PARAMETERS
07/26/83	A0	DECOMPOSED MISSION ELEMENT MATRIX
08/16/83	A1	DECOMPOSED MISSION ELEMENT MISSION DEFINITION
08/15/83	A1	DISCRETE MODEL
08/15/83	A0	ELEMENT PRESSURES
06/10/83	A0	ENGINE RATING
06/20/83	A1	HEAT TRANSFER DATA
08/16/83	A2	HEAT TRANSFER MATERIAL PROPERTIES
06/10/83	A1	HEAT TRANSFER PERFORMANCE DATA
06/20/83	A1	MATERIAL LIFE DATA
06/20/83	A1	METAL TEMPERATURES
06/13/83	A0	MISSION DEFINITION
06/12/83	A2	MISSION PERFORMANCE DATA
08/15/83	A0	MODEL MODIFICATIONS
06/19/83	A2	MODELLING CRITERIA
08/15/83	A0	NODAL TEMPERATURES
06/13/83	A1	PART GEOMETRY
07/26/83	A0	PART HISTORY
07/26/83	A0	SOLUTION CRITERIA
07/26/83	A0	SOLUTION RESULTS
08/16/83	A2	STRUCTURAL BOUNDARY CONDITIONS
08/15/83	A1	STRUCTURAL DATA
08/16/83	A2	STRUCTURAL MATERIAL PROPERTIES

***** DATA DICTIONARY *****

DATE: 08/16/83
REV: A2

DATA FLOW NAME: ANALYSIS CONDITIONS

ALIASES: NONE

DIAGRAM REFERENCE: A4

COMPOSITION:

```
ANALYSIS CONDITIONS =  [Element data:                              ]
                       [   Element Number                          ]
                       [ + {Node Number}                           ]
                       [ + Element Type                            ]
                       [ + Material                                ]
                       [ + Angles for orthotropic properties       ]
                       [ + Plasticity indicator                    ]
                       [ + Creep indicator                         ]
                       [ + Pressure                                ]
                      +[Node Data:                                 ]
                       [   Node Number                             ]
                       [ + X,Y,Z location                          ]
                       [ + Temperature                             ]
                       [ + Force                                   ]
                       [ + Angles                                  ]
                       [ + Boundary Conditions                     ]
```

NOTES:

***** DATA DICTIONARY *****

DATE: 08/15/83
REV: A0

DATA FLOW NAME: ANALYSIS INPUT DECK

ALIASES: NONE

DIAGRAM REFERENCE: A4.3

COMPOSITION:

ANALYSIS INPUT DECK = {Node number}
+ {Element Number}
+ {Temperature}
+ {Pressure}
+ {Boundary Condition}

NOTES:

1. The analysis program being used determines the format of the Analysis Input Deck.

***** DATA DICTIONARY *****

DATE: 08/16/83
REV: A1

DATA FLOW NAME: ANALYSIS OUTPUT CONTROL

ALIASES: NONE

DIAGRAM REFERENCE: A4

COMPOSITION:

ANALYSIS OUTPUT CONTROL = Flag that indicates whether or not a Part History should be generated.

NOTES:

***** DATA DICTIONARY *****

DATE: 08/15/83
REV: A0

DATA FLOW NAME: ANALYSIS RESULTS

ALIASES: NONE

DIAGRAM REFERENCE: A4.3

COMPOSITION:

```
ANALYSIS RESULTS =        {Displacement}
                        + {Reaction Force}
                        + {Stress}
                        + {Strain}
```

NOTES:

***** DATA DICTIONARY *****

DATE: 08/16/83
REV: A2

DATA FLOW NAME: CONFIGURATION DETAIL GEOMETRY

ALIASES: CONFIG DETAIL GEOM

DIAGRAM REFERENCE:

COMPOSITION:

```
CONFIGURATION DETAIL GEOMETRY = ({HOLE})
                              + (INTERNAL PASSAGE GEOMETRY)
                              + (COATING)
```

NOTES:

1. Part of HEAT TRANSFER DATA

***** DATA DICTIONARY *****

DATE: 06/20/83
REV: A5

DATA FLOW NAME: CRITICAL POINT HISTORY

ALIASES: NONE

DIAGRAM REFERENCE: A0

COMPOSITION:

$$\text{CRITICAL POINT HISTORY} = \left\{ \begin{array}{l} \text{TIME} \\ + \text{ STRESS} \\ + \text{ STRAIN} \\ + \text{ DISPLACEMENT} \\ + \text{ TEMPERATURE} \end{array} \right\}$$

NOTES:

1. CRITICAL POINT HISTORY contains information about selected critical points in a mission.

***** DATA DICTIONARY *****

DATE: 06/10/83
REV: A0

DATA FLOW NAME: CRITICAL POINT LIFE

ALIASES: NONE

DIAGRAM REFERENCE: A-0

COMPOSITION:

CRITICAL POINT LIFE = Time/cycles to "failure"

NOTES:

DATA DICTIONARY

DATE: 06/20/83
REV: A1

DATA FLOW NAME: CRITICAL POINT LOCATION

ALIASES: CRITICAL POINT LOC

DIAGRAM REFERENCE: A-0

COMPOSITION:

CRITICAL POINT LOCATION = {COORDINATES OF CRITICAL POINT}

NOTES:

***** DATA DICTIONARY *****

DATE: 06/07/83
REV: A1

DATA FLOW NAME: CYCLE MAP

ALIASES: NONE

DIAGRAM REFERENCE: A-0

COMPOSITION:

CYCLE MAP = {CYCLE CASE}

NOTES:

1. There are 148 cases in a CYCLE MAP.

***** DATA DICTIONARY *****

DATE: 08/16/83
REV: A2

DATA FLOW NAME: DECISION PARAMETERS

ALIASES: DECISION PARAM

DIAGRAM REFERENCE: A-0

COMPOSITION:

```
DECISION PARAMETERS =   Solution Type
                      + Structural Analysis Program
                      + RPM
                      + Acceleration
                      + Number of Nodes
                      + Number of Elements
                      + Number of different materials
                      + Number of Pressure Boundary Conditions
                      + Reference Temperature
                      + Number of Incremental Load Conditions
                      + {Constitutive Equation}
                      + {Output parameter}
                      + {Re-start parameter}
                      + {Solution option}
                      + {Convergence Control}
```

NOTES:

1. Solution Types include:
   Plane Stress
   Plane Strain
   Axisymmetric
   3D
   (with/without Thermal Strain)

***** DATA DICTIONARY *****

DATE: 07/26/83
REV: A0

DATA FLOW NAME: DECOMPOSED MISSION ELEMENT MATRIX

ALIASES: DME MATRIX

DIAGRAM REFERENCE: A4

COMPOSITION:

DME MATRIX = {
  Altitude
+ Mach number
+ Power level
+ Ambient Temperature
+ Bleed
+ Deterioration
}

NOTES:

DATA DICTIONARY

DATE: 08/16/83
REV: A1

DATA FLOW NAME: DECOMPOSED MISSION ELEMENT MISSION DEFINITION

ALIASES: DME MISSION DEFINITION

DIAGRAM REFERENCE: ??

COMPOSITION:

```
DME MISSION DEFINITION = {   Altitude
                          + Mach Number
                          + Power level
                          + Ambient temperature
                          + Bleed
                          + Deterioration
                          + Time to next point  }
```

NOTES:

***** DATA DICTIONARY *****

DATE: 08/15/83
REV: A1

DATA FLOW NAME: DISCRETE MODEL

ALIASES: NONE

DIAGRAM REFERENCE: A0

COMPOSITION:

```
PART MODEL = {NODE}
           + {ELEMENT}
           + {PART GEOMETRY}
```

NOTES:

1. A NODE consists of:
   Node Number
   + X coordinate
   + Y coordinate
   + Z coordinate

2. An ELEMENT consists of:
   Element Number
   + Element Type
   + {Node Number}

***** DATA DICTIONARY *****

DATE: 08/15/83
REV: A0

DATA FLOW NAME: ELEMENT PRESSURES

ALIASES: NONE

DIAGRAM REFERENCE: A4.1

COMPOSITION:

$$\text{ELEMENT PRESSURES} = \left\{ \begin{array}{l} \text{Element Number} \\ + \text{ Pressure} \end{array} \right\}$$

NOTES:

DATA DICTIONARY

DATE: 06/10/83
REV: A0

DATA FLOW NAME: ENGINE RATING

ALIASES: NONE

DIAGRAM REFERENCE: A-0

COMPOSITION:

ENGINE RATING = Maximum power level at a given altitude, mach number, and ambient temperature

---

NOTES:

DATA DICTIONARY

DATE: 06/20/83
REV: A1

DATA FLOW NAME: HEAT TRANSFER DATA

ALIASES: HEAT XFER DATA

DIAGRAM REFERENCE: A-0

COMPOSITION:

```
HEAT TRANSFER DATA =   CONFIGURATION DETAIL GEOMETRY
                     + HEAT TRANSFER MATERIAL PROPERTIES
```

NOTES:

***** DATA DICTIONARY *****

DATE: 08/16/83
REV: A2

DATA FLOW NAME: HEAT TRANSFER MATERIAL PROPERTIES

ALIASES: HEAT XFER MATERIAL PROPERTIES

DIAGRAM REFERENCE:

COMPOSITION:

```
HEAT TRANSFER MATERIAL PROPERTIES = {SPECIFIC HEAT}
                                  + {VISCOSITY}
                                  + {THERMAL CONDUCTIVITY}
                                  + {THERMAL NUMBER}
```

NOTES:

1. Part of HEAT TRANSFER DATA

DATA DICTIONARY

DATE: 06/10/83
REV: A1

DATA FLOW NAME: HEAT TRANSFER PERFORMANCE DATA

ALIASES: HEAT XFER PERFORMANCE DATA

DIAGRAM REFERENCE: A0

COMPOSITION:

$$\text{HEAT TRANSFER PERFORMANCE DATA} = \left\{ \begin{array}{l} \text{CASE NUMBER} \\ + \text{ RPM} \\ + \left\{ \begin{array}{l} \text{GAS PRESSURE} \\ + \text{ GAS TEMPERATURE} \\ + \text{ LOCATION} \end{array} \right\} \end{array} \right\}$$

NOTES:

1. One case for each unique mission defintion point.

***** DATA DICTIONARY *****

DATE: 06/19/83
REV: A1

DATA FLOW NAME: MATERIAL LIFE DATA

ALIASES: NONE

DIAGRAM REFERENCE: A-0

COMPOSITION:

```
MATERIAL DATA = {LOW CYCLE FATIGUE DATA}
              + {RUPTURE LIFE DATA}
              + {CREEP LIFE DATA}
              + {MATERIAL OXIDATION RATE DATA}
```

NOTES:

1. LOW CYCLE FATIGUE DATA: Cyclic life vs stress or strain range and metal temperatures.
2. CREEP/RUPTURE LIFE DATA: Hours to "failure" vs stress and metal temperatures.
3. MATERIAL OXIDATION RATE DATA: Oxidation rates vs metal temperature, gas density, and gas velocity.

***** DATA DICTIONARY *****

DATE: 06/19/83
REV: A1

DATA FLOW NAME: METAL TEMPERATURES

ALIASES: NONE

DIAGRAM REFERENCE: A0

COMPOSITION:

$$\text{METAL TEMPERATURES} = \left\{ \begin{array}{l} \text{CASE NUMBER} \\ + \left\{ \begin{bmatrix} + \text{TEMPERATURE} \\ + \text{ELEMENT NUMBER} \\ + \text{NODE NUMBER} \end{bmatrix} \right\} \end{array} \right\}$$

NOTES:

***** DATA DICTIONARY *****

DATE: 06/13/83
REV: A0

DATA FLOW NAME: MISSION DEFINITION

ALIASES: NONE

DIAGRAM REFERENCE: A-0

COMPOSITION:

```
MISSION DEFINITION =     { ALTITUDE
                         + MACH NUMBER
                         + POWER LEVEL
                         + AMBIENT TEMPERATURE
                         + BLEED
                         + DETERIORATION
                         + TIME TO NEXT POINT }
```

NOTES:

1. A series of points that define a mission

***** DATA DICTIONARY *****

DATE: 06/12/83
REV: A2

DATA FLOW NAME: MISSION PERFORMANCE DATA

ALIASES: MISSION PERF DATA

DIAGRAM REFERENCE: A0

COMPOSITION:

$$\text{MISSION PERFORMANCE DATA} = \text{CASE NUMBER/TIME LIST} + \left\{ \begin{array}{l} \text{CASE NUMBER} \\ + \text{ RPM} \\ + \left\{ \begin{array}{l} \text{GAS PRESSURE} \\ + \text{ LOCATION} \end{array} \right\} \end{array} \right\}$$

NOTES:

1. One case for each unique mission definition point.

2. CASE NUMBER/TIME LIST provides the sequence of CASE NUMBERS that define a mission and the time from each case to the next.

***** DATA DICTIONARY *****

DATE: 08/15/83
REV: A0

DATA FLOW NAME: MODEL MODIFICATIONS

ALIASES: NONE

DIAGRAM REFERENCE: A4.1

COMPOSITION:

MODEL MODIFICATIONS = { Node Number / Element Number + addition-deletion indicator }

NOTES:

***** DATA DICTIONARY *****

DATE: 06/19/83
REV: A2

DATA FLOW NAME: MODELLING CRITERIA

ALIASES: NONE

DIAGRAM REFERENCE: A-0

COMPOSITION:

MODELLING CRITERIA = Parameters used to define discretized mesh

---

NOTES:

***** DATA DICTIONARY *****

DATE: 08/15/83
REV: A0

DATA FLOW NAME: NODAL TEMPERATURES

ALIASES: NONE

DIAGRAM REFERENCE: A4.1

COMPOSITION:

$$\text{NODAL TEMPERATURES} = \left\{ \begin{array}{l} \text{Node Number} \\ + \text{ Temperature} \end{array} \right\}$$

NOTES:

1. Temperature is given in degrees Fahrenheit.

***** DATA DICTIONARY *****

DATE: 06/13/83
REV: A1

DATA FLOW NAME: PART GEOMETRY

ALIASES: NONE

DIAGRAM REFERENCE: A-0

COMPOSITION:

```
PART GEOMETRY = {POINTS}
              + {CURVES}
              + {SURFACES}
              + {REGIONS}
```

NOTES:

***** DATA DICTIONARY *****

DATE: 07/26/83
REV: A0

DATA FLOW NAME: PART HISTORY

ALIASES: NONE

DIAGRAM REFERENCE: A4

COMPOSITION:

$$\text{PART HISTORY} = \left\{ \begin{array}{l} \text{Stress} \\ + \text{ Strain} \\ + \text{ Displacement} \end{array} \right\}$$

NOTES:

***** DATA DICTIONARY *****

DATE: 07/26/83
REV: A0

DATA FLOW NAME: SOLUTION CRITERIA

ALIASES: NONE

DIAGRAM REFERENCE: A4

COMPOSITION:

SOLUTION CRITERIA = Soultion Type
+ ???

NOTES:

***** DATA DICTIONARY *****

DATE: 07/26/83
REV: A0

DATA FLOW NAME: SOLUTION RESULTS

ALIASES: NONE

DIAGRAM REFERENCE: A4

COMPOSITION:

SOLUTION RESULTS = Maximum stress deviation
Maximum strain deviation

NOTES:

***** DATA DICTIONARY *****

DATE: 08/16/83
REV: A2

DATA FLOW NAME: STRUCTURAL BOUNDARY CONDITIONS

ALIASES: STRUCT BOUND COND

DIAGRAM REFERENCE:

COMPOSITION:

```
PART BOUNDARY CONDITIONS = {DISPLACEMENT}
                         + {LOAD}
                         + {STRESS}
                         + {STIFFNESS}
```

NOTES:

1. Part of STRUCTURAL DATA

***** DATA DICTIONARY *****

DATE: 08/15/83
REV: A1

DATA FLOW NAME: STRUCTURAL DATA

ALIASES: NONE

DIAGRAM REFERENCE: A-0

COMPOSITION:

```
STRUCTURAL DATA =   CONFIGURATION DETAIL GEOMETRY
                  + {STRUCTURAL BOUNDARY CONDITION}
                  + {STRUCTURAL MATERIAL PROPERTIES}
                  + {Plasticity indicator}
                  + {Creep indicator}
```

NOTES:

***** DATA DICTIONARY *****

DATE: 08/16/83
REV: A2

DATA FLOW NAME: STRUCTURAL MATERIAL PROPERTIES

ALIASES: STRUCT MATL PROP

DIAGRAM REFERENCE:

COMPOSITION:

```
STRUCTURAL MATERIAL PROPERTIES =  {STRESS/STRAIN CURVES}
                                + CREEP DATA
                                + {Orthotropic angle}
```

NOTES:

1. Part of STRUCTURAL DATA

APPENDIX C

THERMODYNAMIC ENGINE MODEL SPECIFICATION

I. Input

A. Setup information (furnished with model)
   1. Engine performance data; 148 cases per Table I-A-1.
      a. Case parameters per Table I-A-1-a.
   2. Engine rating data - Table I-A-2.1-3.
   3. Power level index matrix, Table I-A-3.

B. User Information
   1. Mission definition data
      a. One line for each mission phase point.
      b. Each line contains the following control data:
         1. Phase #
         2. Mach number
         3. Altitude - feet
         4. Offset from standard day - °F
         5. Power level parameter code #
         6. Power level parameter value
         7. Customer bleed - #/sec.
         8. Deterioration level - °F
         9. Time increment between this phase point and the next, min.
      c. One line, following the mission phase point data line, for each parameter to be offset from its steady state value.
      d. Each offset line shall contain:
         1. Phase #
         2. Parameter #
         3. Offset factor
         4. Offset adder

II. Output

A. A performance case for each mission phase point
   1. Parameters per Table I-A-1-a.
   2. Format similar to Table II-A-2.

III. Technical Basis

A. Each new case will be generated from available cases (I-A-1) by a disciplined interpolation process similar to that currently used in the Life Analysis by Stress and Temperature Simulation (LASTS) program.
   1. All parameters will be transformed to a functional form that has optimal linearity relative to all other parameters.
      a. A study will be performed on CF6-50C2 engine performance data to evaluate and improve the interpolation functions.

III. A. 2. Each transformed parameter will be interpolated by a linear interpolation process and then transformed back to its normal form.
3. The interpolation "targets" shall be specified in the input for each mission phase point (I-B-1-b).
4. The interpolation process for each phase point shall begin with a base case near the desired mission phase point.
5. Each interpolation step will convert the base case (or previously modified case) to the desired level of the target control parameter (i.e., MN).
   a. Linear partials are assumed; interactions are ignored.
   b. Partials will be derived from two or more "partial cases" near the base case conditions.
   c. The interpolation steps will be performed in the sequence in Table I-A-1-a.
   d. The specific power level parameter to be used as an interpolation target is input as "power level #", followed by the target value.
   e. For flight idle and ground idle, a special power level # (one for FI or one for GI) will be entered, followed by a zero parameter value; the standard FI and GI power levels will be used.
   f. For thrust reverse, a special power level # will be used and a value of fan speed will follow; thus thrust reverse power level will always be based on a fan speed target.

B. The LASTS interpolation process will be modified to eliminate the current manual procedure for the generation of interpolation instructions.
1. A set of base case numbers will be provided as a function of altitude and Mach number.
2. A family of pairs or triplets of partials case numbers will be provided as a function of altitude and Mach number for each control parameter.
3. The user will be required to input only the data in I-B-1-b for each mission phase point.

C. The Thermodynamic Engine Model (TDE) shall have the capability to predict the minimum time for speed changes due to throttle actions.
1. The user shall have the option to input zero throttle-action transient times, and the model will calculate appropriate transient times, subtracting them from following phase times.
2. The transient time calculation shall be sensitive to the effects of altitude.

D. The user shall have the option of selecting an appropriate CF6-50C2 power management point, and avoid the need for specifying absolute values of the power level parameter.
1. The power management parameter code shall call for take-off, max climb, or max cruise rating, and the adjacent value shall specify the % derate desired based on % thrust.

III. E. Offsets of specific parameters, relative to the steady state performance cases shall be permitted to simulate take-off transient conditions.

1. Each parameter change shall be specified by a line following the mission phase point data.
2. The parameter offset data shall be:
   a. Case #
   b. Parameter #
   c. Offset factor
   d. Offset adder
3. Offset calculations will be performed after mission phase point interpolations are completed.

IV. Software Characteristics/Interfaces

A. Later (to be integrated with overall software of the COSMOS Program).

TABLE I-A-1
CF6-50C2 PERFORMANCE CASES

					OFFSETS		
	M	A	PCNLR	PCNHR2	ΔTo	WB	DT49 °F
1	0	0	109		0	N	50
2			100				
3			90				
4			75				
5			55				
6				FI			
7				GI			
8	0	0	109		-30	N	50
9			100				
10			90				
11			75				
12			55				
13				FI			
14				GI			
15	0	0	109		+30	N	50
16			100				
17			90				
18			75				
19			55				
20				FI			
21				GI			
22	0	0	109		0	0	50
23			100				
24			90				
25			75				
26			55				
27				FI			
28				GI			
29	0	0	109		0	N	0
30			100				
31			90				
32			75				
33			55				
34				FI			
35				GI			
36	4	5	114		0	N	50
37			104.5				
38			94				
39			78				
40			57				
41				FI			
42				GI			

	M	A	PCNLR	PCNHR2	Δ To	OFFSETS WB	DT49 °F	
43	.4	5	114		18	N	50	
44			104.5					
45			94					
46			78					
47			57					
48				FI				
49	↓	↓		GI	↓	↓	↓	
50	.4	5	114		0	0	50	
51			104.5					
52			94					
53			78					
54			57					
55				FI				
56	↓	↓		GI	↓	↓	↓	
57	.4	5	114		0	N	0	
58			104.5					
59			94					
60			78					
61			57					
62				FI				
63	↓	↓		GI	↓	↓	↓	
64	0	5	114		0	N	50	
65			104.5					
66			94					
67			78					
68			57					
69				FI				
70	↓	↓		GI	↓	↓	↓	
71	.4	0	109		0	N	50	
72			100					
73			90					
74			75					
75			55					
76				FI				
77	↓	↓		GI	↓	↓	↓	
78	.18	0	109		0	N	50	T/R
79			100					
80			90					
81			75					
82	↓	↓	55		↓	↓	↓	↓
83	.4	15	106		0	N	50	
84			94					
85			77					
86			59					
87				FI				
88	↓	↓		GI	↓	↓	↓	
89	.65	15	106		0	N	50	
90	↓	↓	94		↓	↓	↓	

TABLE I-A-1
CF6-50C2 PERFORMANCE CASES

	M	A	PCNLR	PCNHR2	ΔTo	OFFSETS WB	DT49 °F
91	.65	15	77		0	N	50
92			59				
93				FI			
94				GI			
95	.65	15	106		18	N	50
96			94				
97			77				
98			59				
99				FI			
100				GI			
101	.65	15	106		0	0	50
102			94				
103			77				
104			59				
105				FI			
106				GI			
107	.65	15	106		0	N	0
108			94				
109			77				
110			59				
111				FI			
112				GI			
113	.65	35	117		0	N	50
114			104				
115			84				
116			65				
117				FI			
118				GI			
119	.8	15	106		0	N	50
120			94				
121			77				
122			59				
123				FI			
124				GI			
125	.8	35	117		0	N	50
126			104				
127			84				
128			65				
129				FI			
130				GI			
131	.8	35	117		18	N	50
132			104				
133			84				
134			65				
135				FI			
136				GI			
137	.8	35	117		0	0	50
138			104				

TABLE I-A-1
CF6-50C2 PERFORMANCE CASES

	M	A	PCNLR	PCNHR2	ΔTo	OFFSETS WB	DT49 °F
139	.8	35	84		0	0	50
140			65				
141				FI			
142				GI			
143	.8	35	117		0	N	0
144			104				
145			84				
146			65				
147				.FI			
148				GI			

TABLE I-A-1a
ENGINE PERFORMANCE CASE PARAMETERS

P2	Fan Inlet Total Pressure	PSIA
P3	Compressor Discharge Total Pressure	PSIA
P4	Turbine Inlet Total Pressure	PSIA
P49	Turbine Outlet Total Pressure	PSIA
T2	Fan Inlet Total Temperature	°F
T3	Compressor Discharge Total Temperature	°F
T41	Turbine Inlet Total Temperature	°F
T49	Turbine Outlet Total Temperature	°F
W25	Fan Air Flow	#/sec
FNIN1	Installed Thrust	#
DTAMB	Offset from Standard Day Temperature	°F
W41	Turbine Air Flow	#/sec
XNH	Core Speed	RPM
XNL	Fan Speed	RPM
MN	Mach Number	
ALT	Altitude	Feet
WB27/WB3	Customer Bleed	#/sec
DT49	Engine Deterioration Index	°F

TABLE I-A-2.1
APPROX. CF6-50C2 RATING DATA

TAKEOFF

°C T2	Feet ALT	PCNLR	XNLR	ALT	PCNLR	XNLR	ALT	PCNLR	XNLR
-60	0	107.75	3736	1000	110.4	3789	2000	111.1	3814
20									
23									
25.5									
27									
28.5								110.4	3789
30.5					109.75	3767		109.75	3767
50		105.7	3628		105.7	3628		105.7	3628
60		97.8	3357		97.8	3357		97.8	3357

T2	ALT	PCNLR	XNLR	ALT	PCNLR	XNLR	ALT	PCNLR	XNLR
-60	3000	111.85	3839	4000	112.75	3870	≥ 5000	113.82	3907
20									
23								112.75	3870
25.5					111.85	3839		111.85	3839
27		111.1	3814		111.1	3814		111.1	3814
28.5		110.4	3789		110.4	3789		110.4	3789
30.5		109.75	3767		109.75	3767		109.75	3767
50		105.7	3628		105.7	3628		105.7	3628
60		97.8	3357		97.8	3357		97.8	3357

TABLE I-A-2.2
APPROX. CF6-50C2 RATING DATA

MAX CLIMB

°C T2	FEET ALT	PCNLR	XNLR	FEET ALT	PCNLR	XNLR	FEET ALT	PCNLR	XNLR
-60.0	36089	117.1	4019	42000	116.2	3989	30000	113.6	3899
-7.0									
-5.7		116.2	3989						
-1.2		113.6	3899		113.6	3899			
11.0		106.7	3662		106.7	3662		106.7	3662
21.2		103.4	3549		103.4	3549		103.4	3549
34.0		98.5	3381		98.5	3381		98.5	3381
60.0		90.4	3103		90.4	3103		90.4	3103

T2	ALT	PCNLR	XNLR	ALT	PCNLR	XNLR	ALT	PCNLR	XNLR
-60.0	20000	106.7	3662	10000	103.4	3549		98.5	3381
-7.0									
-5.7									
-1.2									
11.0									
21.2		103.4	3549						
34.0		98.5	3381		98.5	3381			
60.0		90.4	3103		90.4	3103		90.4	3103

TABLE I-A-2.3
APPROX. CF6-50C2 RATING DATA

MAX CRUISE

°C T2	FEET ALT	PCNLR	XNLR	FEET ALT	PCNLR	XNLR	FEET ALT	PCNLR	XNLR
-4.5	36089	112.42		30000	109.70		42000	109.25	
-1.0		109.70							
0		109.25			109.25				
9.2		104.45			104.45			104.45	
+20		100.64			100.64			100.64	
+29.2		97.47			97.47			97.47	
+43.7		92.70			92.70			92.70	
+60.0		87.35			87.35			87.35	

T2	ALT	PCNLR	XNLR	ALT	PCNLR	XNLR	ALT	PCNLR	XNLR
-4.5	25000	104.45		20000	100.64		10000	97.47	
-1.0									
0									
9.2									
20.0		100.64							
29.2		97.47			97.47				
43.7		92.70			92.70			92.70	
60.0		87.35			87.35			87.35	

T2	ALT	PCNLR	XNLR
-4.5	0	92.70	
-1.0			
0			
9.2			
20.0			
29.2			
43.7			
60.0		87.35	

TABLE I-A-3

AUTOMATED INTERPOLATION SYSTEM

POWER LEVEL INDEX

CF6-50C2

	PCNLR	
P.L. INDEX	ALT 0	ALT 10000'
1	109.0	119.0
2	100.0	109.0
3	90.0	98.0
4	75.0	81.0
5	55.0	58.0
6	38.0	44.0
7	24.0	34.0
P.L. INDEX	ALT 10000'	ALT 40000'
1	103.5	120.0
2	91.5	106.0
3	75.0	85.0
4	58.0	67.0
5	44.0	48.0
6	34.0	37.0

ORIGINAL PAGE IS
OF POOR QUALITY

TABLE II-A-2

PERFORMANCE DATA OUTPUT FORMAT

* ENGINE PERFORMANCE DATA BY MISSION PHASE *

PHASE #	CASE #	** ENGINE P48	PARAMETER P5	W25	** FNIN1	DTAMB
1	197	14.476	14.476	1.108	0.	1.700
2	190	14.476	14.476	1.108	0.	1.700
3	191	14.476	14.476	1.108	0.	1.700
4	192	15.176	14.476	1.108	0.	1.700
5	193	16.476	16.476	1.108	0.	1.700
6	151	16.912	14.595	38.502	1943.746	1.700
7	151	16.912	14.595	38.502	1943.746	1.700
8	152	80.731	20.930	243.413	42726.324	1.701
9	153	82.835	21.507	245.733	39699.600	2.501
10	154	66.172	18.773	206.290	30540.937	2.502
11	155	63.487	16.305	194.756	21451.468	5.001
12	156	34.321	8.196	105.120	9766.540	12.200
13	157	24.340	5.515	81.158	6421.258	12.200
14	157	24.340	5.515	81.158	6421.258	12.200
15	158	4.588	2.797	19.617	-592.969	12.200
16	159	8.911	6.888	26.739	-1914.288	7.800
17	160	13.099	10.748	35.505	-2310.870	4.200
18	161	16.297	13.944	38.100	894.115	2.500
19	162	27.946	14.707	95.530	7275.440	2.500
20	163	29.131	15.402	99.315	8873.031	1.700
21	164	22.015	14.861	68.412	4493.193	1.700
22	164	22.015	14.861	68.412	4493.193	1.700
23	165	43.788	16.292	145.437	14871.125	1.704
24	166	43.084	16.184	144.799	15603.446	1.700
25	187	16.942	14.622	38.558	1946.327	1.700
26	187	16.942	14.622	38.558	1946.327	1.700
27	194	16.503	16.503	0.974	0.	1.700
28	195	14.503	14.503	0.974	0.	1.700
29	196	14.503	14.503	0.974	0.	1.700
30	186	14.503	14.503	0.974	0.	1.700